JOURNAL OF PETROLOGY

Journal of Petrology, 2019, Vol. 60, No. 1, 19–56
doi: 10.1093/petrology/egy105
Advance Access Publication Date: 19 November 2018
Perspectives

OXFORD

PERSPECTIVES

Modeling Metamorphic Rocks Using Equilibrium Thermodynamics and Internally Consistent Databases: Past Achievements, Problems and Perspectives

Pierre Lanari[1]* and Erik Duesterhoeft[2]

[1]Institute of Geological Sciences, University of Bern, Baltzerstrasse 1 + 3, Bern 3012, Switzerland; [2]CAU University Kiel, Institute of Geosciences, Ludewig-Meyn-Straße 10, Kiel 24118, Germany

*Corresponding author. E-mail: pierre.lanari@geo.unibe.ch

Received June 5, 2018; Accepted November 6, 2018

Pierre Lanari is a Research Associate at the Institute of Geological Sciences of the University of Bern (Switzerland). He earned his PhD in geosciences from the University of Grenoble (France) in 2012. His work aims to understand the conditions and tempo of metamorphic processes by combining high-resolution geochemical analysis with thermodynamic modelling. Pierre has contributed to the development of important tools for community use including the mapping software XMapTools as well as to the theory, technique and application of advanced petrological models. He recently co-edited a volume of the *Reviews in Mineralogy and Geochemistry* series on petrochronology and is associate editor of *Computers and Geosciences*.

Erik Duesterhoeft is a lecturer at the Institute of Geosciences of the Kiel University (Germany). He graduated from the University of Potsdam (Germany) with a doctoral degree in geosciences–geodynamics in 2014. His research focuses broadly on the influence of metamorphic processes on the outcome of geodynamic models. In particular, this involves the improvement of thermodynamic databases and modeling approaches (e.g. computation of seismic velocities or mineral volumes and densities). He is interested in the polymetamorphic evolution of the Central Metasedimentary Belt of the Canadian Grenville Province. Erik is an active member of the Theriak-Domino developers group and released the add-on Theriak_D for implementing thermodynamic analysis into geodynamic models.

ABSTRACT

The astonishing progress of personal computer technology in the past 30 years as well as the availability of thermodynamic data and modeling programs have revolutionized our ability to investigate and quantify metamorphic processes. Equilibrium thermodynamics has played a central role in this revolution, providing simultaneously a physico-chemical framework and efficient modeling strategies to calculate mineral stability relations in the Earth's lithosphere (and beyond) as well as thermobarometric results. This Perspectives contribution provides a review of the ingredients and recipes required for constructing models. A fundamental requirement to perform thermodynamic modeling is an internally consistent database containing standard state properties and activity–composition models of pure minerals, solid solutions, and fluids. We demonstrate how important internal consistency is to this database, and show some of the advantages and pitfalls of the two

main modeling strategies (inverse and forward modeling). Both techniques are commonly applied to obtain thermobarometric estimates; that is, to derive *P–T* (pressure–temperature) information to quantify the conditions of metamorphism. In the last section, we describe a new modeling strategy based on iterative thermodynamic models, integrated with quantitative compositional mapping. This technique provides a powerful alternative to traditional modeling tools and permits use of local bulk compositions for testing the assumption of local equilibrium in rocks that were not fully re-equilibrated during their metamorphic history. We argue that this is the case for most natural samples, even at high-temperature conditions, and that this natural complexity must be taken into consideration when applying equilibrium models.

Key Words: metamorphism; modeling tools; thermobarometry; thermodynamics

INTRODUCTION

The concept of equilibrium thermodynamics has been widely applied for almost two centuries in diverse disciplines studying the transformations of matter and energy. This fundamental principle applies to systems that are in thermal, mechanical, chemical and radiative equilibrium. In geology, equilibrium thermodynamics has proven to be powerful, notably serving as a physical basis for developing thermobarometric tools that have allowed definition of the large variety of lithospheric conditions recorded throughout Earth's history (Brown, 2007). Important scientific progress has also been made in the last three decades in understanding multi-scale geochemical cycles and lithospheric processes, many of them relying on predictions made by equilibrium models (see recent reviews by Spear *et al.*, 2016; Yakymchuk, 2017). These accomplishments have required considerable efforts towards developing tools (Fig. 1) that can easily be applied by a broad community studying a large variety of geological settings. These tools include the following: (1) empirical calibrations of geothermometers or geobarometers based on mineral–mineral and mineral–fluid equilibria; (2) an internally consistent thermodynamic database consisting of a dataset of standard state properties for minerals and fluids, as well as solution models or activity–composition relations (Fig. 1b); (3) computer programs dedicated to solving chemical equilibrium problems in simple and complex systems; (4) software employed for forward or inverse modeling (Fig. 1c).

Calculation of pressure–temperature (*P–T*) equilibrium phase diagrams for a given bulk composition (Hensen, 1971)—these are isochemical phase diagrams, also referred to as pseudosections in the recent literature—has recently been considered the best way to do thermobarometry in metamorphic rocks (Powell & Holland, 2010). These diagrams are the results of a forward model, starting with the causes (pressure, temperature, bulk composition) and calculating the resulting mineral compositions and modes for a given internally consistent thermodynamic database. At present, equilibrium phase diagrams can be generated by four computer programs (THERIAK-DOMINO, PERPLE_X, THERMOCALC and GIBBS; see below), each applying a different numerical strategy. The diversity of modeling techniques and programs partially accounts for the success of equilibrium thermodynamics both as a concept and as a modeling tool, and its impact in petrological studies (e.g. Fig. 3c of Engi *et al.*, 2017) even where samples show evidence of only partial equilibration.

All these methods rely on the assumption of thermodynamic equilibrium, yet if equilibrium were truly maintained, all surface rocks would be 'mud' in a metaphorical sense. The tacit assumption is that equilibrium is achieved at the peak of metamorphism and then quenched, whereas for most metamorphic rocks, it is not self-evident that equilibrium was attained and maintained (e.g. Waters & Lovegrove, 2002; Pattison *et al.*, 2011; Carlson *et al.*, 2015; Lanari & Engi, 2017). In nature, thermodynamic equilibrium is not a tendency but is rather a result; a balanced state of internal energy toward which a thermodynamic system should spontaneously converge. The road to equilibrium for a closed system is 'straight down the Gibbs free energy hill' and travel time (i.e. rate of equilibration) depends on the rates at which matter and energy can flow within the system if the driving forces are sufficient to overcome the kinetic barriers. If conditions change, such that the system needs to react to reach the state of least energy, but some constraint prevents the reaction from proceeding, it is said to be in a metastable equilibrium state. It has long been recognized that natural systems, such as crustal rocks, do not always reach thermodynamic equilibrium along every stage of their *P–T* history (Rubie, 1998), and this may thwart thermobarometric investigations. Features of thermodynamic disequilibrium have been reported in magmatic (e.g. Albarede & Bottinga, 1972; Metcalf *et al.*, 1995; Couch *et al.*, 2001; Davidson *et al.*, 2007) and metamorphic rocks (e.g. Evans & Guidotti, 1966; Loomis, 1975; Carlson, 2002; Waters & Lovegrove, 2002; Evans, 2004; Meth & Carlson, 2005; Pattison & Tinkham, 2009; Carlson *et al.*, 2015; Lanari & Engi, 2017). Both chemical (Brouwer & Engi, 2005; White *et al.*, 2008; Beinlich *et al.*, 2010) and mechanical disequilibrium (Tajčmanová *et al.*, 2015; Centrella *et al.*, 2018) at sample scales have been invoked. Polymineralic rocks are chemically heterogeneous, and compositional gradients are likely to

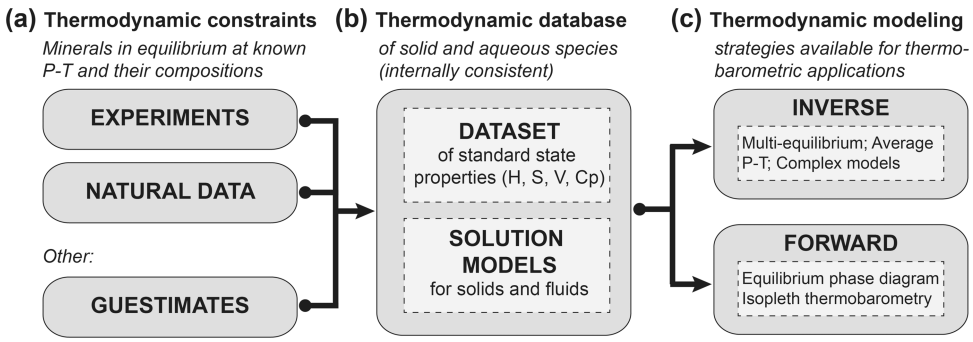

Fig. 1. Strategy for modeling metamorphic rocks using equilibrium thermodynamics and an internally consistent database. (a) Experimental, natural and other constraints used to derive a thermodynamic database. 'Guestimates' represent all the other types of constraint such as mineral assemblage relationships and shape of mineral stability field. (b) The thermodynamic database consists of an internally consistent dataset of standard state properties and solution models. (c) Main modeling strategies used in the literature and described in this review.

be preserved in low- to medium-grade metamorphic rocks, as low inter- and intra-granular rates of elemental diffusion are expected at these low-temperature conditions (Carlson, 1989, 2002). To overcome these issues and help extend the limits of the equilibrium assumption, alternative concepts and strategies have been employed, such as applying the concept of local equilibrium (Korzhinskii, 1936, 1959; Thompson, 1955, 1959, 1970; Carmichael, 1969) and the use of fractionation models to approximate the reactive bulk composition (Spear, 1988*b*; Evans, 2004). Several recent contributions have taken an opposite path, re-emphasizing the role and importance of kinetic phenomena (Waters & Lovegrove, 2002; Carlson & Gordon, 2004; Carlson, 2010; Gaidies *et al.*, 2011; Spear *et al.*, 2014; Carlson *et al.*, 2015; Spear & Pattison, 2017). Overall, these researchers acknowledge that equilibrium calculations are important to model *P–T* conditions, whereas kinetics dictates what can eventually be seen in an exhumed rock (Pattison *et al.*, 2011; Spear & Pattison, 2017).

In this contribution, we emphasize the critical role of modeling techniques and computer programs in the success story of equilibrium thermodynamics, and we present a critical review of the main strategies that have been utilized. The first section is dedicated to the indispensable basis of any reliable thermodynamic model: the thermodynamic database (Fig. 1b). Different strategies have been applied in an attempt to make them 'internally consistent', as it is important that data should not be combined from different sources without testing their consistency. The second section reviews the traditional approaches involving either inverse or forward modeling (Fig. 1c). In the third section a novel modeling strategy based on iterative forward models (IFM) is presented. This technique aims to overcome some conceptual limits of the inverse and forward approaches that are highlighted in this contribution.

THERMODYNAMIC DATABASES

It has long been recognized that standard state thermodynamic data from different sources cannot be combined with impunity because they may be based on different sets of data for entropy, enthalpy or volume and thus introduce systematic errors (Essene, 1989). To be used for accurate prediction of phase relationships in complex chemical systems, the thermodynamic properties of solid and fluid phases must be derived from relevant experimental data and maintained in thermodynamic datasets. Such datasets are distinguished from the final database in this contribution as they often provided the basis from which activity models of solid solutions have been calibrated. It is important to note that for many solid solutions optimal activity models require derivation simultaneously with end-member data (Berman, 1990; Berman & Aranovich, 1996; Spear *et al.*, 2016).

Gibbs free energy of mineral phases and experimental constraints

As shown by J. Willard Gibbs, chemical equilibrium among phases in an isolated system can be described in terms of the energetic behavior of each phase (Gibbs, 1878). For petrologists, the apparent Gibbs free energy $\Delta_a G^{P,T}$ has proven to be the most convenient description of the energetic behavior of a mineral phase. The apparent Gibbs free energy is a function of P and T and is defined as

$$\Delta_a G^{P,T} = \Delta_f G^{P,T} + RT\ln(a) \quad (1)$$

with R the universal gas constant, a the activity of the a component in a phase and $\Delta_f G^{P,T}$ the standard Gibbs free energy of formation of this component (Berman *et al.*, 1986):

$$\Delta_f G^{P,T} = \Delta_f H^{P_0,T_0} - TS^{P_0,T_0} + \int_{T_0}^{T} Cp\,\mathrm{d}T - T\int_{T_0}^{T} \frac{Cp}{T}\,\mathrm{d}T + \int_{P_0}^{P} V\,\mathrm{d}P. \quad (2)$$

$\Delta_f H^{P_0,T_0}$ and S^{P_0,T_0} are the enthalpy of formation from the elements or oxides and third law entropy at P_0 (1 bar) and T_0 (298·15 K), Cp is the heat capacity and V the molar volume of the phase. It should be noted that

equation (2) contains the minimum number of terms needed to compute chemical equilibrium problems and differs slightly from the equation of Helgeson *et al.* (1978) in which the standard state entropy term was defined as $(T - T_0)S$; the same formalism was also used by Holland & Powell (1988) and Holland & Powell (1998).

The apparent Gibbs free energy is not directly measurable, but part of it is, at least in principle, as described by Engi (1992). Standard state properties and an activity or solution model are required to compute the apparent Gibbs free energy of any phase at given P and T conditions. The main standard state properties are $\Delta_f H^{P_0,T_0}$, S^{P_0,T_0} and V^{P_0,T_0}, as well as the parameters for the heat capacity (Cp), thermal expansion and compressibility functions (Newton, 1987). Thermodynamic properties presented in internally consistent databases are derived from both direct measurement of a phase's thermodynamic properties (i.e. H, S, V, Cp) and indirect experiments constraining phase stability relationships and/or compositions (i.e. phase equilibrium data).

Direct experiments aim to determine standard state thermodynamic properties of individual phases using synthetic or well-characterized natural materials. Calorimetric or spectroscopic techniques allow the enthalpy of formation ($\Delta_f H^{P_0,T_0}$), the entropy (S^{P_0,T_0}) and the $Cp(T)$ of a mineral phase to be constrained (e.g. Charlu *et al.*, 1975; Robie *et al.*, 1978; Benisek *et al.*, 2010; Dachs *et al.*, 2012), whereas X-ray diffraction experiments provide measurement of the molar volume (V°), including compressibility and thermal expansivity (e.g. Newton, 1987; Katsura *et al.*, 2009; Nestola *et al.*, 2011). Analytical uncertainties can be high, notably for enthalpies of formation. In addition, enthalpy, entropy and heat capacities are intrinsically linked (second law of thermodynamics) via the G function, and thus cannot be systematically derived together from a single-phase equilibrium experiment. Instead, they are derived from indirect experiments on multiphase equilibria (e.g. phase equilibrium reversals), often performed in different laboratories, which are optimized simultaneously in an attempt to satisfy all of the available experimental constraints.

Ideally, reversed phase relationships are used to ensure the equilibrium position was constrained by the experiment (Holloway & Wood, 1988). These experiments consist of bracketing the P–T conditions for a given equilibrium between two mineral assemblages (e.g. albite = jadeite + quartz; see Holland, 1980). If the P–T range and the P–T slope of a metamorphic reaction are known, it becomes possible to model how the thermodynamic properties of the reaction (ΔH_r°, ΔS_r° and ΔV_r°) change with P and T. This can then be used as a constraint to refine the standard state properties of the mineral phases involved. A variant of such experiments involves 'bracketing' mineral compositions rather than P–T conditions (e.g. Ferry & Spear, 1978; Powneby *et al.*, 1987; Koziol & Newton, 1989), although reversals are apparent compositional brackets that, in many cases, cannot be reversed (Pattison, 1994). Indirect experiments can be applied to simple systems with low-variance assemblages including (or not) solid solutions, or more complex systems closer to nature. Uncertainties in thermodynamic properties derived from indirect experiments are generally smaller than for those obtained by direct methods, but they have complex probability distributions (see below); all kinds of experiments are exposed to all of the usual experimental and analytical errors.

Internally consistent thermodynamic datasets

The early well-documented compilations of thermodynamic properties for solids and fluids were based on only calorimetric and volumetric data (Robie & Hemingway, 1995) without use of phase equilibrium reversals to test and refine thermodynamic properties. The latter step was the huge contribution of Helgeson *et al.* (1978), who provided the first partially internally consistent thermodynamic database built upon a stepwise analysis of phase equilibrium experiments in different compositional systems. Less than 10 years later, thermodynamic properties in multicomponent (e.g. SiO_2–TiO_2–Al_2O_3–FeO–Fe_2O_3–MnO–MgO–CaO–Na_2O–K_2O–H_2O) systems were derived simultaneously by achieving consistency with the large set of experimental constraints (Table 1). A fully internally consistent dataset contains thermodynamic properties that (1) are compatible with basic thermodynamic definitions, (2) adhere to one set of reference values, (3) consider all the experimental data simultaneously and (4) reproduce all primary data within their uncertainties (Berman *et al.*, 1986; Engi, 1992). It should be noted that the term internally consistent has been intensively applied to describe published datasets (Holland & Powell, 1985, 1988, 1990, 1998, 2011; Berman, 1988; Gottschalk, 1997; Chatterjee *et al.*, 1998; Miron *et al.*, 2016, 2017). However, the degree of consistency with primary data (i.e. selection of primary data and fit quality) varies among these, as well as in the final databases—including complex solid solution activity models—that are in use in the modeling programs.

The two main techniques that have been employed for determining internally consistent thermodynamic datasets are the least-squares regression technique (REG; e.g. Helgeson *et al.*, 1978; Holland & Powell, 1985), and the mathematical programming technique (MAP; e.g. Berman *et al.*, 1986); the latter is an extension of the linear programming technique (LIP; Gordon, 1973). The main difference between REG and MAP lies in the way phase equilibrium data are treated (see Fig. 8.1 of Engi, 1992) to refine $\Delta_f H^{P_0,T_0}$ of each phase (Holland & Powell, 1985, 1988, 1998, 2011) or $\Delta_f H^{P_0,T_0}$, S^{P_0,T_0} and V° (Berman, 1988). In REG, the weighted midpoints of brackets are treated as positions where the $\Delta_r G^{P,T} = 0$ (Powell & Holland, 1993*a*), whereas in MAP each half-bracket is treated as a statement of inequality in $\Delta_r G^{P,T}$ [see equation (3) below for a definition of the

Table 1: List of the main thermodynamic datasets (and databases) cited in the text

	Reference	Updates	Technique	Phases	Si	Al	Mg	Ca	Na	K	Ti	Fe	Fe3	Mn	Cr	Li	Be	Zn	Zr	Ni	Cu	Cu_3	Cl	S	H_2O	CO_2	O_2	Citations Google Scholar*
HP85	Holland & Powell (1985)	none	REG	43	x	x	x	x	x	x															x	x		225
B88	Berman (1988)	*JUN92; DEC06*	MAP	67	x	x	x	x	x	x	x	x	x												x	x		2138
HP90	Holland & Powell (1985)	none	REG	123	x	x	x	x	x	x	x	x	x	x											x	x	x	1273
G97	Gottschalk (1997)	none	IREG	94	x	x	x	x	x	x	x	x	x												x	x	x	180
C98	Chatterjee *et al.* (1998)	none	BAYES	148	x	x	x	x	x	x	x	x	x	x	x	x	x	x							x	x	x	79
HP98	Holland & Powell (1998)	*ds3.2*; *ds5.5*	REG	189	x	x	x	x	x	x	x	x	x	x					x	x					x	x	x	3707
HP11	Holland & Powell (2011)	*ds6.2*	REG	254	x	x	x	x	x	x	x	x	x	x	x				x	x	x	x	x	x	x	x	x	419

IREG is an iterative REG.
*In December 2017.

standard Gibbs free energy of a reaction] depending on whether growth of reactants or products was observed experimentally. A range of solutions is obtained using the MAP technique, which ensures the consistency with all the selected primary data (Berman *et al.*, 1985). A selection of the primary data is thus required for MAP because different experimental determinations of the same equilibrium may not all agree. As the square of the residuals is minimized in REG, a unique solution, not really optimal because of the non-normal distribution of uncertainties, is obtained with pseudo-uncertainties determined from the covariance matrix (Engi, 1992). It is important to note that REG does not ensure consistency with all of the data and may introduce retrieval problems in the parameters that are not optimized by REG; for example, the parameters of the *Cp* function (e.g. Lanari *et al.*, 2014*c*).

A third technique has been employed to optimize internally consistent thermodynamic datasets: the Bayesian approach (BAYES; e.g. Chatterjee *et al.*, 1998). BAYES combines the advantages of MAP such as the ability to handle inequalities and equalities and the (necessary) elimination of inconsistent experiments, as well as the advantages of REG, such as the ability to obtain a variance–covariance matrix used to approximate uncertainties (Holland & Powell, 1988). Despite recent improvements in computational capabilities and in Markov chain Monte Carlo methods, the apparent complexity of BAYES has resulted in the limited use of this technique.

Differences between BE and HP datasets

The updated versions of the databases, based on the datasets of Berman (1988) and Holland & Powell (1998), have been most commonly used in metamorphic petrology; the dataset of Holland & Powell (2011) has replaced the 1998 version and is now 'recommended' by the THERMOCALC group. It is important to review the main methodological differences between these databases. For brevity, the datasets of Berman (1988), Holland & Powell (1998) and Holland & Powell (2011) are referred to as *BE88*, *HP98* and *HP11*, respectively.

Mineral volumes are calculated using different equations of state (EOS; see Angel *et al.*, 2014; Duesterhoeft, 2016). The heat capacity of mineral phases is approximated in *HP98* and *HP11* using the formalism of Maier & Kelley (1932) expanded by Robie *et al.* (1978), whereas *BE88* uses the Berman & Brown (1985) equation designed for high-*T* extrapolation. The *PVT* properties of fluid components are calculated with the EOS of Haar *et al.* (1984) and Kerrick & Jacobs (1981) in *BE88*, whereas *HP98* employs a compensated Redlich–Kwong (CORK) equation (Holland & Powell, 1991). This was changed in *HP11*, which relies on the Pitzer & Sterner EOS (Pitzer & Sterner, 1994, 1995). Some activity models compatible with *HP11* have been calibrated, for instance for the H_2O–CO_2–NaCl system (Dubacq *et al.*, 2013).

It is important to note that the mathematical expressions of the EOS define the range of applicability of the entire dataset. The dataset *BE88* is, for example, applicable only below 4 GPa and 1200°C because of the parabolic form of the volume equation (Fig. 2). However, a recent improvement of this EOS can extend this range up to 20 GPa using the same volume parameters as *BE88* (Duesterhoeft, 2016). Some mineral phases are prone to high-temperature order–disorder transitions, such as between α-quartz and β-quartz (Majumdar *et al.*, 1964). To model the order–disorder transitions of quartz, *BE88* uses the Lambda transition approach (Berman & Brown, 1985), and *HP98* (as well as *HP11*) the Landau transition approach (Holland & Powell, 1996*a*, 1998). The Landau transition was incorrectly implemented in *HP98* and resulted in large discrepancies between measured and predicted volumes, which have implications for determining rock density (Duesterhoeft *et al.*, 2012*b*). However, the effects on phase diagrams calculated for crustal conditions were minor, so this mistake was corrected only in the subsequent dataset *HP11*. These are examples of how the choice of an EOS and the possible errors during implementation may affect the results of informed and uninformed users who are using the modeling programs. The implications can be indeed important or relevant only in principle.

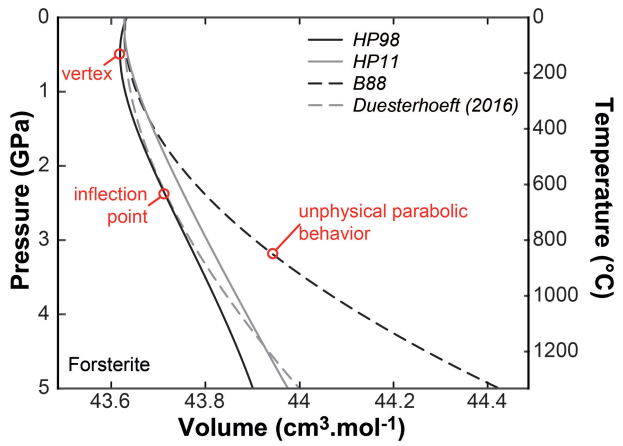

Fig. 2. Molar volume data for forsterite as a function of pressure (or depth), calculated along a thermal gradient of 8°C km^{-1} calculated for different EOS using Theriak_D (Duesterhoeft & de Capitani, 2013). Dataset *HP98* uses the Murnaghan EOS; an inflection point is observed at 24 kbar, which is a typical feature of this type of function; the volume is predicted to decrease from 0 to 6 kbar. Dataset *HP11* uses the modified Tait EOS. Dataset *B88* relies on a Bridgman Power Series, causing an unrealistic volume increase with depth because of the parabolic equation. The EOS of Duesterhoeft (2016) readjusts this volume function, while using the volume parameters of *B88*.

Other datasets for specific applications

The main datasets described in the previous section are large, involving more phases than required in many applications. Smaller optimized datasets or datasets extended to larger chemical systems have also been developed. The *BE88* dataset was used as a basis to develop *MELTS* (Ghiorso & Sack, 1995), *pMELTS* (Ghiorso *et al.*, 2002), the CaO–MgO–Al_2O_3–SiO_2–H_2O database of Grevel (2004), the database for metapelite of Pattison *et al.* (2002) including phosphate minerals (Spear & Pyle, 2010), the *ChIMica* database for low-grade thermobarometry (e.g. Vidal & Parra, 2000; Vidal *et al.*, 2006; Pourteau *et al.*, 2014), the *JUN92* database distributed with the software Theriak-Domino (de Capitani & Petrakakis, 2010) and the *BED92* database extended from *JUN92* (Duesterhoeft, 2017). The Holland & Powell datasets originally designed for the THERMOCALC software package (Powell & Holland, 1988, 2008; Powell *et al.*, 1998) were used as a basis for many databases published by this group over time. For example, the last major update of the *HP98* dataset (the database known as *ds5.5* or *tc55*) included several complex activity solid solution models (e.g. Diener *et al.*, 2007; Green *et al.*, 2007; White *et al.*, 2007; Taylor-Jones & Powell, 2010; Kelsey & Powell, 2011; Diener & Powell, 2012). The same strategy was applied for the *HP11* dataset (*ds6.2* or *tc62*) with activity solid solution models for metapelitic rocks (White *et al.*, 2014) or mafic and ultramafic rocks (e.g. Holland *et al.*, 2013; Wheller & Powell, 2014; Jennings & Holland, 2015; Green *et al.*, 2016).

Other datasets (and/or databases) have also been developed and published; they are not all listed here because of their limited number of applications in metamorphic petrology (Saxena *et al.*, 1993; Fabrichnaya *et al.*, 2003). However, the database of Stixrude & Lithgow-Bertelloni (2005) deserves mention, as it has been intensively applied by the geophysical community to model the phase equilibrium relationships for mantle minerals. This database is provided in the Gibbs free energy minimizer *HeFESTo* (Stixrude & Lithgow-Bertelloni, 2011), Theriak-Domino (de Capitani & Brown, 1987; de Capitani & Petrakakis, 2010) and Perple_X (Connolly, 1990; Connolly & Petrini, 2002).

Solid solution models

Analysis of experimental data is required not only to derive thermodynamic properties of end-members but also to derive compatible activity–composition (*a*–*x*) models. In most silicates, several elements can substitute for each other on each crystallographic site (points on the lattice, which have fixed geometric relations to the adjacent sites) forming complex solid solutions (e.g. Powell, 1978; Spear, 1993). For each solid solution included in a specific database, it is necessary to express the activity–composition relations for the end-members (phase components) involved. An activity model contains the thermodynamic mixing properties of the components reflecting their structural complexity and the elemental substitutions that take place in the solid solution, as well as other phenomena such as ordering and exsolution (Navrotsky, 1987).

Simple and complex solid solution models

In a thermodynamic description, the solid solution model aims to reproduce the energetic behavior of natural mineral phases. To achieve this goal the level of complexity can be variable. The solid solutions were first classified as simple or complex (Brown, 1977). Simple solutions consisted of a set of independent end-members with a size corresponding to the number of chemical components involved in the chemical substitutions. For example, olivine $(Mg,Fe)_2SiO_4$ can be treated as a simple solution if the compositional range is restricted to the Fe–Mg binary system, with a description involving only two independent end-members: forsterite (Mg_2SiO_4) and fayalite (Fe_2SiO_4). In a complex solid solution model, more end-members are required and they can exceed the number of elements involved in the chemical substitutions. Such complex solutions are characteristic of multi-site interactions, each site behaving in a different way, or of reciprocal relationships involving end-members dependent in composition that can be treated as dependent in *G* (Powell & Holland, 1993*b*) or independent (Wood & Nicholls, 1978; Vidal *et al.*, 2005). A model for clinopyroxene involving four end-members—diopside ($CaMgSi_2O_6$), hedenbergite ($CaFeSi_sO_6$), jadeite ($NaAlSi_2O_6$) and omphacite ($Ca_{0.5}Na_{0.5}Al_{0.5}Mg_{0.5}Si_2O_6$)—is complex, because omphacite is a linear combination of diopside and jadeite with respect to composition, but not with respect to *G*, as ordering within the split M2 and M1 sites

makes a contribution to G (e.g. Holland & Powell, 1996*b*). It is important to note that applying complex solution models with reciprocal relationships such as the formulation of Wood & Nicholls (1978) may lead to non-unique mathematical solutions, because for a unique set of end-member activities, there is not an unique solution of end-member compositions (Hunziker, 2003; C. de Capitani, personal communication, 2017); an undesired scenario in minimizing Gibbs free energy. This is not the case for the complex reciprocal formulation of Powell & Holland (1993*b*).

The Gibbs free energy of a mechanical mixture between two end-members is a linear combination of the standard Gibbs free energy $\Delta_f G_1^{P,T}$ and $\Delta_f G_2^{P,T}$ (Fig. 3):

$$G_{mech} = X_1 \Delta_f G_1^{P,T} + X_2 \Delta_f G_2^{P,T} \quad (3)$$

where X_1 and X_2 are the molar fractions. This mixture is made up of the two distinct phases, which are mixed but not combined chemically (like a powder consisting of two phases). If the mixture reacts at given P and T, without heat effect ($\Delta H_S = 0$), and forms a single phase, the change in Gibbs free energy (G_{conf}) is (Greenwood, 1977)

$$G_{conf} = -T\Delta S_S. \quad (4)$$

In this case of ideal mixing, the extensive properties such as volume and enthalpies are the sum of the components ($\Delta V_{\text{ideal mixing}} = \Delta H_{\text{ideal mixing}} = 0$). As shown by equation (4), this is not true for entropy, as the entropy of the new solution increases with a larger number of possible arrangements. In an ideal one-site mixing model, the activity of each end-member is equal to the mole fraction of this end-member.

The ideal model provides a useful reference for the behavior of solid solutions, but comparing real solid solution with the ideal one has led to the concept of excess functions (e.g. Thompson, 1955; Spear, 1993; White, 2013; and references therein). The excess molar Gibbs free energy G_{excess} is defined as the difference between the ideal configurational Gibbs free energy of mixing G_{ideal} and the real Gibbs free energy of mixing of the solid solution G_{real} (Fig. 3). A non-ideal solid solution is thermodynamically described by

$$\Delta G_m = G_{mech} + G_{conf} + G_{excess}. \quad (5)$$

In many cases, it is assumed that G_{excess} is T and P independent (only $\Delta H_{\text{non-ideal mixing}} \neq 0$); it should be noted that it can also be T dependent ($\Delta S_{\text{non-ideal mixing}} \neq 0$) and/or P dependent ($\Delta V_{\text{non-ideal mixing}} \neq 0$). There are usually not enough data to constrain both pressure and temperature dependence in G_{excess} independently. The calibration of such models requires experimental constraints or atomistic modeling techniques to approximate G_{real} and derive G_{excess} for a given range of T and P (e.g. Dubacq *et al.*, 2011).

A large variety of ideal and non-ideal mixing models exist in the literature (see Ganguly, 2001, for a review); in most cases G_{excess} is calculated based on a symmetrical regular model or an asymmetrical sub-regular model (Fig. 4a). These models, first introduced into the geological literature by Thompson (1967), use three independent interaction parameters W_H, W_S and W_V also known as Margules parameter (Margules, 1895):

$$W_G = W_H - TW_S + PW_V. \quad (6)$$

These interaction parameters can be employed to express the non-ideal interaction energy between macroscopic end-members, such as $W_{\text{grs, grs, py}}$ of Berman (1990), or microscopic pair-wise interactions between elements on the same or different sites (site-Margules parameters), such as $W^{M1}{}_{MgFe}$ of Berman (2007). However, (sub)-regular models can only produce smooth, continuous curves representing G_{excess} of a solid solution (Fig. 4a).

Describing more complex solid solutions such as discontinuous curves (e.g. owing to order–disorder effects) is challenging. The expansion of the Margules approach to higher order increases the number of interaction parameters (Anderson, 2005), producing continuous curves with a higher degree of asymmetry. Some alternative approaches include the quasi-chemical approach (Guggenheim, 1952) or the universal thermodynamic equation of Gottschalk (2016). The models that have been most used so far are extended from the classical solution models: the symmetric formalism of Powell & Holland (1993*b*) or the asymmetric formalism of Holland & Powell (2003) that is based on the model from van Laar (1906). These formulations reduce the number of parameters required to describe a solid solution as there is only a limited number of within-site (standard Margules) and cross-site (reciprocal) terms for any solid solution (Powell & Holland, 1993*b*). In addition, the symmetric models can be calibrated with real solid solutions, whereas many intra-site and reciprocal terms cannot be calibrated independently because it is not possible to isolate the substitution to be investigated.

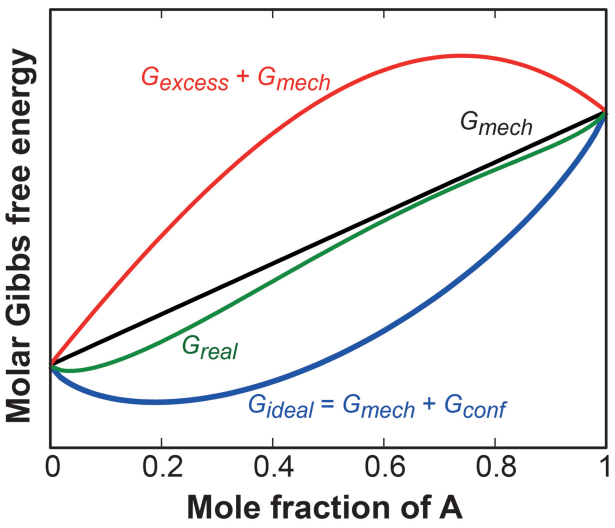

Fig. 3. Molar Gibbs free energy of mixing in a non-ideal solution, giving a graphical illustration of equations (3), (4) and (5).

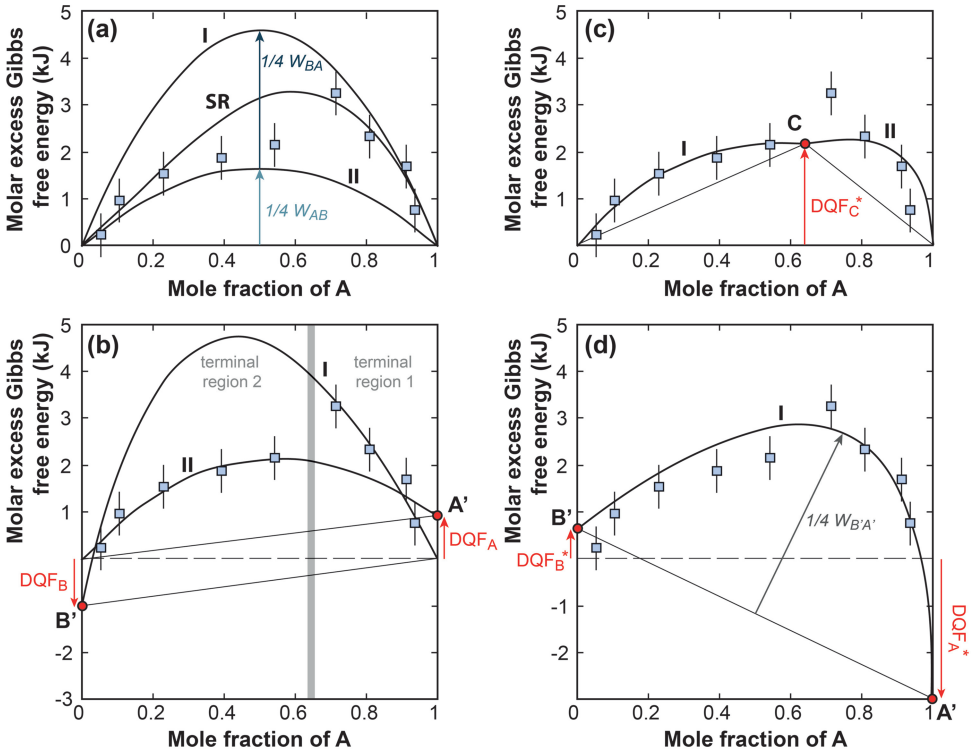

Fig. 4. Illustration of the numerical techniques commonly applied to fit the molar excess Gibbs energy of mixing ΔG_m^{XS} for an asymmetric solid solution inspired by the pyrope–grossular binary join (e.g. Ganguly, 2010). The squares represent hypothetical calorimetric data with their absolute uncertainties. (a) Regular and sub-regular models; curves I and II are regular models described by quadratic functions. The value of the input parameter, referred to as the Margules parameter W_{XY}, is four times higher than the amplitude of the standard parabola. The curve SR shows a sub-regular model defined as the weighted average of the two regular models. In this case, two Margules parameters are required to describe this binary solid solution (here $\frac{1}{4}W_{BA}$ and $\frac{1}{4}W_{AB}$). (b) Darken's quadratic formulation (*sensu stricto*) in which DQF_A is the excess enthalpy of mixing added to the expression of G of end-member A, resulting in a hypothetical end-member A'. Regular model I (between A and B') is valid for the terminal region 1, whereas regular model II (between A' and B) is used for the terminal region 2. Two solid solution models are required, each of them having a single Margules parameter and a *DQF* parameter to define the pseudo end-member. (c) *Pseudo-DQF* type 1 model in which an intermediate pseudo end-member C is defined as C = 0·65A + 0·35B. The Gibbs free energy of formation of C is calculated using a linear combination of the Gibbs free energy of formation of A and B plus an excess enthalpy being the type I *pseudo-DQF* parameter DQF_C*. Consequently, this model is described by the value of DQF_C*, and a single Margules parameter for each of the two regular models (W_{AC}). (d) *Pseudo-DQF* type 2 model in which the Gibbs free energy of formation of both A and B end-members is changed by introducing two type II *pseudo-DQF* parameters DQF_A* and DQF_B*. It should be noted that this type of model never produces reasonable Gibbs free energy values when approaching the end-member compositions ($X_A = 1$ and $X_B = 1$). Two *pseudo-DQF* parameters and a single Margules parameter $W_{B'A'}$ are required to describe this model. The *pseudo-DQF* type 2 could also be used with a single hypothetical end-member.

Internal consistency and the role of DQF *and pseudo-*DQF *parameters (*G *modifications)*

One approach to modeling the non-ideal behavior of solid solutions is Darkens' quadratic formalism (Darken, 1967), calibrated with *DQF* parameters. In this case, three compositional ranges are defined to approximate G_{excess} of a binary solid solution, two terminal regions and a central transitional region (Fig. 4b). The functions of G_{excess} in the two terminal regions are treated separately and approximated using two regular solution models, as shown in Fig. 4b. In the central region G_{excess} can be expressed as the weighted average of those of the terminal regions, similar to the asymmetric sub-regular solution model. Darken (1967) and Powell (1987) showed that the two terminal regions are wide, and the central region is very narrow, thus it can be neglected. For complex activity–composition relationships, the Darken quadratic formalism has more realistic objectives; it provides a better description than the sub-regular models. For instance, Powell (1987) showed that G_{excess} for olivine can be described by two regular solution models: one for $X_{Mg} > 0{\cdot}85$, involving thermodynamic data for real forsterite but fictive fayalite, and one for $X_{Mg} < 0{\cdot}85$, involving thermodynamic data for real fayalite but fictive forsterite. One of the most successful applications of *DQF* is the solid solution model for plagioclase by Holland & Powell (1992). The G_{excess} function of plagioclase is modeled as two regular models: one for the first terminal region [$X_{An} < 0{\cdot}5$ at 700°C and $X_{An} < 0{\cdot}7$ at 1200°C, labeled *C1* by Holland & Powell (1992)] and one for the second terminal region [labeled *I1* by Holland & Powell (1992)]. The user has to select the correct solid solution model depending on the compositional range of plagioclase that would be stable. Two *DQF* models cannot be used together in a Gibbs free energy minimization framework

(e.g. in Fig. 4b where the model *I* would be more stable than *II* for $X_{An} < 0{\cdot}02$ in the terminal region 2).

In the last decade, the usage of *DQF* parameters has significantly increased. However, most of these have little in common with *DQF sensu stricto*, as described above. For the sake of clarity, we refer to these here as *pseudo-DQF*. Two types of *pseudo-DQF* were defined by White *et al.* (2014). Type 1 *pseudo-DQF* (Fig. 4c) is an excess enthalpy (ΔH) added to the expression for the standard state Gibbs energy of a non-dataset end-member; for example, a phase not present in the internally consistent dataset but required in a solution model. This new phase is defined as a linear combination of several dataset end-members with addition of the DQF excess enthalpy. For example, in the study by White *et al.* (2014) the ordered biotite end-member *obi* is a combination of $\frac{2}{3}$phlogopite (phl) and $\frac{1}{3}$annite (ann); the Gibbs free energy becoming $G_{obi} = \frac{2}{3}G_{phl} + \frac{1}{3}G_{ann} + DQF_{obi}$, with $DQF_{obi} = -2$ kJ (White *et al.*, 2014).

Type 2 *pseudo-DQF* (Fig. 4d) results in a change of the standard state Gibbs free energy of a dataset end-member compared with the original internally consistent dataset. For example, annite has been modified by a DQF_{ann} of –3 kJ in the study by White *et al.* (2014) compared with Holland & Powell (2011). This may generate inconsistencies with primary data. It should be noted that the *pseudo-DQF* from White *et al.* (2014) both represent an adjustment ΔG_i of the *G* function of an end-member *i*. The Type 1 *pseudo-DQF* and Type 2 *pseudo-DQF* were redefined by Green *et al.* (2016) as ΔG_i^{make} and ΔG_i^{mod}, respectively. The two terminologies *DQF* and ΔG have been used in the literature since that time. The THERMOCALC group recommends using the ΔG notation (E. C. R. Green, personal communication, 2018).

The type 1 *pseudo-DQF* (ΔG_i^{make}) is a thermodynamically valid procedure for adding a new phase to an already existing internally consistent dataset. The usage of type 2 *pseudo-DQF* (ΔG_i^{mod}) is, however, not compatible with the philosophy of an internally consistent dataset. The thermodynamic properties of single end-members cannot be changed without consideration of all relevant experimental data or the database will no longer be (fully?) internally consistent. Even though the *pseudo-DQF* type 2 (ΔG_i^{mod}) is being applied only to end-members of solid solutions, this approach contradicts the philosophy of Darken: a single regular activity model is used over the entire compositional range, instead of splitting the compositional range into terminal regions (Fig. 4d). The solid solution model will not be 'valid' for compositions close to the end-member A to which the type 2 *pseudo-DQF* (ΔG_i^{mod}) has been applied.

As an example, let us consider the forsterite–fayalite binary join shown in Fig. 5. The two melting points corresponding to the olivine end-members are shifted down by 100°C if arbitrary type 2 *pseudo-DQF* (ΔG_i^{mod}) values of –10 kJ and –9 kJ are applied to the melt components forsterite–liquid and fayalite–liquid (Fig. 5). If type 2 *pseudo-DQF* (ΔG_i^{mod}) values are changed to zero,

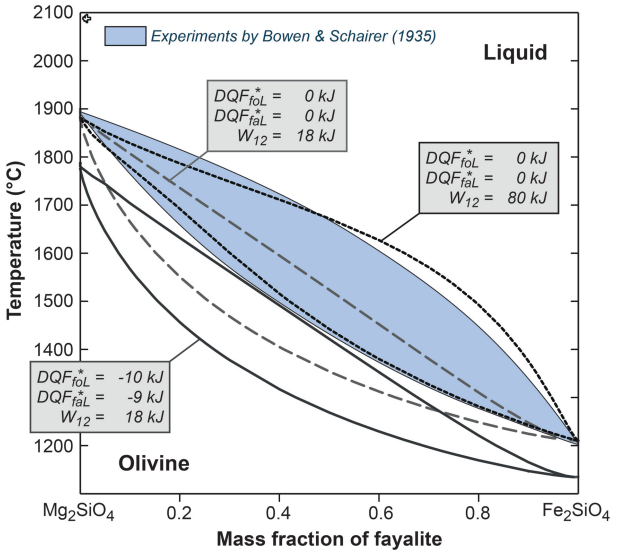

Fig. 5. Possible effects of *DQF*, *pseudo-DQF* and Margules parameters on the reactions in the olivine–melt system compared to the experimental results of Bowen & Schairer (1935). The parameters DQF_{foL}* and DQF_{faL}* were applied to the enthalpy values of the species *forsterite.liq* (Mg_2SiO_4) and *fayalite.liq* (Fe_2SiO_4) of the melt model; W_{12} is the Margules parameter applied for the join between *forsterite.liq* and *fayalite.liq*. This example shows that an acceptable fit to an intermediate region of solution behavior may fail close to an end-member composition.

the original parameters from the internally consistent thermodynamic dataset are applied, and both melting points are consistent with the experimental data of Schairer & Bowen (1935). The melting temperature for the end-member compositions matches the experimental results, but this is not the case for the intermediate compositions using a regular solution model (gray dashed line in Fig. 5). A similar result is obtained if the Margules parameter W_{12} is set to an unreasonably high value of 80 kJ (black dashed line in Fig. 5). Even though other contributions to the free energy, such as miscalculation of the configurational entropy, can be lumped into Margules parameters, such high values can cause problems, such as accidentally generating solvi (e.g. Green *et al.*, 2016).

Further developments of thermodynamic databases

Internal consistency remains a central issue of thermodynamic databases, as these are widely used in modeling programs. Even if an original thermodynamic dataset is guaranteed to be internally consistent—for instance, because MAP was used to derive it—the development of complex solid solution models can, as discussed above, result in the loss of internal consistency in a formal statistical sense. In a more informal sense, the solution models are 'consistent' with the dataset, because they are parameterized so that they predict appropriate phase relations when used with the dataset for samples used for calibration purposes.

For the purpose of comparisons, it would be most useful to have a computer program to evaluate the internal consistency of any given database. The development of such a tool is in progress (to be included in Theriak-Domino; C. de Capitani, personal communication, 2017). It will enable any user to test a given database against all of the experimental data that have been used to refine the dataset and the solid solution models. We are essentially in a monopoly situation at the present time, because only a small group of scientists is currently producing thermodynamic datasets and databases on which many geologists and geophysics strongly depend. An optimistic alternative would be the creation of a community-approved working group to develop a scheme whereby the thermodynamic properties could be accessed by plug-in modules including an open-source computing framework for database fitting, testing and petrological modeling.

Further improvements in the estimation of absolute uncertainties would require (1) using the BAYES method to derive the database (i.e. the dataset and the complex solid solution models together), but also (2) a sustained program of high-precision experiments to generate better constraints. In a recent study, Geiger & Dachs (2018) showed that a better determination of critical thermodynamic properties such as S^{P_0,T_0} values can be obtained via new technological development of low-T relaxation calorimetry. Whereas the number of end-members in thermodynamic databases (Holland & Powell, 1988, 1998, 2011) has been increasing over the past 20 years (see Table 1) the number of new experimental publications has continually decreased in the same time (Spear *et al.*, 2016). In the *HP11* dataset, ~30% of all the standard state properties are only approximated using oxide summation techniques (see below) and do not rely on direct experimental data or even natural constraints. In the dataset *HP11*, the percentage of references to experimental constraints published between 2006 and 2010 is only 4·5%. This figure goes up to 12·5% for the period 2001–2005 and 16% for the period 1996–2000. Among the reasons for the paucity of new experiments are the amount of time and effort required to produce high-quality data and the low funding probability. The scientific impact of such studies may seem to be hidden as soon as the data are 'incorporated' into a thermodynamic dataset, which will be highly cited. A major rethink of the citing policy of users of thermodynamic databases would be necessary to ensure that the data behind high-quality thermodynamic data receive appropriate recognition.

Predictive models and the age of data mining for the calibration of solution models

Simple predictive models are available to estimate standard state properties of phases for which experimental data are not yet available. These models are based on the observation that thermodynamic functions of complex compounds may be estimated by summing—in stoichiometric proportions—the functions of simpler chemical entities such as oxide and hydroxide components. For example, the heat capacity coefficients can be estimated within 2% uncertainty by summation of oxide component *Cp* coefficients tabulated by Berman & Brown (1985); the entropy using the entropy–volume–coordination model of Holland (1989); the enthalpy of formation using the estimation technique of Chermak & Rimstidt (1989). The predictive methods can be updated for a specific mineral group when new experimental data are available (e.g. Vieillard, 2010; Blanc *et al.*, 2015). Such calibrations are especially useful for phases so complex or so impure that reliable calorimetric measurements are not possible, or for phases stable at low-temperature conditions (Vidal & Dubacq, 2009; Sánchez-Roa *et al.*, 2018) where experiments are difficult to perform because of very low reaction rates. Recent developments involve the approximation of $\Delta_f H^0$ using density functional theory (Benisek & Dachs, 2018) or the regularization approach to build a set of mutually consistent activity models and corresponding new end-members not present in the original dataset (using *pseudo-DQF type I*) of Powell *et al.* (2014).

Oxide summation techniques are insufficient, however, to constrain activity models with non-ideal contributions to mixing. In the early days, Margules parameters were derived based on experimental data or determined graphically (De Capitani & Peters, 1982). Today activity models are often refined using mineral compositions in natural rocks (e.g. Dubacq *et al.*, 2010; Lanari *et al.*, 2014*c*; White *et al.*, 2014; Green *et al.*, 2016), which require that the phases of interest have formed at equilibrium and that the calculated *P*–*T* conditions are accurate and precise enough (Spear *et al.*, 2016).

A more robust technique to derive excess functions is to use lattice energy estimation such as the *Js* method (e.g. Dove *et al.*, 2000; Bosenick *et al.*, 2001; Dove, 2001) combined with Monte Carlo simulations to estimate the Gibbs free energy of mixing along binary solid solutions. The idea is (1) to look at all of the energetic variations that occur when forcing the dilution of one end-member by another end-member, (2) to estimate the energetic state and the degree of ordering of the most stable structures, and (3) to infer the Gibbs free energy of mixing from the non-linearity between two end-members. Lattice energy calculations have been employed, for example, to investigate the energetic behavior of binary systems such as barite–celestite (Becker *et al.*, 2000), diopside–jadeite (Vinograd *et al.*, 2007), muscovite–pyrophyllite (Dubacq *et al.*, 2011), pyrite–arsenopyrite (Reich & Becker, 2006) and Ca–Sr fluorapatite (Goryaeva *et al.*, 2013). These data mining techniques are time-consuming, but they open new avenues to constrain the Gibbs free energy of mixing in complex solid solution systems. However, it will be not possible to make a better dataset unless there are better or new constraints (i.e. experiments).

MODELING TECHNIQUES FOR THERMOBAROMETRY

Thermobarometry aims to retrieve the equilibrium conditions (P and T) from mineral compositions and/or assemblages thought to represent a preserved equilibrium state in a rock. The early developments of thermobarometry were thus based on empirically calibrated temperature-dependent and pressure-dependent reactions or element fractionation systematics involving mineral phases that represent thermodynamic equilibrium. For example, the Fe–Mg fractionation among minerals is T-dependent (thermometry), whereas the Al content in minerals can be either P-dependent (barometry; e.g. in mica or amphibole) or T-dependent (thermometry; e.g. in chlorite). This behavior is controlled by the changes of the entropy and volume of the reaction as shown by the Clausius–Clapeyron relation, $\frac{dP}{dT} = \frac{\Delta S}{\Delta V}$. Several empirical calibrations and methods were developed in the 1980s, covering a broad range of minerals, mineral–mineral and mineral–fluid equilibria (see, for example, the reviews by Essene, 1989; Spear, 1993; Reche & Martinez, 1996; Ravna & Paquin, 2003). However, some significant inconsistencies between P–T results emerged from such efforts. These empirical (or semi-empirical) techniques are usually referred to as 'conventional' or 'traditional' thermobarometry (e.g. Powell & Holland, 2008) in the literature. Several programs such as GTB (from Spear & Kohn) and PTQUICK (from Dolivo-Dobrovolsky) include a large set of published geothermometers and geobarometers. Rather than giving a historical perspective on conventional or traditional methods we emphasize here major conceptual advances in the types of modeling used (inverse, forward; see Fig. 6).

As discussed above, the refinement of internally consistent thermodynamic datasets and databases (Berman, 1988; Holland & Powell, 1988) together with the progress made in developing a new generation of modeling software (Berman *et al.*, 1987; de Capitani & Brown, 1987; Powell & Holland, 1988; Spear, 1988*a*; Connolly, 1990; Berman, 1991; Connolly & Petrini, 2002; de Capitani & Petrakakis, 2010) created the dynamic needed to stimulate further improvements in thermobarometry with the main goal of obtaining more reliable results. It should be noted that as experimental and natural data are used to derive the thermodynamic databases, the models described in this review remain, in essence, semi-empirical.

Two strategies relying on internally consistent thermodynamic data have been pursued to retrieve the equilibrium conditions recorded by crustal rocks, thus

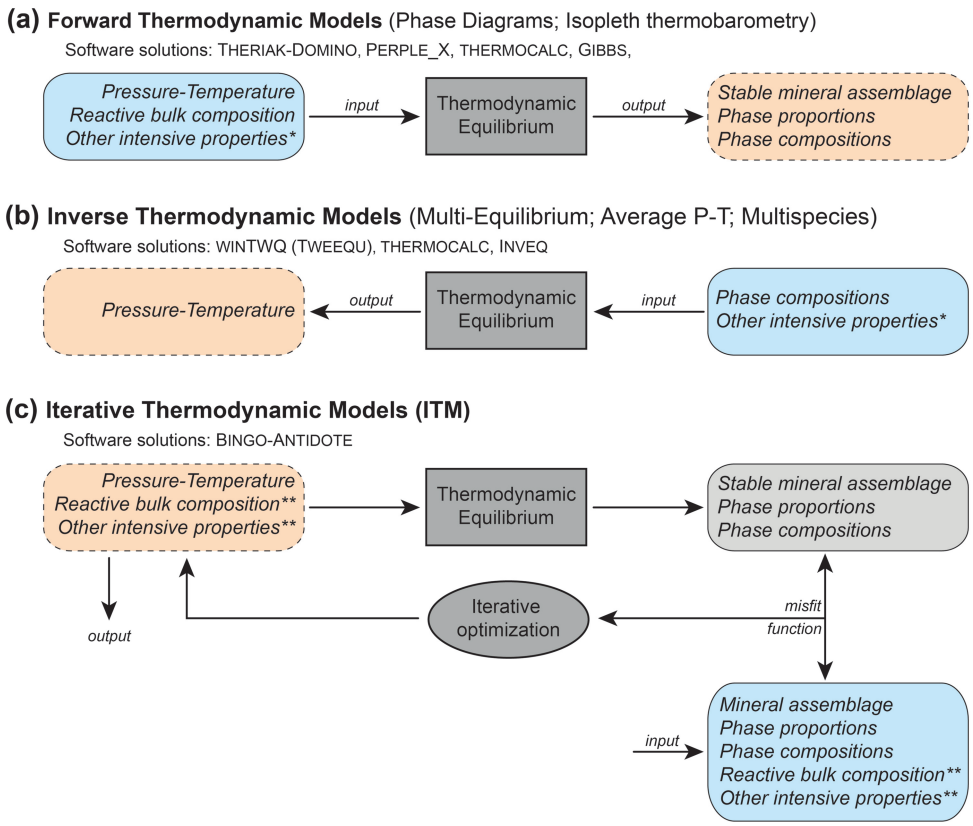

Fig. 6. Forward, inverse and iterative modeling techniques in thermobarometry. The references to the software descriptions are given in the text. *Properties that can be refined using complex inverse or automated forward methods [e.g. CHLMICAEQUI from Lanari (2012) (originally known as PTLINES); GRTMOD from Lanari *et al.* (2017)]. **Properties optimized by BINGO-ANTIDOTE.

relying on the concept of chemical equilibrium (Fig. 6a and b). Inverse thermodynamic models (e.g. multi-equilibrium thermobarometry) aim to retrieve equilibrium conditions from local phase compositions analyzed in a natural sample, specifically from an assemblage of minerals, which are postulated to have retained their equilibrium compositions. By contrast, forward thermodynamic models (e.g. phase diagrams) apply the principle of minimum Gibbs free energy to predict the stable mineral assemblage at fixed equilibrium conditions (P, T, a_{H_2O}, a_{CO_2}, f_{O_2}, etc.); these models yield the modes and compositions of phases for any reactive bulk composition and can be directly compared with natural observations. The advantages and limits of both strategies are separately highlighted in the following sections. We then introduce a hybrid modeling technique that relies on iterative thermodynamic modeling (ITM). This approach combines the mains strengths of forward and inverse techniques.

Inverse thermodynamic modeling and its application in petrology

The inverse modeling techniques described in the following all derive from the idea that more than one independent thermometer and barometer can be combined to minimize the possible bias in each calibration. In a purely empirical approach, each thermometer or barometer is independently calibrated, either directly by experimental results or indirectly from empirical data. The main problem is the absence of consistency among independent calibrations. One way to increase the consistency, as we have shown in the previous section, is to use an internally consistent thermodynamic database. Their development in the late 1990s promoted the application of mutually consistent inverse techniques (Powell & Holland, 1988, 1994; Berman, 1991; Gordon, 1992). Rather than having to make a selective and subjective choice of individually calibrated reactions, it became possible to use all the reactions (or an independent set of reactions) that can be written between the phase components (end-members of each mineral phase or species of each fluid phase) in a particular assemblage. These mutually consistent inverse calculations maximize the benefits of having an internally consistent thermodynamic database.

Theoretical basis and computer programs for multi-equilibrium, least-squares and multispecies thermobarometry

For a balanced reaction involving n phase components (end-members) in a particular assemblage, the equilibrium condition can be written as

$$\Delta_r G^0 = -RT\ln(K) \tag{7}$$

where $\Delta_r G^0$ is the standard Gibbs free energy of reaction of the pure phase components at P and T, and K is the equilibrium constant of this reaction. The standard Gibbs free energy of reaction is computed from

$$\Delta_r G^0 = \sum_i^n v_i \Delta_a G_i^{P,T} \tag{8}$$

with v_i the stoichiometric reaction for phase component i coefficient and $\Delta_a G_i^{P,T}$ the apparent Gibbs free energy of formation of any phase component at P and T [see equation (1)]. The apparent Gibbs free energy of a phase component can be estimated using the standard state properties of any internally consistent thermodynamic dataset that contains this phase component [see equation (1)]. The equilibrium constant K is given by

$$K = \prod_i^n a_i \tag{9}$$

with a_i the activity of phase component i.

In a system with c system components, the maximum number of reactions N_r^{max} that can be written between n phase components is

$$N_r^{max} = \frac{n!}{(c+1)![n-(c+1)]!} \tag{10}$$

and the number of independent reactions $N_r^{ind.}$ is (van Zeggren & Storey, 1970)

$$N_r^{ind.} = n - c. \tag{11}$$

It is important to notice that once a set of $N_r^{ind.}$ independent reactions has been chosen, all the other reactions—which are dependent by definition—can be generated from linear combinations of the independent reactions (Powell & Holland, 1988).

Three major programs have been developed to perform mutually consistent inverse calculations: TWEEQU (by R. Berman), *Average P-T*, which is part of the THERMOCALC package (by R. Powell), and INVEQ (by T. M. Gordon); two of them have turned out to be very popular in the community over the years (TWEEQ has recorded more than 1000 citations since 1991 in Google Scholar and *Average P-T* ~450 citations since 1994).

The first program, TWEEQU (Thermobarometry With Estimation of EQUilibration state), allows multi-equilibrium thermobarometry by calculating the possible equilibria implied by selected phase components from an internally consistent thermodynamic database of end-member properties and mixing models for some common minerals (Berman, 1991). Sixteen years later, TWEEQU evolved to WINTWQ (Berman, 2007). This version recommends calculating average P–T results from intersections of an independent set of equilibria that are considered as more robust; for example, because they are calibrated directly by reliable experimental constraints (Berman, 1991). The selected equilibria may also take into account different inferred closure temperatures; for example, that the Al content of orthopyroxene in assemblages with garnet often records higher temperatures than the Fe–Mg exchange equilibrium

between these two phases (Bégin & Pattison, 1994; Pattison *et al.*, 2003). At the present time, the WINTWQ software utilizes the internally consistent database of Berman (1988) together with compatible solution models (Berman, 1990; Mäder *et al.*, 1994) as well as a smaller database of phases that better account for relevant phase equilibrium experiments by virtue of the simultaneous derivation of end-member and mixing properties (Berman & Aranovich, 1996). The latest version of this software is available for download at http://twq.petrochronology.org/.

The second program, *Average P-T*, allows least-squares thermobarometry and is distributed in the software package THERMOCALC (Powell & Holland, 1988; Powell *et al.*, 1998). The original version of this program, known as *Average P*, was first published by Powell & Holland (1988), then refined and further developed in 1990 to become *Average P-T* (Powell & Holland, 1994). *Average P-T* (sometimes referred to as *avPT* or $\overline{PT}$) can only be used with the successive databases included in THERMOCALC (e.g. *HP98*: *ds3.2*, *ds5.5*; *HP11*: *ds6.2*). The major feature of *Average P-T* is that it uses a weighted least-squares scheme applied to a set of independent reactions to adjust the linearized data and retrieve optimal *P*–*T* conditions. Estimated uncertainties on formation enthalpies and solid solution models are used, as well as their correlations. This was a critical aspect for the authors as they demonstrated that any set of independent reactions represents all of the equilibria, provided that the uncertainties and uncertainties correlations of the ln(*K*) values are part of the optimization (Powell & Holland, 1988, 1994). In this case, the correlations derive mainly from uncertainties on the activities of the end-members, which cannot be evaluated statistically in the absence of a comprehensive set of direct experimental data (Kohn & Spear, 1991). A formulation of default uncertainty for activities has been proposed by Powell & Holland (1988)—and is incorporated in THERMOCALC (Powell & Holland, 2008)—but it remains difficult to appreciate how this approximation actually matches the real uncertainties, especially near the end-member compositions if *pseudo-DQF* corrections are applied (see above). The latest version of this software is available for download at http://www.metamorph.geo.uni-mainz.de/thermocalc/.

The third program, INVEQ, allows multispecies thermobarometry and was published by Gordon (1992). An interactive scientific software WEBINVEQ was released 6 years later (Gordon, 1998), but unfortunately it is no longer maintained. This method is similar in essence to the least-squares thermobarometry of *Average P-T*, but rather than minimizing the sum of squares of errors in equilibrium equations, the problem is formulated as the minimization of the sum of squares of errors in the free energy approximations for individual species (e.g. Fig. 4 of Spear *et al.*, 2016). This algorithm does not separate the constant and *T*-dependent contributions to the calculation. Examples of application included sensitivity tests in which the effects of perturbing each partial molar free energy equation by a constant amount can be observed and quantified (Gordon *et al.*, 1994).

This brief overview shows that the development of computer programs has been critical in popularizing the inverse technique. However, a general program for inverse modeling working with several databases (from different teams) regrettably is not available so far. The database dependence of any program represents a limitation that seriously reduces its capabilities. Although inverse thermodynamic modeling has become very popular in the last 20 years and did improve the reliability and ease of thermobarometric calculations to some extent, the challenges regarding the uncertainties may preclude the use of sophisticated statistical techniques such as least squares. Some authors rely on a rough approximation of errors and their correlations (the absolute uncertainty is generally larger, in the range $\pm 50^{\circ}$C and $\pm 0{\cdot}25$ GPa; Essene, 1989; Berman, 1991), whereas others put more emphasis on the scientific capabilities of the investigator to interpret the results. An essential point to emphasize is that true overall uncertainties must also incorporate 'geologic uncertainty' (Kohn & Spear, 1991), most importantly how well characterized and understood are a rock's mineral compositions, and their variations, which are utilized in the calculations. Which method should be favored in a specific case is outside the scope of this review, but we can conclude that these techniques have all paved the way to complex inverse techniques that were introduced at the dawn of the 21st century and are discussed below.

Refinement of compositional variables in complex inverse models

It has long been recognized that mutually consistent inverse calculations can be used for the optimization of compositional (e.g. $X(Fe^{3+})_{mineral}$) or activity (e.g. a_{H_2O}, a_{CO_2}) variables that cannot be analyzed (Powell & Holland, 1994). Well-equilibrated rocks are required for thermobarometry based on equilibrium thermodynamics, and high-variance assemblages (parageneses) are also promising targets for multi-equilibrium inverse techniques. This is particularly evident in low-grade metamorphic rocks lacking index minerals, where thermobarometry is otherwise challenging (e.g. Parra *et al.*, 2002*b*; Lanari *et al.*, 2012; Pourteau *et al.*, 2013; Cantarero *et al.*, 2014). For instance, chlorite and K-white mica are ubiquitous minerals present together in rocks of various bulk-rock compositions from greenschist- to amphibolite-facies metamorphic conditions. Modeling assemblages with chlorite and K-white mica is complicated as complex chemical substitutions are involved (Holland *et al.*, 1998; Vidal *et al.*, 2001; Parra *et al.*, 2002*a*; Dubacq *et al.*, 2010; Trincal & Lanari, 2016), and direct experimental constraints of the equilibria between the phases involved are rare (Parra *et al.*, 2005). Complex inverse models are defined here as inverse models that include the optimization of some activity or compositional variables. They have been

developed and have proven most useful for thermobarometric applications in such situations. The equilibrium conditions of chlorite + quartz + H_2O in the system SiO_2–Al_2O_3–FeO–Fe_2O_3–MgO–H_2O are represented by a *P–T* line along which the $X(Fe^{3+})_{chl}$ varies as shown in Fig. 7a (Lanari, 2012). For a given chlorite composition this *P–T* line indicates a temperature; this model was used mostly as a chlorite thermometer permitting the estimation of $X(Fe^{3+})_{chl}$ at a fixed pressure (Vidal *et al.*, 2006; Grosch *et al.*, 2012; Cantarero *et al.*, 2014, 2018). It was shown that the predictions of $X(Fe^{3+})_{chl}$ are in line with speciation analyses available for natural chlorite (Lanari *et al.*, 2014*c*). A similar strategy has been employed by Dubacq *et al.* (2010) for K-white mica thermobarometry that refined a solid-solution model with hydrated pyrophyllite-like thermodynamic end-members to account for the variable hydration observed in natural smectite, interlayered illite–smectite, illite, and phengite. As shown in Fig. 7b, the equilibrium conditions of K-white-mica + quartz + H_2O in the system SiO_2–Al_2O_3–FeO–Fe_2O_3–MgO–CaO–Na_2O–K_2O–H_2O is a *P–T* line along which the interlayer H_2O content $[X(H_2O)_{KWM}]$ varies (Dubacq *et al.*, 2010). This model can be used as a thermometer at fixed pressures or as a barometer at fixed temperatures (e.g. Scheffer *et al.*, 2016; Lanari *et al.*, 2018). For thermobarometry, it is possible to combine the *chlorite + quartz + H_2O* thermometer and *K-white mica + quartz + H_2O* barometer to derive the *P–T* conditions as well as $X(Fe^{3+})_{chl}$ and $X(H_2O)_{KWM}$ (Ganne *et al.*, 2012; Lanari *et al.*, 2012, 2014*a*; Giuntoli *et al.*, 2018*a*). The solid-solution models described above can also be used to plot all the simultaneous equilibria of the assemblage *chlorite + K-white mica + quartz + H_2O* (Fig. 7c and d).

A chlorite–phengite pair from Oman investigated by Agard *et al.* (2010) is used here to illustrate how complex inverse models can be applied to chlorite and K-white mica thermobarometry. *P–T* conditions were evaluated for a metasediment from a series of tectonic units bounded by high-strain ductile shear zones to

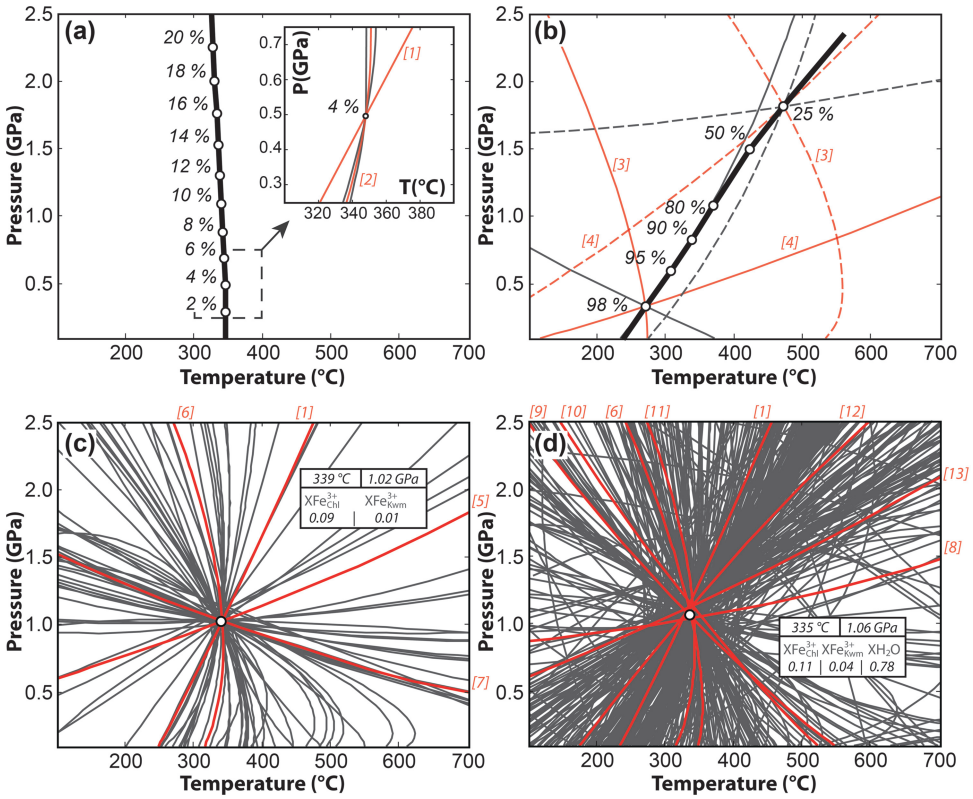

Fig. 7. Multi-equilibrium investigations of a high-variance assemblage from Oman involving chlorite, K-white mica, quartz and H_2O; the mineral compositions are taken from Agard *et al.* (2010). The reactions used for optimization are shown in red and are provided in Supplementary Data S4. The activity of H_2O was assumed to be unity in all the computations. (a) *Chlorite + Quartz + H_2O* thermometry: the thick line is the *Chlorite + Quartz + H_2O* equilibrium curve along which $X(Fe^{3+})_{chl}$ varies; the dots show *P–T* conditions for fixed values of $X(Fe^{3+})_{chl}$; inset: *Chlorite + Quartz + H_2O* equilibria for an $X(Fe^{3+})_{chl}$ value of 4%. (b) *K-white mica + Quartz + H_2O* thermobarometry: *K-white mica + Quartz + H_2O* equilibrium curve (thick) along which $X(H_2O)_{KWM}$ varies; *K-white mica + Quartz + H_2O* equilibria for $X(H_2O)_{KWM}$ values of 25% (dashed) and 98% (continuous). (c) *Chlorite + K-white mica + Quartz + H_2O* equilibria with optimization of $X(Fe^{3+})_{chl}$ and $X(Fe^{3+})_{KWM}$; optimal *P–T* conditions: 339°C and 1·02 GPa for $X(Fe^{3+})_{chl} = 0{\cdot}09$ and $X(Fe^{3+})_{KWM} = 0{\cdot}01$. (d) *Chlorite + K-white mica + Quartz + H_2O* equilibria with optimization of $X(Fe^{3+})_{chl}$ and $X(Fe^{3+})_{KWM}$ and $X(H_2O)_{KWM}$; optimal *P–T* conditions: 335°C and 1·06 GPa for $X(Fe^{3+})_{chl} = 0{\cdot}11$, $X(Fe^{3+})_{KWM} = 0{\cdot}04$ and $X(H_2O)_{KWM} = 0{\cdot}78$. The optimizations were performed with ChlMicaEqui 1.5 (Lanari, 2012). The dependent equilibria are shown in gray in (c) and (d); it should be noted that in the absence of reliable uncertainties on the end-member properties and solid solution models the different sets of equilibria do not result in the same *P–T* estimates.

demonstrate that the metasediments experienced similar *P* conditions to the mafic eclogites of adjacent units (Agard *et al.*, 2010). The equilibria between *chlorite* + *K-white mica* + *quartz* + H_2O shown in Fig. 7 were calculated using the program CHLMICAEQUI [an improved version of the program PTLines described by Lanari (2012)]; the models employed were from (1) Vidal *et al.* (2006) for chlorite and Parra *et al.* (2002*a*) for K-white mica (64 reactions, four of them independent; Fig. 7c), as well as (2) Vidal *et al.* (2006) for chlorite and Dubacq *et al.* (2010) for K-white mica (358 reactions, eight of them independent; Fig. 7d). Optimal *P*–*T* conditions and compositional values for $X(Fe^{3+})_{chl}$, $X(Fe^{3+})_{KWM}$ and $X(H_2O)_{KWM}$ were obtained by minimizing

$$\text{minimize} \sum_{N=1}^{N_r^{ind.}} (\Delta_r G_i)^2 \quad (12)$$

the Gibbs free energy of reaction *i* is defined as

$$\Delta_r G = \Delta_r G^0 + RT\ln(K). \quad (13)$$

In this example, similar *P*–*T* conditions (335°C, 1·0 GPa) were obtained with the K-white mica calibrations of Parra *et al.* (2002*a*) and Dubacq *et al.* (2010) (Fig. 6), suggesting that the models are mutually consistent. Similar *P*–*T* results for the two calibrations were reported in several studies (Pourteau *et al.*, 2013; Airaghi *et al.*, 2017*a*), but other researchers reported different *P*–*T* conditions (e.g. Dubacq *et al.*, 2010) caused by the successive refinements of each activity solid solution model generating inconsistencies between the models.

Application examples—reconstruction of P–T paths using inverse models

As previously shown for the example from Oman, inverse calculations can be used to retrieve the equilibrium conditions of a single *P*–*T* stage during which the mineral formed. As compositional zoning is common in metamorphic rocks (Tracy, 1982; Kohn, 2014*a*), this technique may be applied to several local equilibrium domains to retrieve *P*–*T* trajectories. If the same mineral assemblage (e.g. chlorite, K-white mica and quartz) is used to model different domains of a rock or different rock samples, then relative thermometry (ΔP or ΔT) is much more precise than the absolute values. The systematic uncertainties associated with the modeled thermodynamic properties are essentially the same for each domain or rock sample, so can be eliminated from the uncertainty in the relative pressure or temperature (Worley & Powell, 2000). Two additional examples are given in the following to illustrate the power of mutually consistent inverse thermobarometry.

The first example is taken from García-Casco *et al.* (2008), who investigated amphibolite and trondhjemitic segregations from the remnants of subducted oceanic crust in the Sierra del Convento mélange (Cuba). The *P*–*T* conditions shown in Fig. 8a were obtained by García-Casco *et al.* (2008) from low-variance assemblages using *Average P-T* in THERMOCALC 3.25 with the thermodynamic database *tc55*. In the amphibolites, pre-peak conditions were based on the composition of inclusions in garnet and the assemblage garnet + amphibole + epidote + quartz, peak conditions relied on garnet and the matrix assemblage amphibole + epidote ± quartz ± clinopyroxene, and retrograde conditions relied on the assemblage glaucophane + chlorite + epidote + garnet (rims) + albite ± quartz. In trondhjemitic segregations, the solidus conditions were based on the assemblage amphibole + epidote + paragonite + quartz + plagioclase, and retrograde conditions on the assemblage amphibole + chlorite + epidote +

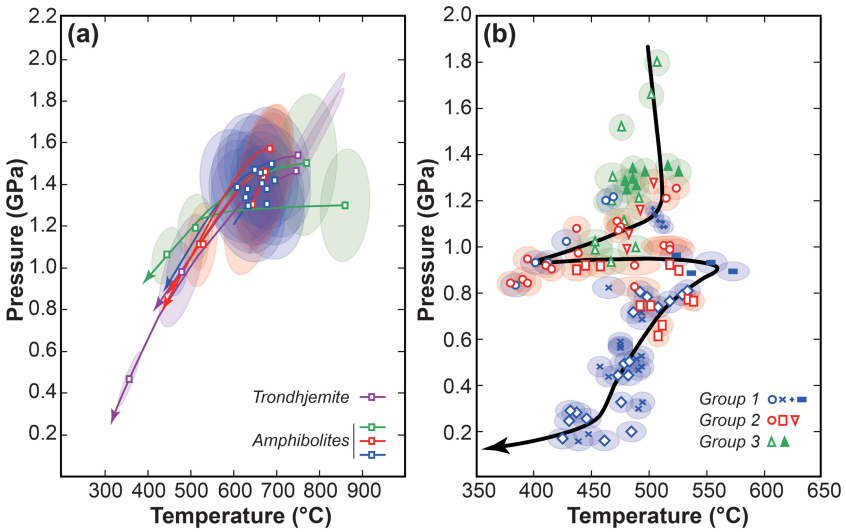

Fig. 8. *P*–*T* paths retrieved using mutually consistent inverse calculations for (a) Sierra del Convento mélange (modified from García-Casco *et al.*, 2008) and (b) Cycladic Blueschist unit on Tinos (modified from Parra *et al.*, 2002*b*). Ellipsoids show the *P*–*T* uncertainties (1σ). Uncertainties only in the thermodynamic model (a) or in the microprobe analyses (b) were used. The symbols used in (b) correspond to different samples from groups 1, 2 and 3; they are the same as used by Parra *et al.* (2002*b*).

paragonite + quartz + albite ± lawsonite. The *P–T* results show a retrograde *P–T* trajectory (Fig. 8a). Even though different assemblages were used for modeling, the relative differences between the *P–T* trajectories are much smaller than the absolute uncertainties (ellipsoids, 1σ) obtained by *Average P-T*. This observation supports the conclusion of García-Casco et al. that these blocks underwent similar retrograde *P–T* trajectories and that 'operator errors' (i.e. the mistakes the petrologist makes in interpreting reaction history or correlating mineral compositions; see Kohn, 1993) have not obscured the true *P–T* path trend. Such high uncertainty ellipses may also reflect the selection of equilibria that are too insensitive to provide any refinement of the *P–T* constraints (Pattison & Vogl, 2005).

The second example is taken from Parra *et al.* (2002*b*), who investigated metapelites from the Cycladic Blueschists unit on Tinos (Greece). The *P–T* conditions shown in Fig. 8b were obtained by Parra *et al.* (2002*b*) from low- and high-variance assemblages using TWEEQU with the thermodynamic database of Berman (1988) and modified solid solution models (Berman, 1990; Evans, 1990; McMullin *et al.*, 1991; Vidal *et al.*, 2001; Parra *et al.*, 2002*a*). The equilibrium conditions were based on the assemblage chlorite + phengite + quartz + H_2O ± glaucophane ± albite ± paragonite ± garnet ± biotite. The results show a fair agreement between the *P–T* results obtained for different minerals involved in key micro-structural sites at thin-section scale; this supports the notion of local equilibrium (Fig. 8b). Parra *et al.* (2002*b*) applied a Monte Carlo method to produce ellipsoids depicting the relative uncertainty of any *P–T* estimate based on the precision of the microprobe analyses (see also Vidal & Parra, 2000). In this case, the uncertainties for the standard state properties are not considered. A two-stage exhumation process can be distinguished from this dataset (Fig. 8).

Challenges—re-equilibration versus preservation of equilibrium archives

P–T estimates obtained using inverse models rely on the assumption of a frozen-in state of equilibrium. This assumption cannot be valid for high-temperature rocks in which different elements have different diffusivities and thus the equilibrium compositions are no longer preserved after cooling (e.g. Bégin & Pattison, 1994; Pattison *et al.*, 2003). It is important to reaffirm here that we cannot prove that local equilibrium was attained and the mineral compositions preserved using a purely inverse modeling approach. The mineral assemblage of a single *P–T* metamorphic stage that is used to calculate the position of the mineral equilibria may or may not (for kinetic reasons) have been at the minimum Gibbs free energy for the reactive bulk composition. The convergence of reactions, ideally intersecting at one *P–T–X* point, is an insufficient argument if the objective is to prove chemical equilibrium; it only shows that mineral composition is consistent with chemical equilibrium having been achieved at these *P–T* conditions. If the intersections scatter widely, the minerals cannot be modeled as an equilibrium assemblage. In this case, the problem can be either an incorrect interpretation of the rock record or uncertainties in the thermodynamic models. Although the equilibrium among mineral phases cannot be proven, microtextural relationships (e.g. Vernon, 1977) and compositional criteria based on quantitative compositional maps (e.g. Vidal *et al.*, 2006; Lanari *et al.*, 2012, 2013; Scheffer *et al.*, 2016) may help to decide which minerals, and more importantly which mineral compositions, may represent a frozen-in local state of equilibrium.

In their study, Scheffer *et al.* (2016) used such quantitative compositional maps that reveal distinct *P–T* conditions for sheet silicates as a function of their structural, microstructural and microtextural positions. In Fig. 9, each generation of phengite (blue) and chlorite (green) is compositionally distinct, but found in differing proportions in both S_1 and S_2 fabrics. This highlights the process responsible for the later generation—chemical replacement rather than growth during D_2 deformation. Greenschist- and amphibolite-facies metasediments are examples for which is difficult to assess, without the help of compositional maps, which composition should be used for modeling [other examples have been given by Lanari *et al.* (2012) and Airaghi *et al.* (2017*b*)].

Finding criteria for the stable coexistence of minerals has been a long-standing problem of metamorphic petrology [see Vernon (1977) for a review]. At the grain scale, texture is useful to judge the degree of (dis)equilibrium; inclusion relations are a good example. Figure 9b displays a map showing the fractions of almandine in garnet and jadeite in omphacite; the data are for a mafic eclogite boudin from the Atbashi Range in the Kyrgyz South Tien Shan (Loury *et al.*, 2015, 2018). The qualitative evolution of *P–T* conditions during garnet growth can be retrieved from inclusion–porphyroblast relationships (e.g. Vernon, 1978). Garnet cores contain inclusions of glaucophane, phengite, and low-jadeite omphacite, suggesting blueschist conditions, whereas a first garnet overgrowth (mantle 1) contains inclusions of omphacite with a high jadeite fraction and quartz, which are characteristics of eclogite-facies conditions. Garnet mantle 2 and rims show a progressive decrease in jadeite contents, caused either by decompression or by fractionation of the reactive bulk-rock composition. However, the composition of omphacite in chemical equilibrium with garnet at any stage of growth is difficult to assess, as every inclusion shows compositional zoning (Fig. 9b). This example demonstrates how complex relationships can be, even in relating compositions of trapped inclusions to their host when both are heterogeneous.

The two examples discussed here show that textural relationships can be complex, and they may be misleading in many cases if the purpose is to apply an

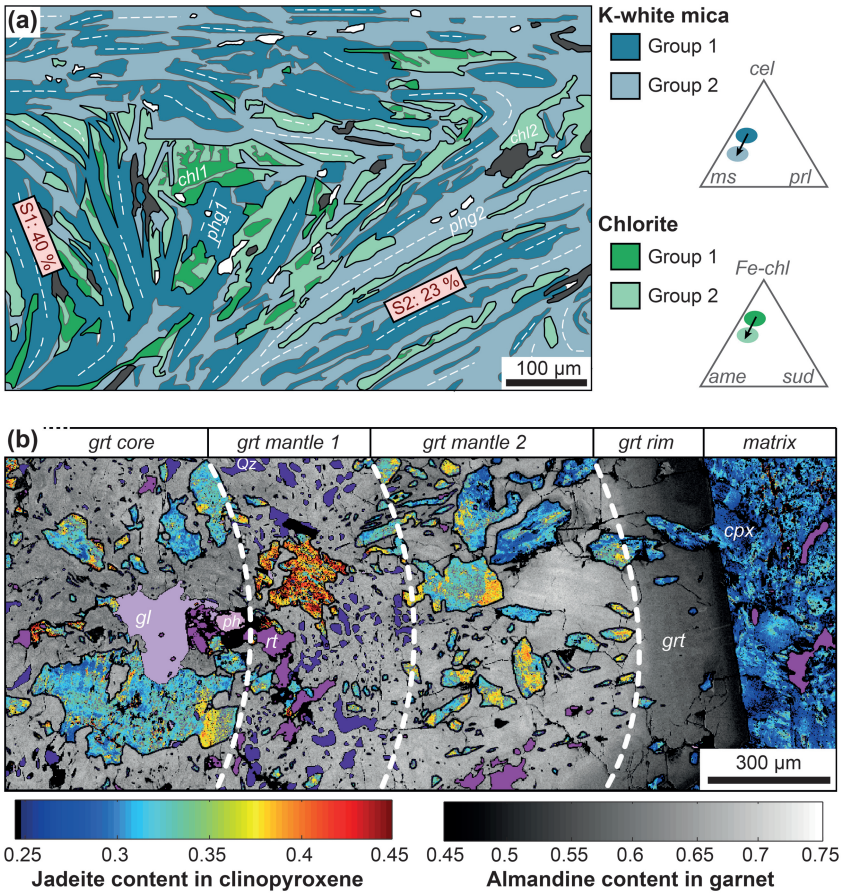

Fig. 9. Example of partial re-equilibration in metamorphic rocks leading to ambiguous microtextural relationships. (a) Spatial distribution of chlorite and phengite compositional groups in a metapelite sample from the western Attic–Cycladic metamorphic complex (modified from Scheffer *et al.*, 2016). Percentages shown in S_1 and S_2 domains are the degree of preservation of group 1 compositions in the related microstructure. (b) Spatial distribution and compositional zoning of omphacite inclusions in garnet porphyroblast in mafic eclogites from the Atbashi Massif (modified from Loury *et al.*, 2015).

equilibrium model. Textural relationships still remain, however, essential for understanding what the actual rock reactions might have been (e.g. Waters & Lovegrove, 2002; Pattison & Spear, 2018). In general, it is challenging to identify a frozen-in state of equilibrium suitable for inverse thermodynamic modeling. In the following sections, we discuss alternative modeling techniques that may be used to test the hypothesis of chemical equilibrium.

Forward thermodynamic modeling—the success of phase diagrams

Forward thermodynamic models (Fig. 6) take their power from the internally consistent databases, and this makes them attractive and apparently simple, as they can be used to generate a large variety of equilibrium phase diagrams among which is the popular isochemical phase diagram (or pseudosection). Duhem's theorem assures that 'the equilibrium state of an isothermal–isobaric closed system, for which the bulk composition is given, is completely determined by two independent variables'. The selection of P and T as independent variables allows isochemical P–T phase diagrams to be computed. These diagrams depict the evolution with P and T of the stable mineral assemblage for a given bulk system composition (X_{sys}). The stable assemblage at any P–T–X_{sys} conditions is the mineral assemblage (i.e. the modal abundance and chemical composition of all phases) for which the total Gibbs free energy of the system G_{sys} is minimal. Field boundaries in isochemical phase diagrams are conditions for which the mode of one phase goes to zero. The mineral equilibria described in the inverse modeling section lie in theory within a stability field, provided that the minerals used for modeling are stable for the bulk composition of the system at these P–T conditions.

A numerical method must be employed for the computation of multi-component multiphase equilibria. The first attempts [see Wood (1987) for a review] to minimize G_{sys} with ideal solid solutions included the 'rocking tangent-plane' method of Brown & Skinner (1974), generalized for non-ideal solutions by de Capitani & Brown (1987), but also the pseudo-compound technique of Connolly & Kerrick (1987). Today, four main software solutions for forward thermodynamic analysis are

widely used in the metamorphic petrology community (see Fig. 3 of Engi *et al.*, 2017): Theriak-Domino (de Capitani & Brown, 1987; de Capitani & Petrakakis, 2010); Perple_X (Connolly & Kerrick, 1987; Connolly, 1990, 2005); thermocalc (Powell & Holland, 1988, 2008; Powell *et al.*, 1998) and Gibbs (Spear, 1988*a*). The availability of these software packages resulted in an impressive proliferation of isochemical phase diagrams for many bulk-rock compositions. Each program has its own advantages and limits that are briefly summarized in the following.

Determining the stable mineral assemblage—a matter of program?

The modeling programs used to generate phase diagrams are classified into two fundamentally different groups—phase equilibrium calculators versus Gibbs free energy minimizers—and they also employ different numerical methods.

thermocalc and Gibbs are phase equilibrium calculators; they both apply non-linear equation solvers to determine the mineral assemblage at given *P*–*T* conditions. The *P*–*T* position of a field boundary or isoline (contour of phase proportions and/or mineral compositions) relies on an algorithm combining Newton–Raphson iterations and quadratic interpolations to solve equation (13) (for $\Delta_r G = 0$), constrained by a series of mass-balance equations (Powell & Holland, 1988). In Gibbs, isolines are calculated using a differential thermodynamics method (Spear, 1988*a*). Univariant equilibria are drawn using Schreinemakers analysis combined with intuition and experience—a time-consuming iterative approach for each diagram. Each iteration consists of (1) defining the starting assemblage and the bulk composition of the system, (2) setting the mode of one phase of the assemblage to zero, and (3) obtaining the compositions of all the coexisting phases for any given *P* (or *T*). Although thermocalc calculates the composition of coexisting phases, it does not test the stability of the equilibrated assemblage for a specific bulk composition at the *P*–*T* of interest; this can, however, be done at chosen conditions by supplying an appropriately comprehensive set of phases. The considered mineral assemblage may be metastable (i.e. not at the minimum G_{sys}), hence the user has to manually perform Schreinemakers analysis. Applying non-linear equation solvers always requires an *a priori* knowledge of phase stabilities and thus strongly relies on the expertise of the user. This problem is illustrated in Fig. 10a. If one assumes that this binary system is only represented by phase P_1 and P_2, it will not be recognized that this assemblage is metastable with respect to the assemblage $\alpha + \beta$, which has a lower G_{sys}. This is the reason why many workers use a free energy minimizer for a quick reconnaissance and then follow up in detail with thermocalc. The program Gibbs is based on a similar strategy taking advantage of the Gibbs–Duhem relation (Spear, 1988*a*) and also offering alternative tools for automated Schreinemarkers analysis, if a petrogenic grid is available for the same chemical system and the same thermodynamic database. In the late 1990s an algorithm calculating every possible assemblage and finding the one with the lowest Gibbs free energy was added to the program. This elegant solution is unfortunately not a viable strategy for petrological programs unless the number of phases under consideration is small. The more recent developments of Gibbs (unpublished, F. Spear, personal communication, 2018) include a hybrid Gibbs free energy minimization routine and a grid scheme similar to that of de Capitani & Petrakakis (2010), calculating isochemical phase diagrams or contouring any isolines.

By contrast to the above, Perple_X and Theriak-Domino are Gibbs free energy minimizers: with the system and its state fixed (*P*, *T*, all X_{sys}), an efficient algorithm minimizes G_{sys}. The result includes the stable mineral assemblage at these conditions; that is, the modes and compositions of all phases (Fig. 6a). Determining the minimum Gibbs free energy surface for an assemblage composed only of pure phases is a simple linearization problem, and several algorithms are in use, such as the alphabetic method of de Capitani & Brown (1987) implemented in Theriak-Domino (Fig. 10b) or the simplex algorithm implemented in Perple_X (Connolly & Kerrick, 1987). If solid solutions are involved the problem becomes non-linear. Perple_X linearizes the problem and uses linear programming to solve it, approximating solid solution functions with pseudo-compounds (Fig. 10e). Theriak applies a succession of linear and non-linear programming steps (Fig. 10b–d). The recent review by Connolly (2017) provides a detailed description of how the two algorithms work and a discussion of the advantages and limits of each technique. The Gibbs free energy minimizers compute mineral assemblages for *P*–*T*–X_{sys} points (i.e. within stability fields) rather than the position of field boundaries. To delineate the stability fields, a multilevel grid strategy is required, with interpolation between stability fields (e.g. Connolly & Petrini, 2002; Connolly, 2005; de Capitani & Petrakakis, 2010) to generate phase diagrams.

Phase equilibrium calculators rely on the petrological expertise of the user to decide which mineral phases should be considered (or not) in a specific case. Gibbs free energy minimizers consider all of the phases present in a given thermodynamic database. Gibbs free energy minimizers might converge to local minima (if non-linear programming is used), so precautions such as higher resolution scanning stages and random sampling are taken to prevent that risk (Connolly, 2017). Phase equilibrium calculators yield an exact solution of the problem as the composition of each phase is fixed. It is possible to restrict the algorithm to the phase composition ranges where a particular solution model is applicable, but the solution may not correspond to a minimum in free energy.

Both Theriak-Domino and Gibbs create high-quality and ready-to-use vector graphics. All four software

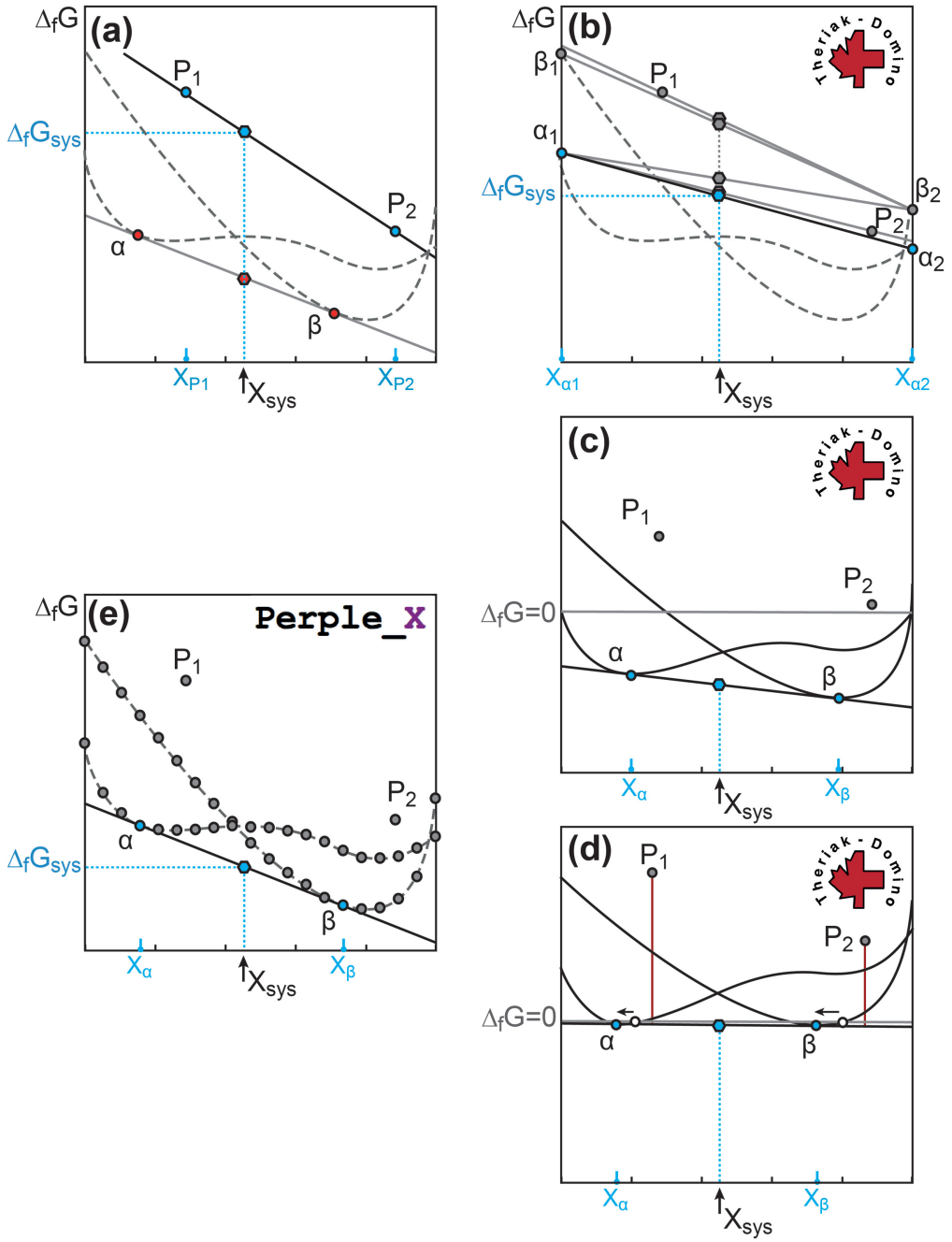

Fig. 10. Illustration of the numerical techniques employed to produce an equilibrium assemblage diagram in a binary system including solid solutions. The virtual thermodynamic database used in this example contains two pure phases P_1 and P_2 and two solid solution models α and β with two pure end-members (α_1, α_2 and β_1, β_2). The bulk composition of the system X_{sys} is ~0·45 moles of the second component. (a) The non-linear equation solver of the phase equilibrium calculators finds the equilibrium compositions of the assumed stable assemblage $\alpha+\beta$ (red dots) tangent to the $\Delta_f G$–X surface at a given P and T. The solution is exact on the basis of mass-balance calculations. However, if one assumes that the system is only represented by phases P_1+ P_2 (blue dots), it will not be recognized that both phases are metastable with respect to the assemblage $\alpha+\beta$. (b–d) The Gibbs free energy minimizer THERIAK-DOMINO applies a succession of linear (b) and non-linear programming steps (c, d) to minimize $\Delta_f G_{sys}$. The initial solution of the problem is obtained by considering the end-members only, in this example P_1, P_2, α_1, α_2, β_1 and β_2. The initial solution is $\alpha_1+\alpha_2$ [black line in (b)], as this assemblage has the lowest $\Delta_f G_{sys}$. The reference state of the system is then transformed, whereas the stability relations of all phases remain the same [black lines in (c)]. The G–X plane of the initial solution becomes horizontal [grey line in (c)]. A new minimum with $\alpha+\beta$ is obtained using non-linear minimization. This procedure is repeated [e.g. in (d)] until convergence to a stable solution. (e) The Gibbs free energy minimizer PERPLE_X uses pseudo-compounds for solid solutions (α_1, α_2, α_3... and β_1, β_2, β_3...) to linearly approximate the Gibbs free energy of non-linear solutions. Pseudo-compounds have fixed compositions and the algorithm searches the combination of pseudo-compounds with the lowest Gibbs free energy, here $\alpha_4+\beta_{15}$. The accuracy of the equilibrium solution compositions depends on the compositional resolution between two pseudo-compounds.

packages produce postscript files. Each program comes with a collection of thermodynamic databases, as follows.

1. THERMOCALC supports the datasets and solid solution models produced by Holland & Powell and their collaborators [e.g. *ds3.2*, *ds5.5* (*HP98*), *ds6.2* (*HP11*)].
2. GIBBS incorporates the datasets *HP98*, *HP11* (e.g. *ds6.2*) and the database SPaC (Spear, Patisson & Cheney) based on *BE88* and optimized for application to pelitic schists (Pattison *et al.*, 2002; Pattison & DeBuhr, 2015). This database also includes phosphate phases (Spear & Pyle, 2010).
3. PERPLE_X contains several datasets (e.g. *HP98*, *HP11*) with an extensive collection of models from various authors. It also contains the database of Stixrude & Lithgow-Bertelloni (2011) for geophysical applications.
4. THERIAK-DOMINO incorporates the main databases from Holland & Powell (*tc3.2*, *tc5.5*, *tc6.2*) with additional solid solution models from other authors. The databases *JUN92* (de Capitani & Petrakakis, 2010) and *BED92* (Duesterhoeft, 2017) are based on *BE88* with updated solid solution models available only in this program.

It is important to mention that the distribution of software code to the scientific community (e.g. by open source; see Mader & Schenk, 2017) is critical to maintain and enhance development. This principle has been largely followed by THERIAK-DOMINO, PERPLE_X and GIBBS. As a result, several add-ons and extensions have been developed: LitMod (Afonso *et al.*, 2008), LitMod3D (Fullea *et al.*, 2009), PreMDB (Siret *et al.*, 2009), PHMEGP (Zunino *et al.*, 2011) and Rcrust (Mayne *et al.*, 2016) for PERPLE_X; Theriak_D (Duesterhoeft & de Capitani, 2013), Theria_G (Gaidies *et al.*, 2008), GRTMOD (Lanari *et al.*, 2017) and myDomino (by E. Kelly) for THERIAK-DOMINO.

Applications of forward thermodynamics modeling

Forward phase equilibria modeling has progressively become a major petrological tool to investigate metamorphic processes and retrieve *P–T* conditions from metamorphic assemblages (Spear, 1988*b*; Powell & Holland, 2008). Other applications have also explored thermodynamic modeling of hydrothermal alteration (Helgeson *et al.*, 1969; Helgeson, 1970, 1971, 1979; Greenwood, 1985; Tanger & Helgeson, 1988; Shock *et al.*, 1989; Dolejš & Wagner, 2008; Wagner *et al.*, 2012; Marsala & Wagner, 2016) and reactive transport processes (Oliveira *et al.*, 2018). Studies have upscaled metamorphic phenomena into geodynamic models (Connolly, 2009; Duesterhoeft *et al.*, 2012*a*, 2014; Engi *et al.*, 2018), the prediction of global geochemical cycles (Baxter & Caddick, 2013; Evans & Powell, 2015), and the interpretation of geophysical signals (Nagel *et al.*, 2018). For additional examples and references, the reader is referred to the recent review by Yakymchuk (2017).

Petrological applications—isochemical phase diagrams and isopleth thermobarometry

The construction of equilibrium phase diagrams for specific bulk-rocks of interest—producing isochemical phase diagrams—requires choosing (1) a database, (2) an appropriate chemical system and (3) a representative bulk composition of the sample volume assumed to have been chemically reactive. The last has been variably termed the reactive bulk composition (Lanari & Engi, 2017) or the effective bulk composition (Evans, 2004). These choices are critical as they strongly affect the resulting diagrams (e.g. Symmes & Ferry, 1992; Tinkham & Ghent, 2005; for the effect of Mn on garnet stability); they are the object of intense discussions in the reviews of Kelsey & Hand (2015), Lanari & Engi (2017), Yakymchuk (2017) and Yakymchuk *et al.* (2017). An equilibrium phase diagram allows the mineral assemblages predicted for a given X_{sys} to be compared with the natural record of a metamorphic rock. If the peak assemblage is no longer preserved because of retrogression, an inferred peak assemblage can be defined (Kelsey *et al.*, 2003; Warren & Waters, 2006; Lanari *et al.*, 2013). If the observed mineral assemblage agrees with a computed stability field in *P–T* space, it is desirable further to refine the *P–T* conditions within that field; this requires comparison of the mineral modes and phase compositions. For that purpose, equilibrium phase diagrams can be contoured for phase proportions and/or mineral compositions (see Fig. 1 of Powell & Holland, 2008). Such contours are referred to as isolines or isopleths. Quantitative comparison of observed and predicted mineral compositions can also be aided by an automated strategy with a weighting scheme that reflects the relative uncertainty in the electron probe microanalysis (EPMA) data (Moynihan & Pattison, 2013; Lanari *et al.*, 2017). If a *P–T* trajectory can be constrained [i.e. a segment of the *P–T* path represented in the sample by (partial) relic assemblages] it can be helpful to produce diagrams showing variations in mineral mode along this *P–T* trajectory (Connolly, 2005; Konrad-Schmolke *et al.*, 2008; de Capitani & Petrakakis, 2010; Rubatto *et al.*, 2013; Airaghi *et al.*, 2017*b*). The resulting mode-box diagrams [e.g. Yakymchuk *et al.* (2017) for typical metamorphic rocks and *P–T* paths] allow checking of the amounts grown and destroyed along the path—an important test of the match between model and sample.

An example of such an approach is the case study of McCarron *et al.* (2014), which has been reinvestigated in this study (Fig. 11). These researchers constructed isochemical phase diagrams and applied garnet isopleth thermobarometry to study the metamorphic gradient in ~1 Gyr old metasediments of the Flinton Group of the Canadian Grenville Province. Here we focus on their sample 12TM16 (McCarron *et al.*, 2014), a metapelite

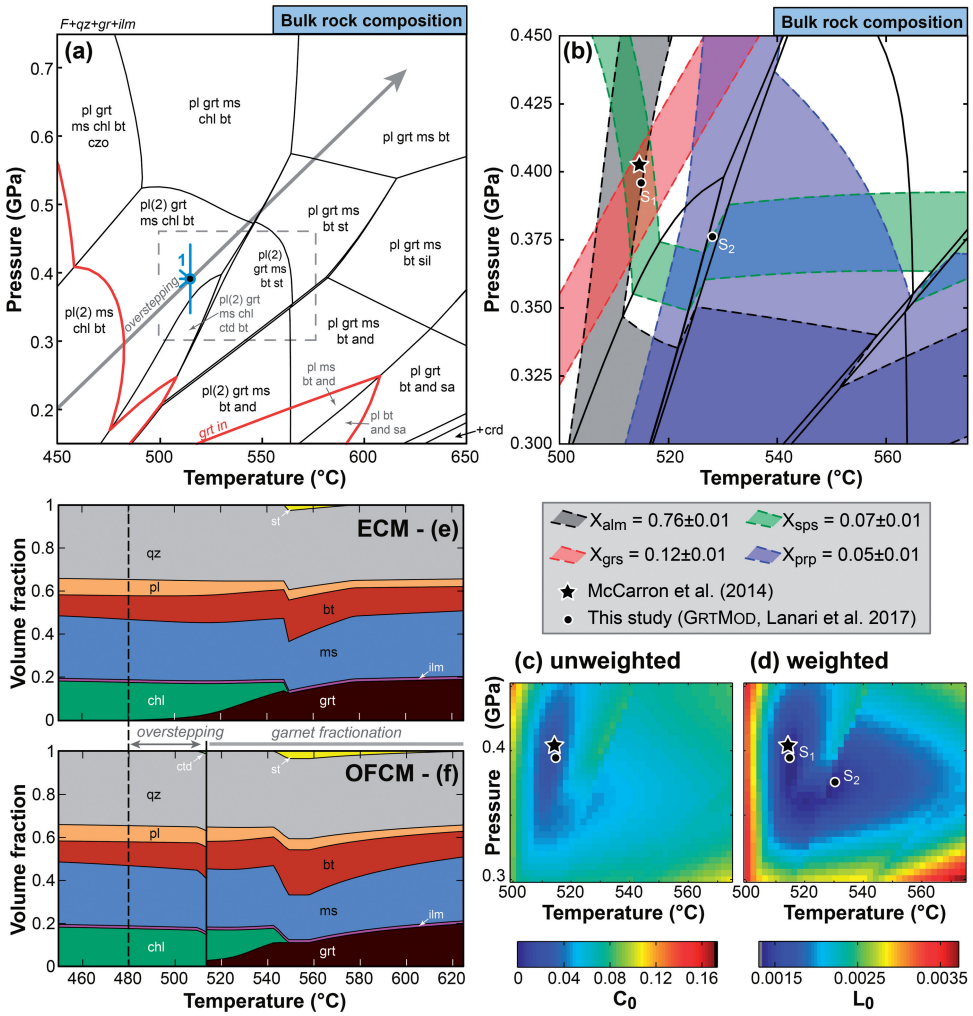

Fig. 11. Example of forward thermodynamic analysis of the metapelite 12TM16 from the Flinton Group of the Canadian Grenville Province (modified from McCarron *et al.*, 2014). (a) Isochemical phase diagram computed for the same bulk-rock composition and thermodynamic database as used by McCarron *et al.* (2014). The optimal *P*–*T* conditions of garnet cores were obtained using GRTMOD (Lanari *et al.*, 2017) and are shown in blue (noted 1). The red curve marks the garnet-in reaction. The dashed rectangle marks the *P*–*T* region investigated for isopleth thermobarometry (b–d). The gray line shows the *P*–*T* trajectory used to generate the box-diagrams (e, f). (b) *P*–*T* diagram showing the range of garnet isopleths (X_{alm}, X_{prp}, X_{grs}, X_{sps}) for garnet core compositions. The star is the best match empirically derived by McCarron *et al.* (2014); the circles mark the two solutions obtained by GRTMOD (see text). (c) Unweighted and (d) weighted objective functions of GRTMOD, corresponding to C_0 and L_0 of Lanari *et al.* (2017). (e, f) Mode-box diagrams showing the evolution of modal abundances with *T* calculated along the *P*–*T* trajectory shown in (a). (e) ECM, equilibrium crystallization model; (f) OFCM, overstepping and fractional crystallization model for garnet. A vertical dashed line marks the position of the garnet-in reaction. Mineral abbreviations are from Whitney & Evans (2010).

comprising fine-grained muscovite, ilmenite, rutile and quartz, with porphyroblasts of garnet and biotite. Diamond-shaped patches of coarse-grained muscovite were interpreted as staurolite pseudomorphs in that study.

To reassess the evolution of sample 12TM16, the isochemical phase diagram shown in Fig. 11a was computed here for the bulk-rock composition—obtained by wavelength-dispersive X-ray fluorescence (XRF) analysis—using THERIAK-DOMINO and the exact same thermodynamic database as was used by McCarron *et al.* (2014). The range of garnet isopleths (X_{alm}, X_{grs}, X_{sps}, X_{prp}) corresponding to the observed composition of garnet cores is reported in Fig. 11b. At the *P*–*T* conditions of garnet nucleation proposed by McCarron *et al.* (2014) (star in Fig. 11b), the mole fraction of pyrope is the only one outside the range of ±0·01. This means that there is no perfect match between modeled and predicted garnet compositions. To improve this situation, optimal conditions were derived by means of the program GRTMOD, using a weighting procedure, as documented by Lanari *et al.* (2017), that takes into account the relative uncertainties in the EPMA data. Two solutions were found (S_1 and S_2 in Fig. 11), with similar residuals. S_1 has the lowest residual, and its *P*–*T* values are close to the unweighted conditions [see equation (13) of Lanari *et al.* (2017)] and the solution proposed by McCarron *et al.* (2014) (Fig. 11c), whereas S_2 has a slightly higher residual (still within an acceptable range; see Fig. 11d), and lies in the staurolite stability field.

Although the intersection of isopleths would seem tighter at S_1 when judged visually, the two solutions are equivalent if the uncertainties are taken into account. In this case, the *P–T* differences are rather small (∼0·025 GPa and ∼15°C) but S_2 is of interest because it suggests that garnet may have grown in equilibrium with staurolite. This example indicates that the *P–T* conditions determined by isopleth thermobarometry may not be optimal if all the compositional variables (and the modes) are not used, or if a weighting scheme taking into account the analyses' uncertainty is not applied.

Challenges—assessing the reactive bulk composition

The evolution of the mineral modes—and the mineral compositions—of sample 12TM16 (McCarron *et al.*, 2014) can be modeled along a *P–T* trajectory from 450°C and 0·2 GPa to 625°C and 0·7 GPa using an equilibrium crystallization model (ECM, Fig. 11e). This type of modeling can help to interpret the microstructural record in metamorphic rocks (Vernon *et al.*, 2008; Airaghi *et al.*, 2017*b*). In the present model, garnet nucleates at the garnet-in reaction (∼480°C) and readjusts its composition during growth as the whole system is assumed by the model to reach thermodynamic equilibrium at every step. Therefore, this model cannot predict compositional zoning of mineral phases. Minor garnet resorption marked by a net decrease of garnet mode is observed at 545°C when staurolite becomes stable.

A more realistic model accounts for disequilibrium processes such as reaction overstepping (Pattison *et al.*, 2011; Kelly *et al.*, 2013; Spear *et al.*, 2014) and partial re-equilibration. Reaction overstepping—assuming that the composition of the nucleating garnet can be predicted by equilibrium thermodynamics—and garnet fractional crystallization have been included in the model (overstepping and fractional crystallization model OFCM in Fig. 11). The garnet core is assumed to nucleate with a thermal overstepping of 25°C (Fig. 11a) as recorded by the garnet core composition (see above). The corresponding reaction affinity, calculated using the method of Pattison *et al.* (2011), is 281 J mol^{-1} oxygen in garnet. This overstepping has been included in the first part of the model (up to 515°C; see Fig. 11f) by preventing garnet from becoming stable in THERIAK-DOMINO. Once garnet starts to grow, the reactive bulk composition begins to evolve because the components stored in garnet are progressively fractionated from the bulk-rock composition [see Fig. 5 of Lanari & Engi (2017)]. A new reactive bulk is modeled at each step by subtracting the composition of the newly grown garnet from the previous reactive bulk composition. The differences between the two mode-box diagrams show how reaction overstepping and fractional crystallization affect the predictions of the model. As the garnet porphyroblasts in sample 12TM16 exhibit compositional zoning, a fractional crystallization model is in this case required for accurate thermobarometry.

An alternative strategy that does not require any assumption about the *P–T* trajectory is to determine the optimal *P–T* conditions for each growth zone using the program GRTMOD to perform the required fractionation calculation [Lanari *et al.* (2017); a similar strategy for modeling garnet growth was proposed by Moynihan & Pattison (2013)]. The results for Grt_2 and Grt_3 in sample 12TM16 are shown in Fig. 12, as well as the effect on the geometry of the isochemical phase diagrams. The position of the *P–T* stability field of the inferred peak assemblage (plagioclase, garnet, muscovite, biotite and staurolite shown in gray in Fig. 12) and the garnet isopleths are progressively shifted in the diagram as the reactive bulk composition changes (McCarron *et al.*, 2014). Other semi-automated (Spear, 1988*b*; Konrad-Schmolke *et al.*, 2008; de Capitani & Petrakakis, 2010) and automated methods (Gaidies *et al.*, 2008; Moynihan & Pattison, 2013; Vrijmoed & Hacker, 2014; Kelly *et al.*, 2015) were discussed by Lanari *et al.* (2017).

The presence of metastable relics and the observation of compositional zoning in most (if not all) metamorphic minerals (Fig. 9) demonstrate that large-scale (e.g. thin-section scale) thermodynamic equilibrium is rarely attained in nature (Carlson *et al.*, 2015), questioning the use of the bulk-rock composition as an approximation of the reactive bulk composition. In addition, many researchers have recently raised concern concerning our ability to estimate the *P–T* conditions of garnet nucleation using equilibrium thermodynamics if garnet is nucleating with a significant degree of overstepping (Spear *et al.*, 2014; Castro & Spear, 2017; Spear & Pattison, 2017). Consequently, it can be challenging to identify a frozen-in state of equilibrium suitable to determine a reactive bulk composition for forward thermodynamic modeling. In the following section, we show how iterative thermodynamic models can be employed to test the assumption of chemical equilibrium.

PERSPECTIVE: TOWARDS ITERATIVE THERMODYNAMIC MODELING

As shown in the previous section [and previously mentioned by Powell & Holland (2008)], thermobarometric studies based on forward models remain in most instances largely qualitative. The forward models are quantitative because they are based on Gibbs free energy minimization; however, for the purpose of thermobarometry, it is necessary to compare the mineral compositions and modes with the observations and analytical data obtained from rock samples. This comparison often considers just the mineral assemblage, sometimes augmented by a few diagnostic mineral compositions (isopleth thermobarometry), but rarely uses modal abundances. This 'inverse part' is thus largely qualitative and incomplete. In this section, we present a theoretical framework that allows the quantitative comparison between the observations and the predictions made by Gibbs free energy minimization

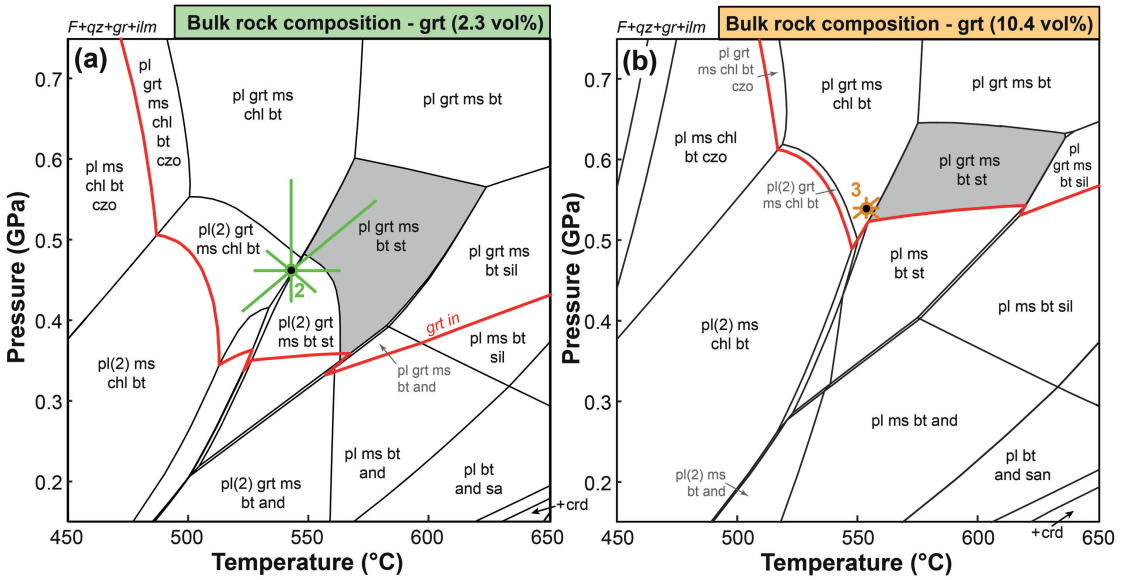

Fig. 12. Effect of garnet fractionation on isochemical phase diagrams using the same sample (12TM16) as in Fig. 11 (modified from McCarron *et al.*, 2014). (a) Isochemical phase diagram computed using the bulk-rock composition minus 2·3 vol. % of garnet cores. (b) Isochemical phase diagram computed using the bulk-rock composition minus 2·3 vol. % of garnet 1 (core) and 8.1 vol. % of garnet 2 (mantle). The optimal conditions for the corresponding growth zones obtained using GrtMod are shown in each figure. Mineral abbreviations are from Whitney & Evans (2010).

(Fig. 6c). This strategy can be employed to derive, via an iterative method, optimal *P*–*T*–(*X*) conditions based on locally delimited bulk compositions.

Bingo-Antidote—a software solution for iterative thermodynamic modeling

The modeling program Bingo-Antidote (Lanari & Duesterhoeft, 2016; Lanari & Engi, 2017) is deployed as an add-on to the compositional mapping software XMapTools (Lanari *et al.*, 2014*b*, 2018). Quantitative compositional maps from XMapTools can be handled readily using Bingo-Antidote, which offers an independent graphical user interface to visualize and select areas of interest within a map. Gibbs free energy minimization is performed using Theriak (de Capitani & Brown, 1987) and any compatible thermodynamic database. The software is divided into two parts: subroutine Bingo contains a scoring technique to quantitatively compare modeled and observed mineral assemblages, modes and compositions; subroutine Antidote includes a heuristic search method to invert the forward model and determine optimal *P*–*T*–*X* conditions (see below).

Philosophy, strategy, advantages

The ITM strategy presented in this study combines advantages of both forward and inverse models (Fig. 6c). Predictions are obtained from the forward part of the model and compared with the observations in a quantitative way, making the assumption of equilibrium easily testable for any delimited local domain of a rock at given *P*–*T* conditions. If the reactive bulk composition is fixed, the problem can be inverted allowing the *P*–*T* conditions as well as some activity and compositional variables (*X*) to be optimized.

This modeling technique involves four steps, as follows.

1. *Quantitative compositional mapping on a polished thin section of rock*. This allows the natural compositional variability of minerals to be measured in two dimensions (Kohn & Spear, 2000; Vidal *et al.*, 2006; Lanari *et al.*, 2018; Ortolano *et al.*, 2018) and also provides a reliable estimate of the local bulk composition of any domain in the mapped area (Lanari & Engi, 2017).
2. *Selection of a domain for estimating the local bulk-rock composition and the mineral proportions*. The average mineral compositions, their uncertainties, and the mineral modes are determined within this domain. Phases assumed to be non-reactive, such as porphyroblast interiors or accessory phases, can be excluded from the assumed reactive part of the rock (e.g. garnet interiors, Marmo *et al.*, 2002; Tinkham & Ghent, 2005).
3. *Quantitative comparison between observations and model prediction.* For any set of *P*–*T* conditions program Bingo determines the 'quality' of the model predictions based on three factors evaluating the quality of the match between predicted and observed assemblage (Q_{asm}), mineral modes (Q_{vol}) and mineral compositions (Q_{cmp}). The mathematical procedure used for Q_{asm}, Q_{vol} and Q_{cmp} is given in Supplementary Data S1 (supplementary data are available for downloading at http://www.petrology.oxfordjournals.org). The values of each quality factor range between 0% (low quality) and 100%

(excellent match). The factors Q_{vol} and Q_{cmp} can also be determined for individual minerals. A global evaluation factor

$$Q_{tot} = \frac{1}{3}\left(Q_{ass} + \frac{Q_{ass}}{100}Q_{vol} + \frac{Q_{ass}}{100}Q_{cmp}\right)$$

can also be displayed.

4. *Optimization of* P–T*(–*X*) conditions (*Antidote*).* Among the results from Bingo any quality factor (such as $-Q_{tot}$) can be used as an objective function that compares the predictions of the model with the observations. The iterative optimization involves several steps of mapping of the objective function in *P–T–X* space to identify possible local minima, combined with non-linear minimizations applying the simplex method [see Lanari *et al.* (2017) for the description of a simple case involving only one phase]. Compositional (e.g. X_{fluid}) and/or activity variables (e.g. a_{CO_2}) can also be part of the optimized variables.

One of the key features of this modeling technique is the correspondence between the local bulk composition taken as the reactive bulk composition and the direct observations in the same volume. This mutual correspondence permits users to build a fully quantitative comparison between model and observations and allows the quality of the model to be evaluated. In other approaches, for instance if the bulk-rock composition determined by XRF is used for modeling, the bulk composition is generally obtained for a different volume of rock than the one documented by direct microscopic observations and for which mineral compositions were analyzed.

In theory, equilibrium can be assessed, via ITM, provided that (1) the investigated rock volume is devoid of compositional heterogeneities, such as compositional zoning in solid solution phases, and (2) the model predictions match the observations and analytical data within their uncertainties. This method can also be applied to more complex cases involving the metastable persistence of mineral phases or other chemical heterogeneities (see below).

Example of application

A metapelite from the Higher Himalayan Crystalline Sequence exposed in Sikkim (India), previously studied by Rubatto *et al.* (2013), was reinvestigated. This sample (TG8C-03) exhibits an apparently 'well-equilibrated' HT–LP assemblage made of quartz, plagioclase, sanidine, biotite, garnet, sillimanite and ilmenite. Polycrystalline inclusions in garnet and melt pseudomorphs indicate that a small fraction of melt was episodically present during the equilibration of this assemblage. The peak assemblage is expected to be relatively well equilibrated, as this sample experienced a HT metamorphic event lasting at least 5–7 Myr and peaking at ~800°C (Rubatto *et al.*, 2013).

The models presented below are calculated for the system SiO_2–TiO_2–Al_2O_3–FeO–MnO–MgO–CaO–Na_2O–K_2O–H_2O, based on the thermodynamic database *tc6.2* including the dataset *HP11* (Holland & Powell, 2011) and the solid solution models of White *et al.* (2014). Melt was systematically included in the models and treated as a 'solid phase' for the estimation of Q_{asm}.

Quantitative petrography based on compositional maps

The investigated area (see Appendix A for a description of the analytical technique) has two distinct mineralogical domains that define a metamorphic layering (Fig. 13a). The dark layer is made of garnet, biotite, quartz, plagioclase, and sanidine. The light domain consists of quartz and sillimanite only. Kyanite relics have been reported by Rubatto *et al.* (2013). The accessory minerals are ilmenite (with a few small rutile cores), apatite, monazite and zircon. Most of them are present only in the dark layers.

Garnet shows slight compositional zoning from core (grt_1, $Alm_{64}Prp_{27}Grs_6Sps_2Adr_2$) to rim ($grt_2$, $Alm_{65}Prp_{29}Grs_3Sps_2Adr_2$) with a tiny rim (5–10 μm) showing Mn kick-up (grt_3, $Alm_{70}Prp_{22}Grs_3Sps_3Adr_2$) where in contact with biotite (Fig. 13b). Plagioclase shows slight zoning between sparse relic cores (pl_0, $Ab_{76}An_{21}San_3$), mantle (pl_1, $Ab_{74}An_{22}San_4$), and rim (pl_2, $Ab_{72}An_{25}San_3$). Coarse-grained sanidine is relatively homogeneous in composition (san_1, $San_{76}Ab_{23}An_1$), with only narrow rims and smaller grains displaying a different composition (san_2, $San_{81}Ab_{19}An_1$). Biotite grains exhibit compositional zoning dependent on their microstructural position: in the vicinity of garnet, biotite (bt_g) has $X_{Mg} = 0{\cdot}55$ and a Ti content of 0·28 atoms per formula unit (a.p.f.u.), whereas biotite away from garnet (bt_m) has lower X_{Mg} (0·52) and slightly higher Ti (0·33 a.p.f.u.).

The major minerals in this sample all exhibit slight compositional zoning. This observation suggests either that they had only partially re-equilibrated at the peak conditions, thus preserving prograde information, or that they formed or partially re-equilibrated later, during retrogression.

Assessing the peak metamorphic assemblage—scale of equilibrium or disequilibrium

The first advantage of ITM is the quantitative approach employed to determine the local bulk composition (Lanari & Engi, 2017). However, what needs testing is whether any composition is representative of the equilibration volume at the metamorphic stage in question. For the example discussed here, sensitivity tests were performed at the inferred conditions for the peak assemblage (i.e. 790°C and 0·64 GPa; Fig. 14). To this end, several arbitrary domains based on petrographic textures were selected for modeling.

The first local bulk composition LBC_1 was extracted from the sillimanite-absent layer consisting of garnet,

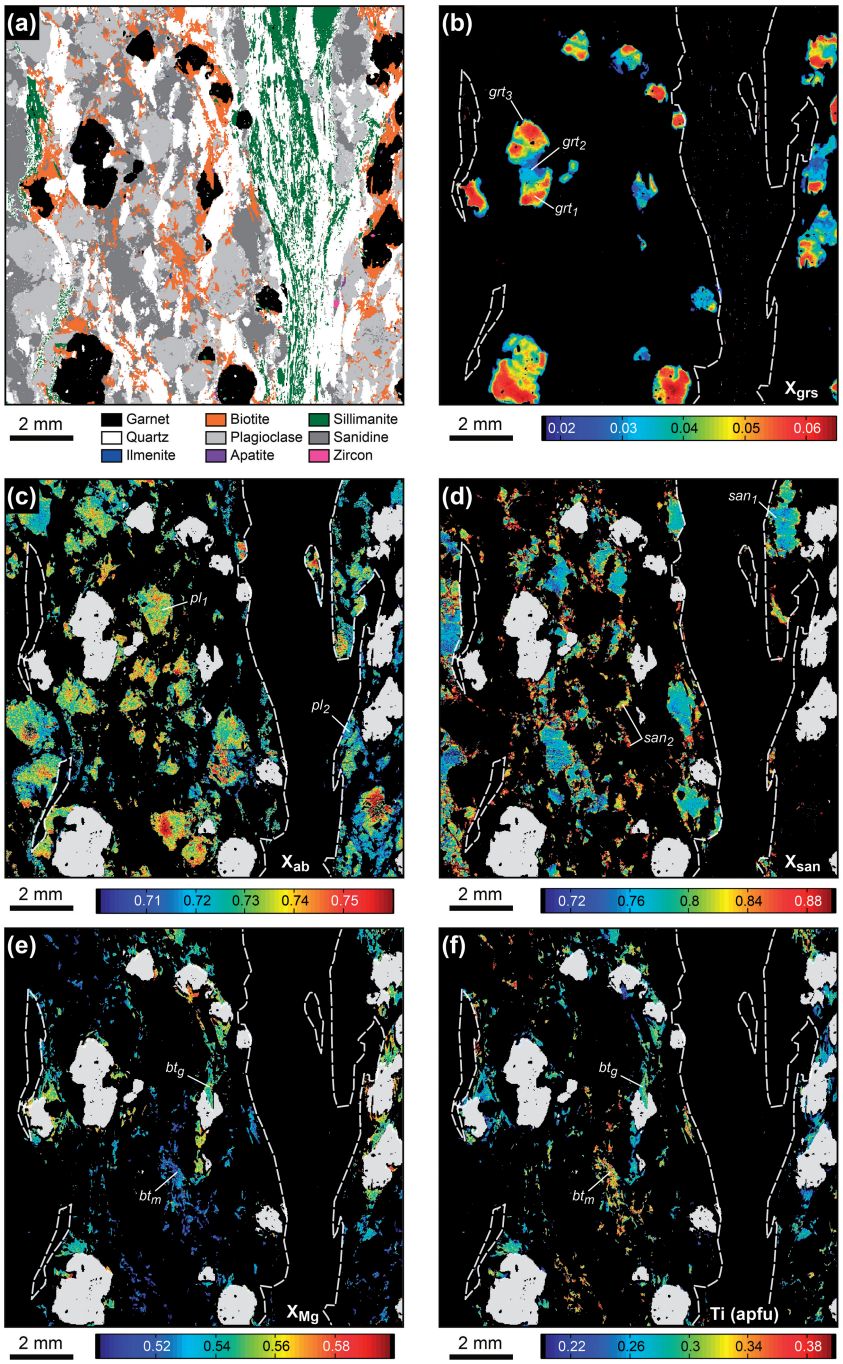

Fig. 13. Selection of quantitative compositional maps for sample TG8C-03 (see text), a metapelite from the Higher Himalayan Crystalline Complex exposed in Sikkim (India). (a) Map showing the distribution of the mineral phases in the mapped area. (b) Map of grossular content (X_{grs}) in garnet. (c) Map of albite content (X_{ab}) in plagioclase. (d) Map of sanidine content (X_{san}) in K-feldspar. (e) Map of X_{Mg} in biotite. (f) Map of Ti content in biotite, in atoms per formula unit (a.p.f.u.). The domains used to define the groups of each phase are shown in the compositional maps (b–f). Mineral abbreviations are from Whitney & Evans (2010).

biotite, plagioclase, sanidine and quartz (Fig. 14a), assuming that the two layers should be regarded as closed systems. In this scenario, the sillimanite–quartz layer is considered to reflect a discrete seam caused by metasomatism. The modeled mineral assemblage and mineral modes are in line with the observations (Fig. 14a). The second local bulk composition LBC_2 was obtained from a larger domain area (Fig. 14b) that included both layers. In this case, a global equilibrium assumption is invoked (i.e. all the minerals are assumed to have coexisted in equilibrium at the peak conditions). The modeled mineral assemblage and mineral modes are again in line with the observations (Fig. 14b).

The mineral assemblages and mineral modes match the observations in both cases, showing the strong effect of the mass-balance equation on the results of

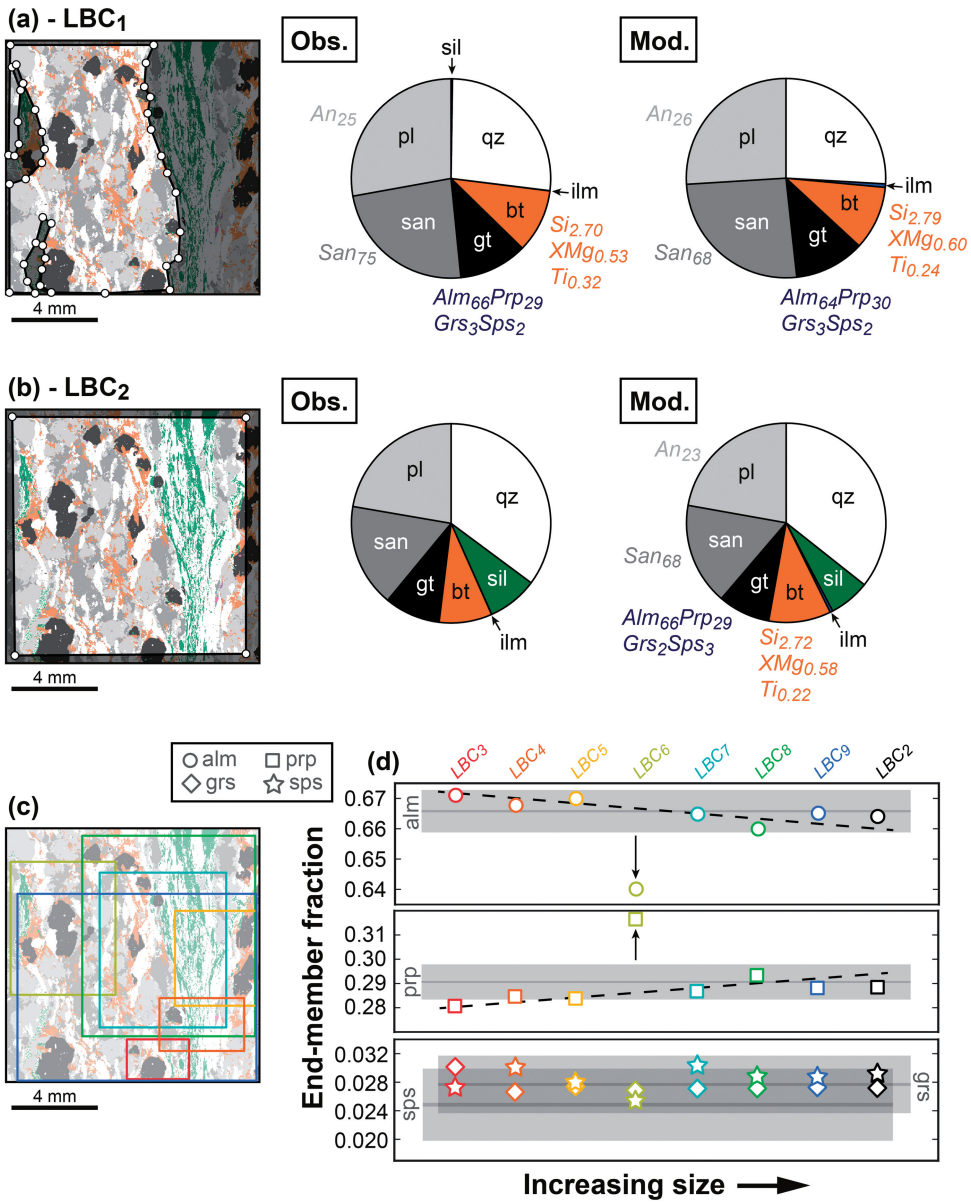

Fig. 14. Sensitivity test performed for peak conditions (790°C, 0·64 GPa), using different equilibrium volumes. *LBC*, local bulk composition; *Obs.*, observed mineral modes extracted from the same domain; *Mod.*, Modeled mineral modes. The nine domains from which the *LBC* were obtained are shown on the maps and labeled from LBC_1 to LBC_9. (a) LBC_1 from the sillimanite-absent domain. The small fraction of sillimanite reported in the observations is neglected as it results from the false classification of mixed pixels. (b) LBC_2. (c) Sensitivity test with increasing surface from LBC_3 to LBC_9. (d) Evolution of the predicted garnet composition with the increasing size of the domain; circle, X_{alm}; square, X_{prp}; star, X_{sps}; diamond, X_{grs}. The colors used in (d) correspond to the color used to contour the domain shapes in (c). LBC_2 from (b) is also used for comparison. Mineral abbreviations are from Whitney & Evans (2010).

Gibbs free energy minimizations. However, the predicted mineral compositions of plagioclase, garnet and biotite differ significantly between the two cases (Fig. 14). Although it cannot be completely excluded that these differences are related to inaccuracies in the thermodynamic models, this result rather suggests that the selection of the assemblage and the domain to be investigated has an effect on the modeled mineral compositions. Similar results were obtained by Lanari & Engi (2017) and interpreted to be an effect of garnet geometry—only thin slices of each garnet grain were analyzed—on the bulk composition. In the present example, the compositional zoning in garnet (and in other phases) is minor and cannot explain such differences. The main difference between LBC_1 and LBC_2 is the presence or the absence of sillimanite in the stable assemblage, which affects the chemical potential of alumina μ_{Al2O3} (–1776 kJ mol^{-1} for LBC_1 and –1773 kJ mol^{-1} for LBC_2). In LBC_2, sillimanite imposed its chemical potential in the intergranular medium, even where it was not physically in contact with the rest of the assemblage. As μ_{Al2O3} obtained for LBC_1 is lower, sillimanite is not

predicted to be stable. For a system in equilibrium, the chemical potential of each component is not different in one phase from what it is in any other. In this example, at least one of the phases controlling μ_{Al2O3} in the first model (using LBC_1) was apparently not in equilibrium with sillimanite at the peak conditions.

A second sensitivity test was conducted to quantify the effects of domain size and mineral proportions on the modeled garnet composition (Fig. 14c). For a system that is at a uniform temperature and pressure and is composed of a number of mineral phases in equilibrium, the same mineral compositions must be predicted by Gibbs free energy minimization, independently of the mineral proportions chosen to generate the reactive bulk composition, as the Gibbs free energy of a mineral phase is dictated by only *P*, *T* and activity [see equation (1)]. The selection of any arbitrary subsystem (domain) should not affect the model predictions at the *P*–*T* conditions of equilibrium. It should be noted that this rule does not apply if *P*–*T* conditions change (e.g. in isochemical phase diagrams) because the positions of many reactions are controlled by the reactive bulk composition (Palin *et al.*, 2016). In the present example, seven new domains containing the same assemblage (garnet, biotite, sillimanite, plagioclase, sanidine, quartz and ilmenite) were arbitrarily defined and their local bulk compositions ($LBC_{3–9}$) were used to predict the garnet compositions stable at the inferred peak conditions of 790°C and 0·64 GPa. In this case, LBC_1 is not included as it contains a different mineral assemblage. With increasing size of the domain, a linear trend of decreasing almandine and increasing pyrope contents is observed (dashed lines in Fig. 14c), but this variation remains essentially within the uncertainty of the EPMA data. The only outlier is LBC_6, for which almandine and pyrope are shifted by 0·03; also, a difference in the mineral modes is found: the proportion of plagioclase and sanidine is higher (53 vol. %) than in the other domains (between 13 and 37 vol. %). This second sensitivity test questions again the preservation of an equilibrium assemblage at peak conditions as changes in the mineral proportions significantly affect the model predictions.

Optimization of compositional (or activity) variables

The most direct benefit of ITM is the optimization of compositional variables that control the activity of components. The strategy is somewhat similar to the complex inverse technique described in the modeling section. Variables such as n_{H_2O}, a_{H_2O} and f_{O_2} can be optimized in Antidote either at fixed *P* and *T* or together with the optimization of *P* and *T*. Only the first case is presented below.

Figure 15 shows an example in which the amount of H_2O is optimized for the inferred peak conditions of 790°C and 0·64 GPa, assuming a single compromise bulk composition LBC_2. The assemblage is modeled at these *P*–*T* conditions for a restricted range of H_2O in the system (0·21–0·34 wt %). For lower H_2O contents, rutile is predicted to be stable instead of ilmenite because the modal abundance of biotite, the other carrier of Ti, is lower (Fig. 15c). For higher H_2O contents, a significant fraction of melt is predicted to be stable, whereas the petrological observations rather support the presence of a small melt fraction. Within the restricted range considered, both the quality factors of the predicted mineral abundances Q_{vol} and compositions Q_{cmp} gently increase with increasing H_2O (Fig. 15a). As the observed compositions of garnet and biotite are better modeled for higher amount of H_2O, the optimal value of 0·32 wt % (red line in Fig. 15) is selected as optimal and is used in the following discussion.

Optimal conditions of equilibration in partially re-equilibrated rocks

In this same example, the modeled and observed mineral assemblage (i.e. modes and compositions) were quantitatively compared using Antidote in the range of 600–900°C and 0·35–1·3 GPa. Figure 16 depicts the results as quality factor maps. The quality factor of the inferred peak assemblage Q_{asm} reaches 100% in the range of 600–800°C and 0·4–0·6 GPa, where this assemblage is accurately modeled (Fig. 16a). In this stability field, Q_{vol} is above 96% (Fig. 16b). A similar result is obtained at higher pressures in the rutile stability field. The quality of predicted mineral compositions Q_{cmp} is lower in these fields (84–92%), and the best match (>95%) is found at 680–720°C and 0·8–1 GPa (Fig. 16c) in the kyanite stability field. This solution corresponds to the 'optimal' isopleth intersection considering all the compositional variables of each solid solution (the list is given in Supplementary Data S1). The 'optimal conditions' of 687°C and 0·6 GPa were obtained by minimizing $-Q_{tot}$ in Antidote.

The discrepancy between Q_{asm}, Q_{vol} and Q_{cmp} is too large to be caused by uncertainties in the thermodynamic database and rather suggests that the minerals were not in equilibrium at any stage along the *P*–*T* trajectory of this rock. This interpretation is also supported by petrological observations, such as the presence of kyanite, which is predicted to be stable at higher-pressure conditions (interestingly enough, where the higher values of Q_{cmp} are found; see Fig. 16c). To explore the causes of or implications for such discrepancies, it is helpful to look at the quality factors for each mineral involved [equations (SP1)–(SP4) in Supplementary Data S1], the aim being to distinguish potentially co-genetic generations. Quality factor maps for each compositional group of garnet (grt_1, grt_2), biotite (bt_g, bt_m), plagioclase (pl_1) and sanidine (san_1) are shown in Fig. 16. Garnet cores are modeled at 750°C and 0·92 GPa ($Q_{cmp}^{grt1} = 100\%$, Fig. 16d) and the rims at 780°C and 0·61 GPa ($Q_{cmp}^{grt2} = 100\%$, Fig. 16g). Solutions within the cordierite stability field (e.g. 850°C, 0·58 GPa in Fig. 16g) are not considered, as cordierite was not observed in this sample. The biotite quality factor is

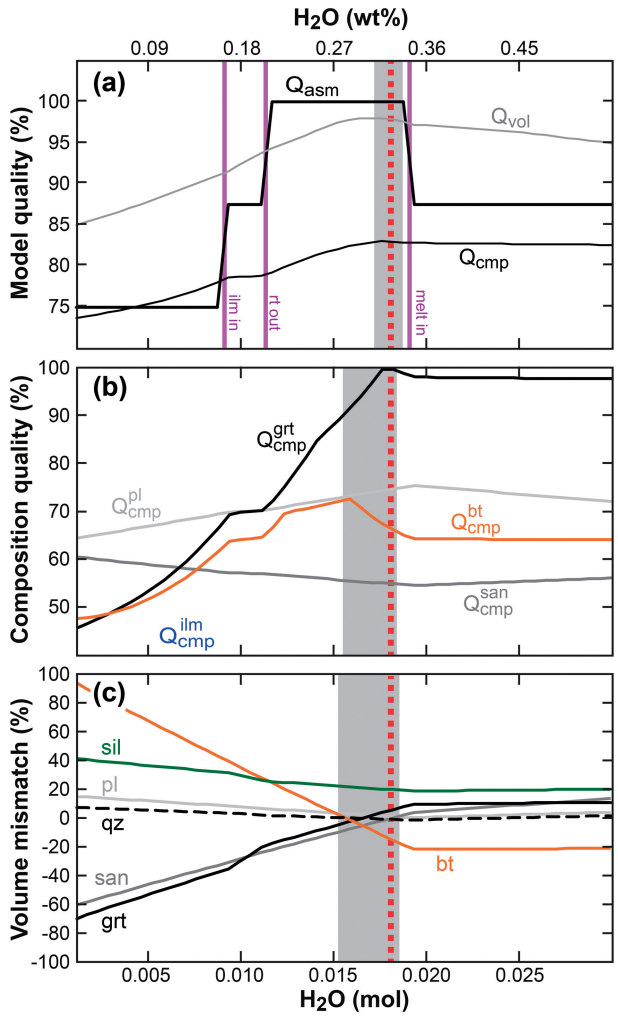

Fig. 15. Optimization of the amount of H_2O used in the reactive bulk composition at peak conditions (790°C, 0·64 GPa). The amount of H_2O is reported as mass fraction (upper axis) and molar abundance (lower axis). (a) Quality of the model for variable H_2O content shown as Q_{asm}, Q_{vol}, Q_{cmp}. A few selected reactions are shown by purple thick lines. (b) Evolution of the composition quality factors for garnet (grt_1), biotite (bt_g), plagioclase (pl_1) and sanidine (san_1). (**c**) Evolution of the misfit between predicted and observed modes (in per cent relative to the observations) for garnet, biotite, sanidine, plagioclase, sillimanite and quartz. The gray domains show the range of optimal H_2O content in each diagram. Mineral abbreviations are from Whitney & Evans (2010).

generally lower (Fig. 16e and h). An optimal solution is found at 770–800°C between 0·95 and 0·6 GPa for both bt_g ($Q_{cmp}^{bt_m} = 79\%$, see Fig. 16e) and 775°C and 0·6 GPa for bt_m ($Q_{cmp}^{bt_m} = 80\%$, Fig. 16e). The main plagioclase group pl_1 is modeled at lower *P–T* conditions (i.e. 600–710°C and 0·58–0·92 GPa; $Q_{cmp}^{pl1} = 100\%$, Fig. 16f) and the main sanidine group san_1 is modeled at 670–730°C ($Q_{cmp}^{san1} = 100\%$, Fig. 16i). It should be noted that the addition of a small fraction of melt at peak conditions (using a higher H_2O content; see Fig. 15) does not affect the positions of the optimal *P–T* conditions for the compositional groups investigated in this study.

Because these metamorphic minerals indicate a range of *P–T* conditions, the main conclusion is that they formed at different stages along the *P–T* trajectory, so only some—or parts—of them are representative of the peak conditions. The results are summarized in a *P–T* diagram (Fig. 17), with the addition of pl_2 and san_2. The *P–T* conditions obtained for pl_1, san_1 and grt_1 define a prograde trajectory between 600°C, 0·62 GPa and 780°C, 1 GPa. All of these minerals (generation 1) were metastable at peak conditions; they did not fully re-equilibrate, neither by recrystallization nor by intragranular diffusion. Diffusion probably altered the composition of garnet, so the results for grt_1 reflect re-equilibration rather than growth conditions. The metastable persistence of plagioclase and sanidine at the peak conditions can explain why the model predictions are biased if sillimanite is not included in the equilibration volume (see Fig. 14). The *P–T* conditions obtained for bt_m and grt_2 are attributed to peak conditions around 800°C and 0·6 GPa. The *P–T* conditions of pl_2 and san_2 reflect retrogression below 650°C at 0·5 GPa. An optimistic interpretation is that the condition of equilibration of each mineral group defines a continuous *P–T* trajectory, reflecting the successive metamorphic conditions experienced by this rock. Such detailed results can be of great help in supporting petrochronological interpretations (Engi *et al.*, 2017).

Open questions and future developments

Why are some quality factors in the example far below 100%? The predictions strongly depend on the thermodynamic dataset and the solid solution models. Systematic mismatch may indicate unrealistic behavior of solution models. For the present example, similar *P–T* conditions for each mineral group were reached with higher Q_{cmp} values using the biotite model of Tajčmanová *et al.* (2009) within the thermodynamic database *tc55* or using *JUN92.bs*. The choice of the database is critical because it may affect the *P–T* predictions and thus the geological interpretations (Pattison *et al.*, 2002; Pattison & Vogl, 2005; Pattison & DeBuhr, 2015; Guevara & Caddick, 2016).

Can reaction kinetics such as overstepping significantly affect the P–T *predictions of nucleation?* It has been shown that if a mineral nucleates with a significant degree of overstepping and from a re-equilibrated matrix, the *P–T* predictions can be flawed (Waters & Lovegrove, 2002; Spear *et al.*, 2014; Castro & Spear, 2017; Spear & Pattison, 2017). Other researchers concluded that the degree of overstepping is limited in metamorphic rocks (Kelly *et al.*, 2015; George & Gaidies, 2017) or that garnet nucleation can be modeled using equilibrium thermodynamics (Laurent *et al.*, 2018) as the mineral matrix does not seem to continuously re-equilibrate during prograde metamorphism (Airaghi *et al.*, 2017*b*). These hypotheses can be tested with independent thermobarometric methods such as *QuiG* barometry and *TitaniQ* thermometry (Thomas *et al.*, 2010; Kohn, 2014*b*; Thomas & Spear, 2018).

If the mineral assemblage did not fully (re-)equilibrate at specific conditions, can such deviations from

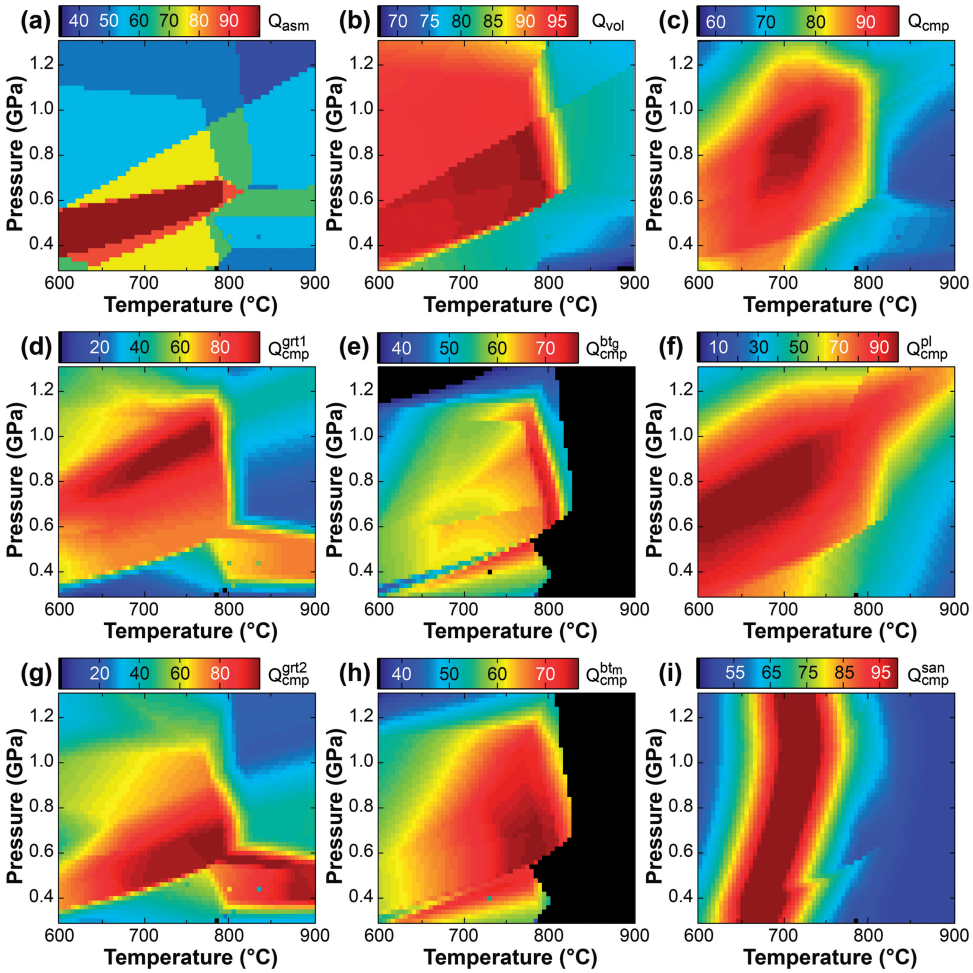

Fig. 16. Maps of quality factors calculated by Antidote using the bulk composition of LBC_2. (a) Q_{asm}; (b) Q_{vol}; (c) Q_{cmp}; (d) Q_{cmp} of grt_1; (e) Q_{cmp} of bt_g; (f) Q_{cmp} of pl_1; (g) Q_{cmp} of grt_2; (h) Q_{cmp} of bt_m; (i) Q_{cmp} of san_1. The same color scale is applied for the compositional groups of the same mineral. Mineral abbreviations are from Whitney & Evans (2010).

equilibrium affect the P–T *predictions?* It is well established that mineral fractionation can significantly affect thermobarometric estimates (Spear, 1988*b*; Evans, 2004; Konrad-Schmolke *et al.*, 2008; McCarron *et al.*, 2014; Lanari & Engi, 2017). Examples shown in Fig. 14 demonstrate how metastable persistence of plagioclase and sanidine can affect the model predictions, depending on the size of the selected domain. In theory, the mineral relics (here pl_1, san_1, grt_1 and bt_1) should not contribute to the reactive bulk composition used to model the peak assemblage. An attempt to use a smaller reactive domain, excluding plagioclase and sanidine, was made and resulted in similar *P–T* results for the peak conditions. We anticipate metastable persistence to be more a rule than an exception in metamorphic rocks. It will be critical in the future to evaluate how this process can affect the results of the forward models based on bulk-rock compositions. Serious problems can be anticipated if an inverse method such as *Average P-T* is applied to the Himalayan sample. The *P–T* conditions based on the inferred peak assemblage garnet + biotite + plagioclase + sanidine + quartz + sillimanite + ilmenite would be flawed (as shown by the map of Q_{cmp}) as these minerals apparently did not reach the state of equilibrium with the peak assemblage garnet + biotite + sillimanite + ilmenite at any stage along the *P–T* path of this rock.

SUMMARY AND CONCLUSIONS

The success of equilibrium thermodynamics in modeling metamorphic processes relies on several developments, notably (1) thermodynamic databases, (2) complex modeling strategies and (3) modeling software. Equilibrium thermodynamics remains a powerful basis to obtain thermobarometric data for metamorphic rocks. Where metastable persistence indicates that equilibrium was not achieved or maintained, suitable precautions must be taken. One way to address that problem is to integrate the textural insight and corresponding compositional data into the model, aiming to identify which minerals (compositional groups) may or may not have coexisted in equilibrium at any metamorphic stage. An iterative thermodynamic modeling

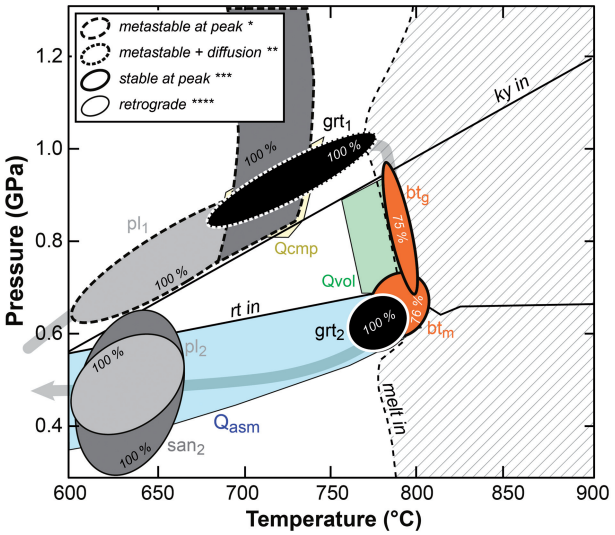

Fig. 17. Synthetic *P–T* diagram showing the optimal conditions derived for each compositional group of solid solutions based on the quality factors (Q_{cmp}) shown in Fig. 16 as well as the kyanite-in, rutile-in and melt-in reactions. The optimal ranges of *P–T* conditions are reported for garnet (black domains), biotite (orange), albite (light gray), sanidine (dark gray). The diagonally hatched domain shows the stability fields in which melt is present assuming an H_2O value of 0·32 wt % (see text). To select the optimal solutions, it was assumed that san_1 formed in the kyanite stability field; pl_2 and san_2 in the ilmenite stability field. *Prograde minerals, metastable at the peak conditions of 790°C and 0·64 GPa. **Prograde minerals (or compositional groups), metastable at the peak conditions, for which the compositional record was probably altered by intragranular diffusion. In this case, the *P–T* conditions do not represent growth conditions. ***Minerals stable at the peak conditions. ****Retrograde phases forming (or re-equilibrated) after the peak conditions. Mineral abbreviations are from Whitney & Evans (2010).

strategy, delivered with the software Bingo-Antidote, was developed. It provides a tool that aims to integrate part of the complexity evident in texture into models that rely on local equilibrium, admitting that its attainment may have been spatially limited. By setting up the models so they can be iteratively refined to account for textural information (inert mineral relics, resorption, etc.) partial re-equilibration can be addressed using equilibrium thermodynamics as a robust theoretical basis.

ACKNOWLEDGEMENTS

We are grateful to Marian Holness, who offered us the opportunity to write this Perspectives paper. We would like to thank both our lifeguards and the sharks; the former taught us to enter the pool of science, the latter how to be fast swimmers. Motivation and inspiration are the key for scientific developments and we are grateful to our mentors Olivier Vidal, Martin Engi and Joerg Hermann (P.L.), and Roland Oberhänsli, Romain Bousquet and Christian de Capitani (E.D.) for their direct and indirect contributions to this work. This paper has also benefited from interactions with colleagues over the past 3 years and it has been partly inspired by the contribution of many PhD students. We thank Travis McCarron for sharing his database and Daniela Rubatto for providing the sample TG8C-03. Careful reading from Martin Engi, Rob Berman, Joerg Hermann, Thorsten Nagel, Olivier Vidal and Alice Vho is acknowledged, as are their suggestions that significantly improved the original paper. Eleanor Green, Dave Pattison, Frank Spear and Dave Waters are thanked for their thoughtful and critical reviews and for pointing out some deficiencies and omissions in the original version.

SUPPLEMENTARY DATA

Supplementary data for this paper are available at *Journal of Petrology* online.

APPENDIX: QUANTITATIVE COMPOSITIONAL MAPPING

An area of 12·3 mm × 12·3 mm of sample TG8C-03 was analyzed using a JEOL JXA-8200 superprobe at the Institute of Geological Sciences of the University of Bern on a polished thin section, following the procedure described by Lanari *et al.* (2017) and Giuntoli *et al.* (2018*b*). X-ray maps of Si, Ti, Al, Fe, Mn, Mg, Ca, Na and K were obtained by wavelength-dispersive spectrometry, whereas for Zr, P, S, Ce, and La energy-dispersive spectrometry was used, all at 15 keV accelerating voltage, using a specimen current of 100 nA, and a dwell time of 150 ms per pixel with a pixel size of 12 μm. The total acquisition time was 100 h, including 87 h for mapping; more than a million quantitative analyses were obtained and are used in the following. The X-ray maps were corrected for time-related drift and surface irregularities using the TOPO map (Lanari *et al.*, 2018). All the pixels were classified and calibrated using the internal standardization procedure and the pseudo-background correction available in XMapTools 2.4.4 (Lanari *et al.*, 2014*b*, 2018). The analytical conditions and standardization procedures are described in Supplementary Data S2. Representative mineral compositions are given in Supplementary Data S3.

REFERENCES

Afonso, J. C., Fernàndez, M., Ranalli, G., Griffin, W. L. & Connolly, J. A. D. (2008). Integrated geophysical–petrological modeling of the lithosphere and sublithospheric upper mantle: methodology and applications. *Geochemistry, Geophysics, Geosystems* **9**, 1–36.

Agard, P., Searle, M. P., Alsop, G. I. & Dubacq, B. (2010). Crustal stacking and expulsion tectonics during continental subduction: *P–T* deformation constraints from Oman. *Tectonics* **29**, 1–19.

Airaghi, L., de Sigoyer, J., Lanari, P., Guillot, S., Vidal, O., Monié, P., Sautter, B. & Tan, X. (2017a). Total exhumation across the Beichuan fault in the Longmen Shan (eastern Tibetan plateau, China): constraints from petrology and thermobarometry. *Journal of Asian Earth Sciences* **140**, 108–121.

Airaghi, L., Lanari, P., de Sigoyer, J. & Guillot, S. (2017b). Microstructural vs compositional preservation and pseudomorphic replacement of muscovite in deformed metapelites from the Longmen Shan (Sichuan, China). *Lithos* **282–283**, 262–280.

Albarede, F. & Bottinga, Y. (1972). Kinetic disequilibrium in trace element partitioning between phenocrysts and host lava. *Geochimica et Cosmochimica Acta* **36**, 141–156.

Anderson, G. M. (2005). *Thermodynamics of Natural Systems*. Cambridge: Cambridge University Press.

Angel, R. J., Alvaro, M. & Gonzalez-Platas, J. (2014). EosFit7c and a Fortran module (library) for equation of state calculations. *Zeitschrift für Kristallographie—Crystalline Materials* **229**, 405–419.

Baxter, E. F. & Caddick, M. J. (2013). Garnet growth as a proxy for progressive subduction zone dehydration. *Geology* **41**, 643–646.

Becker, U., Fernández-González, A., Prieto, M., Harrison, R. & Putnis, A. (2000). Direct calculation of thermodynamic properties of the barite/celestite solid solution from molecular principles. *Physics and Chemistry of Minerals* **27**, 291–300.

Bégin, N. J. & Pattison, D. R. M. (1994). Metamorphic evolution of granulites in the Minto Block, northern Québec: extraction of peak *P–T* conditions taking account of late Fe–Mg exchange. *Journal of Metamorphic Geology* **12**, 411–428.

Beinlich, A., Klemd, R., John, T. & Gao, J. (2010). Trace-element mobilization during Ca-metasomatism along a major fluid conduit: eclogitization of blueschist as a consequence of fluid–rock interaction. *Geochimica et Cosmochimica Acta* **74**, 1892–1922.

Benisek, A. & Dachs, E. (2018). The accuracy of standard enthalpies and entropies for phases of petrological interest derived from density-functional calculations. *Contributions to Mineralogy and Petrology* **173**, 90.

Benisek, A., Dachs, E. & Kroll, H. (2010). A ternary feldspar-mixing model based on calorimetric data: development and application. *Contributions to Mineralogy and Petrology* **160**, 327–337.

Berman, R. G. (1988). Internally consistent thermodynamic data for minerals in the system Na_2O–K_2O–CaO–MgO–FeO–Fe_2O_3–Al_2O_3–SiO_2–TiO_2–H_2O–CO_2. *Journal of Petrology* **29**, 445–522.

Berman, R. G. (1990). Mixing properties of Ca–Mg–Fe–Mn garnets. *American Mineralogist* **75**, 328–344.

Berman, R. G. (1991). Thermobarometry using multi-equilibrium calculations: a new technique, with petrological applications. *Canadian Mineralogist* **29**, 833–855.

Berman, R. G. (2007). winTWQ (version 2.3): a software package for performing internally-consistent thermobarometric calculations. *Geological Survey of Canada* 41. Open file Report 5462, pp. 41, Geological Survey of Canada.

Berman, R. G. & Aranovich, L. Y. (1996). Optimized standard state and mixing properties of minerals: I. Model calibration for olivine, orthopyroxene, cordierite, garnet, and ilmenite in the system FeO–MgO–CaO–Al_2O_3–SiO_2–TiO_2. *Contributions to Mineralogy and Petrology* **126**, 1–24.

Berman, R. G. & Brown, T. H. (1985). Heat capacity of minerals in the system Na_2O–K_2O–CaO–MgO–FeO–Fe_2O_3–Al_2O_3–SiO_2–TiO_2–H_2O–CO_2: representation, estimation, and high temperature extrapolation. *Contributions to Mineralogy and Petrology* **89**, 168–183.

Berman, R. G., Brown, T. H. & Greenwood, H. J. (1985). *An Internally Consistent Thermodynamic Data Base for Minerals in the System Na2O–K2O–CaO–MgO–FeO–Fe2O3–Al2O3–SiO2–TiO2–H2O–C2O*. Chalk River, ON: SSDO, Atomic Energy of Canada.

Berman, R. G., Brown, T. H. & Perkins, E. H. (1987). GEØ-CALC: software for calculation and display of *P–T–X* phase diagrams. *American Mineralogist* **72**, 861–862.

Berman, R. G., Engi, M., Greenwood, H. J. & Brown, T. H. (1986). Derivation of internally-consistent thermodynamic data by the technique of mathematical programming: a review with application to the system MgO–SiO_2–H_2O. *Journal of Petrology* **27**, 1331–1364.

Blanc, P., Vieillard, P., Gailhanou, H., Gaboreau, S., Gaucher, É., Fialips, C. I., Madé, B. & Giffaut, E. (2015). A generalized model for predicting the thermodynamic properties of clay minerals. *American Journal of Science* **315**, 734–780.

Bosenick, A., Dove, M. T., Myers, E. R., Palin, E. J., Sainz-Diaz, C. I., Guiton, B. S., Warren, M. C., Craig, M. S. & Redfern, S. A. T. (2001). Computational methods for the study of energies of cation distributions: applications to cation-ordering phase transitions and solid solutions. *Mineralogical Magazine* **65**, 193–219.

Bowen, N. L. & Schairer, J. F. (1935). The system MgO-FeO-SiO_2. *American Journal of Science* **170**, 151–217.

Brouwer, F. M. & Engi, M. (2005). Staurolite and other high-alumina phases in Alpine eclogite: analysis of domain evolution. *Canadian Mineralogist* **43**, 105–128.

Brown, T. H. (1977). Introduction to non-ideal and complex solutions. In: Greenwood, H. J. (ed.) *Short Course in Application of Thermodynamics to Petrology and Ore Deposits*. Quebec, QC: Mineralogical Association of Canada, pp. 126–135.

Brown, M. (2007). Metamorphic conditions in orogenic belts: a record of secular change. *International Geology Review* **49**, 193–234.

Brown, T. H. & Skinner, B. J. (1974). Theoretical prediction of equilibrium phase assemblages in multicomponent systems. *American Journal of Science* **274**, 961–986.

Cantarero, I., Lanari, P., Vidal, O., Alías, G., Travé, A. & Baqués, V. (2014). Long-term fluid circulation in extensional faults in the central Catalan Coastal Ranges: *P–T* constraints from neoformed chlorite and K-white mica. *International Journal of Earth Sciences* **103**, 165–188.

Cantarero, I., Alías, G., Cruset, D., Carola, E., Lanari, P. & Travé, A. (2018). Fluid composition changes in crystalline basement rocks from ductile to brittle regimes. *Global and Planetary Change* doi:10.1016/j.gloplacha.2018.1003.1002.

Carlson, W. D. (1989). The significance of intergranular diffusion to the mechanisms and kinetics of porphyroblast crystallization. *Contributions to Mineralogy and Petrology* **103**, 1–24.

Carlson, W. D. (2002). Scales of disequilibrium and rates of equilibration during metamorphism. *American Mineralogist* **87**, 185–204.

Carlson, W. D. (2010). Dependence of reaction kinetics on H_2O activity as inferred from rates of intergranular diffusion of aluminium. *Journal of Metamorphic Geology* **28**, 735–752.

Carlson, R. W. & Gordon, C. L. (2004). Effects of matrix grain size on the kinetics of intergranular diffusion. *Journal of Metamorphic Geology* **22**, 733–742.

Carlson, W. D., Pattison, D. R. M. & Caddick, M. J. (2015). Beyond the equilibrium paradigm: how consideration of kinetics enhances metamorphic interpretation. *American Mineralogist* **100**, 1659–1667.

Carmichael, D. M. (1969). On the mechanism of prograde metamorphic reactions in quartz-bearing pelitic rocks. *Contributions to Mineralogy and Petrology* **20**, 244–267.

Castro, A. E. & Spear, F. S. (2017). Reaction overstepping and re-evaluation of peak *P–T* conditions of the blueschist unit, Sifnos, Greece: implications for the Cyclades subduction zone. *International Geology Review* **59**, 548–562.

Centrella, S., Putnis, A., Lanari, P. & Austrheim, H. (2018). Textural and chemical evolution of pyroxene during hydration and deformation: a consequence of retrograde metamorphism. *Lithos* **296–299**, 245–264.

Charlu, T. V., Newton, R. C. & Kleppa, O. J. (1975). Enthalpies of formation at 970 K of compounds in the system

$MgO–Al_2O_3–SiO_2$ by high temperature solution calorimetry. *Geochimica et Cosmochimica Acta* **39**, 1487–1497.

Chatterjee, N. D., Krüger, R., Haller, G. & Olbricht, W. (1998). The Bayesian approach to an internally consistent thermodynamic database: theory, database, and generation of phase diagrams. *Contributions to Mineralogy and Petrology* **133**, 149–168.

Chermak, J. A. & Rimstidt, J. D. (1989). Estimating the thermodynamic properties (ΔG°_f and ΔH°_f) of silicate minerals at 298 K from the sum of polyhedral contributions. *American Mineralogist* **74**, 1023–1031.

Connolly, J. A. D. (1990). Multivariate phase diagrams: an algorithm based on generalized thermodynamics. *American Journal of Science* **290**, 666–718.

Connolly, J. A. D. (2005). Computation of phase equilibria by linear programming: a tool for geodynamic modeling and its application to subduction zone decarbonation. *Earth and Planetary Science Letters* **236**, 524–541.

Connolly, J. A. D. (2009). The geodynamic equation of state: what and how. *Geochemistry, Geophysics, Geosystems* **10**, 1–19.

Connolly, J. A. D. (2017). A primer in Gibbs energy minimization for geophysicists. *Petrology* **25**, 526–534.

Connolly, J. A. D. & Kerrick, D. M. (1987). An algorithm and computer program for calculating composition phase diagrams. *Calphad* **11**, 1–55.

Connolly, J. A. D. & Petrini, K. (2002). An automated strategy for calculation of phase diagram sections and retrieval of rock properties as a function of physical conditions. *Journal of Metamorphic Geology* **20**, 697–708.

Couch, S., Sparks, R. S. J. & Carroll, M. R. (2001). Mineral disequilibrium in lavas explained by convective self-mixing in open magma chambers. *Nature* **411**, 1037.

Dachs, E., Geiger, C. A., Benisek, A. & Grevel, K. D. (2012). Grossular: a crystal-chemical, calorimetric, and thermodynamic study. *American Mineralogist* **97**, 1299–1313.

Darken, L. S. (1967). Thermodynamics of binary metallic solutions. *Metallurgical Society of AIME Transactions* **239**, 80–89.

Davidson, J., Morgan, D., Charlier, B., Harlou, R. & Hora, J. (2007). Microsampling and isotopic analysis of igneous rocks: implications for the study of magmatic systems. *Annual Review of Earth and Planetary Sciences* **35**, 273–311.

de Capitani, C. & Brown, T. H. (1987). The computation of chemical equilibrium in complex systems containing non-ideal solutions. *Geochimica et Cosmochimica Acta* **51**, 2639–2652.

de Capitani, C. & Peters, T. (1982). Corresponding states in binary solutions, and graphical determination of Margules parameters. *Contributions to Mineralogy and Petrology* **81**, 48–58.

de Capitani, C. & Petrakakis, K. (2010). The computation of equilibrium assemblage diagrams with Theriak/Domino software. *American Mineralogist* **95**, 1006–1016.

Diener, J. F. A. & Powell, R. (2012). Revised activity–composition models for clinopyroxene and amphibole. *Journal of Metamorphic Geology* **30**, 131–142.

Diener, J. F. A., Powell, R., White, R. W. & Holland, T. J. B. (2007). A new thermodynamic model for clino- and orthoamphiboles in the system $Na_2O–CaO–FeO–MgO–Al_2O_3–SiO_2–H_2O–O$. *Journal of Metamorphic Geology* **25**, 631–656.

Dolejš, D. & Wagner, T. (2008). Thermodynamic modeling of non-ideal mineral–fluid equilibria in the system Si–Al–Fe–Mg–Ca–Na–K–H–O–Cl at elevated temperatures and pressures: implications for hydrothermal mass transfer in granitic rocks. *Geochimica et Cosmochimica Act* **72**, 526–553.

Dove, M. T. (2001). Computer simulations of solid solutions. In: Geiger, C. A. (ed.) *Solid Solutions in Silicate and Oxide Systems*. Mineralogical Society of Great Britain and Ireland.

Dove, M. T., Bosenick, A., Myers, E. R., Warren, M. C. & Redfern, S. A. T. (2000). Modelling in relation to cation ordering. *Phase Transitions* **71**, 205–226.

Dubacq, B., Vidal, O. & De Andrade, V. (2010). Dehydration of dioctahedral aluminous phyllosilicates: thermodynamic modelling and implications for thermobarometric estimates. *Contributions to Mineralogy and Petrology* **159**, 159–174.

Dubacq, B., Vidal, O. & Lewin, E. (2011). Atomistic investigation of the pyrophyllitic substitution and implications on clay stability. *American Mineralogist* **96**, 241–249.

Dubacq, B., Bickle, M. J. & Evans, K. A. (2013). An activity model for phase equilibria in the $H_2O–CO_2–NaCl$ system. *Geochimica et Cosmochimica Acta* **110**, 229–252.

Duesterhoeft, E. (2016). A volume equation of state that extends thermodynamic datasets, using the Bridgman Power Series, to very high pressures (20 GPa). *American Journal of Science* **316**, 578–589.

Duesterhoeft, E. (2017). *BED92.v1—Theriak-Domino Database*. ResearchGate.

Duesterhoeft, E. & de Capitani, C. (2013). Theriak_D: an add-on to implement equilibrium computations in geodynamic models. *Geochemistry, Geophysics, Geosystems* **14**, 4962–4967.

Duesterhoeft, E., Bousquet, R., Wichura, H. & Oberhänsli, R. (2012a). Anorogenic plateau formation: the importance of density changes in the lithosphere. *Journal of Geophysical Research: Solid Earth* **117**, 1–13.

Duesterhoeft, E., Zaehle, M., de Capitani, C., Bousquet, R. & Oberhänsli, R. (2012b). Discrepancies of mineral volumes predicted by thermodynamic databases. *Geophysical Research Abstracts* EGU2012-5549.

Duesterhoeft, E., Quinteros, J., Oberhänsli, R., Bousquet, R. & de Capitani, C. (2014). Relative impact of mantle densification and eclogitization of slabs on subduction dynamics: a numerical thermodynamic/thermokinematic investigation of metamorphic density evolution. *Tectonophysics* **637**, 20–29.

Engi, M. (1992). Thermodynamic data for minerals: a critical assessment. In: Price, G. D. & Ross, N. L. (eds) *The Stability of Minerals*. London: Chapman & Hall, pp. 267–328.

Engi, M., Lanari, P. & Kohn, M. J. (2017). Significant ages—an introduction to petrochronology. In: Kohn, M. J., Engi, M. & Lanari, P. (eds) *Petrochronology: Methods and Applications. Mineralogical Society of America and Geochemical Society, Reviews in Mineralogy and Geochemistry* **83**, 1–12.

Engi, M., Giuntoli, F., Lanari, P., Burn, M., Kunz, B. & Bouvier, A.-S. (2018). Pervasive eclogitization due to brittle deformation and rehydration of subducted basement. Effects on continental recycling? *Geochemistry, Geophysics, Geosystems* **19**, 865–881.

Essene, E. J. (1989). The current status of thermobarometry in metamorphic rocks. In: Daly, J. S., Cliff, R. A. & Yardley, B. W. D. (eds) *Evolution of Metamorphic Belts. Geological Society, London, Special Publications* **43**, 1–44.

Evans, B. W. (1990). Phase relations of epidote-blueschists. *Lithos* **25**, 3–23.

Evans, B. W. & Guidotti, C. V. (1966). The sillimanite–potash feldspar isograd in Western Maine, U.S.A. *Contributions to Mineralogy and Petrology* **12**, 25–62.

Evans, K. A. & Powell, R. (2015). The effect of subduction on the sulphur, carbon and redox budget of lithospheric mantle. *Journal of Metamorphic Geology* **33**, 649–670.

Evans, T. P. (2004). A method for calculating effective bulk composition modification due to crystal fractionation in

garnet-bearing schist; implications for isopleth thermobarometry. *Journal of Metamorphic Geology* **22**, 547–557.

Fabrichnaya, O. B., Lukas, H. L., Effenberg, G. & Aldinger, F. (2003). Thermodynamic optimization in the Mg–Y system. *Intermetallics* **11**, 1183–1188.

Ferry, J. M. & Spear, F. S. (1978). Experimental calibration of the partitioning of Fe and Mg between biotite and garnet. *Contributions to Mineralogy and Petrology* **66**, 113–117.

Fullea, J., Afonso, J. C., Connolly, J. A. D., Fernàndez, M., García-Castellanos, D. & Zeyen, H. (2009). LitMod3D: an interactive 3D software to model the thermal, compositional, density, seismological, and rheological structure of the lithosphere and sublithospheric upper mantle. *Geochemistry, Geophysics, Geosystems* **10**, 1–21.

Gaidies, F., de Capitani, C. & Abart, R. (2008). THERIA_G: a software program to numerically model prograde garnet growth. *Contributions to Mineralogy and Petrology* **155**, 657–671.

Gaidies, F., Pattison, D. R. M. & de Capitani, C. (2011). Toward a quantitative model of metamorphic nucleation and growth. *Contributions to Mineralogy and Petrology* **162**, 975–993.

Ganguly, J. (2001). Thermodynamic modelling of solid solution. *EMU Notes in Mineralogy* **3**, 37–69.

Ganguly, J. (2010). Cation diffusion kinetics in aluminosilicate garnets and geological applications. In: Zhang, Y. & Cherniak, D. J. (eds) *Diffusion in Minerals and Melts. Mineralogical Society of America and Geochemical Society, Reviews in Mineralogy and Geochememistry* **72**, 559–601.

Ganne, J., De Andrade, V., Weinberg, R. F., Vidal, O., Dubacq, B., Kagambega, N., Naba, S., Baratoux, L., Jessell, M. & Allibon, J. (2012). Modern-style plate subduction preserved in the Palaeoproterozoic West African craton. *Nature Geoscience* **5**, 60–65.

García-Casco, A., Lázaro, C., Rojas-Agramonte, Y., Kröner, A., Torres-Roldán, R. L., Núñez, K., Neubauer, F., Millán, G. & Blanco-Quintero, I. (2008). Partial melting and counterclockwise *P–T* path of subducted oceanic crust (Sierra del Convento Mélange, Cuba). *Journal of Petrology* **49**, 129–161.

Geiger, C. A. & Dachs, E. (2018). Recent developments and the future of low-*T* calorimetric investigations in the Earth sciences: consequences for thermodynamic calculations and databases. *Journal of Metamorphic Geology* **36**, 283–295.

George, F. R. & Gaidies, F. (2017). Characterisation of a garnet population from the Sikkim Himalaya: insights into the rates and mechanisms of porphyroblast crystallisation. *Contributions to Mineralogy and Petrology* **172**, 57.

Ghiorso, M. S. & Sack, R. O. (1995). Chemical mass transfer in magmatic systems. IV. A revised and internally consistent thermodynamic model for the interpolation and extrapolation of liquid–solid equilibria in magmatic systems at elevated temperatures and pressures. *Contributions to Mineralogy and Petrology* **119**, 197–212.

Ghiorso, M. S., Hirschmann, M. M., Reiners, P. W. & Kress, V. C. I. (2002). The pMELTS: a revision of MELTS aimed at improving calculation of phase relations and major element partitioning involved in partial melting of the mantle at pressures up to 3 GPa. *Geochemistry, Geophysics, Geosystems* **3**, doi: 10.1029/2001GC000217.

Gibbs, J. W. (1878). On the equilibrium of heterogeneous substances. *American Journal of Science* **16**, 441–458.

Giuntoli, F., Lanari, P., Burn, M., Kunz, B. E. & Engi, M. (2018a). Deeply subducted continental fragments—part 2: insight from petrochronology in the central Sesia Zone (western Italian Alps). *Solid Earth* **9**, 191–222.

Giuntoli, F., Lanari, P. & Engi, M. (2018b). Deeply subducted continental fragments—part 1: fracturing, dissolution–precipitation, and diffusion processes recorded by garnet textures of the central Sesia Zone (western Italian Alps). *Solid Earth* **9**, 167–189.

Gordon, T. M. (1973). Determination of internally consistent thermodynamic data from phase equilibrium experiments. *Journal of Geology* **81**, 199–208.

Gordon, T. M. (1992). Generalized thermobarometry: solution of the inverse chemical equilibrium problem using data for individual species. *Geochimica et Cosmochimica Acta* **56**, 1793–1800.

Gordon, T. M. (1998). WEBINVEQ thermobarometry: an experiment in providing interactive scientific software on the World Wide Web. *Computers and Geosciences* **24**, 43–49.

Gordon, T. M., Aranovich, L. Y. & Fed'kin, V. V. (1994). Exploratory data analysis in thermobarometry; an example from the Kisseynew sedimentary gneiss belt, Manitoba, Canada. *American Mineralogist* **79**, 973–982.

Goryaeva, A. M., Urusov, V. S. & Eremin, N. N. (2013). Atomistic simulations of mixing properties and the local structure of the $(Ca, Sr)_{10}[PO_4]6F_2$ solid solution. *European Journal of Mineralogy* **25**, 947–955.

Gottschalk, M. (1997). Internally consistent thermodynamic data for rock-forming minerals in the system SiO_2–TiO_2–Al_2O_3–Fe_2O_3–CaO–MgO–FeO–K_2O–Na_2O–H_2O–CO_2. *European Journal of Mineralogy* **9**, 175–223.

Gottschalk, M. (2016). Beyond the Margules equation: a universal thermodynamic equation for solid solutions including coupled substitution, long- and short-range order. *European Journal of Mineralogy* **28**, 219–244.

Green, E. C. R., Holland, T. J. B. & Powell, R. (2007). An order–disorder model for omphacitic pyroxenes in the system jadeite–diopside–hedenbergite–acmite, with applications to eclogitic rocks. *American Mineralogist* **92**, 1181–1189.

Green, E. C. R., White, R. W., Diener, J. F. A., Powell, R., Holland, T. J. B. & Palin, R. M. (2016). Activity–composition relations for the calculation of partial melting equilibria in metabasic rocks. *Journal of Metamorphic Geology* **34**, 845–869.

Greenwood, H. J. (1977). Entropy, randomness, and activity. In: Greenwood, H. J. (ed.) *Short Course in Application of Thermodynamics to Petrology and Ore Deposits*. Mineralogical Association of Canada, Vancouver, BC, pp. 38–46.

Greenwood, H. J. (1985). Fluid exchange between reacting bodies of rock. In: Helgeson, H. C. (ed.) *Chemical Transport in Metasomatic Processes*. Dordrecht: Reidel, pp. 153–168.

Grevel, K. D. (2004). Intern konsistente thermodynamische Daten für ausgewählte Hochdruckphasen im System CaO–MgO–Al_2O_3–SiO_2–H_2O. Habilitation thesis, Ruhr-University Bochum 124 pp.

Grosch, E. G., Vidal, O., Abu-Alam, T. & McLoughlin, N. (2012). *P–T* constraints on the metamorphic evolution of the Paleoarchean Kromberg type-section, Barberton greenstone belt, South Africa. *Journal of Petrology* **53**, 513–545.

Guevara, V. E. & Caddick, M. J. (2016). Shooting at a moving target: phase equilibria modelling of high-temperature metamorphism. *Journal of Metamorphic Geology* **34**, 209–235.

Guggenheim, E. A. (1952). *Mixtures: The Theory of the Equilibrium Properties of Some Simple Classes of Mixtures, Solutions and Alloy*. Oxford: Clarendon Press.

Haar, C., Gallagher, J. S. & Kell, G. S. (1984). *NBS/NRC Steam Tables. Thermodynamic and Transport Properties and Computer Programs for Vapor and Liquid States of Water in SI Units*. Washington, DC: Hemisphere.

Helgeson, H. C. (1970). A chemical and thermodynamic model of ore deposition in hydrothermal systems. *Mineralogical Society of America* **3**, 155–186.

Helgeson, H. C. (1971). Kinetics of mass transfer among silicates and aqueous solutions. *Geochimica et Cosmochimica Acta* **35**, 421–469.

Helgeson, H. C. (1979). Mass transfer among minerals and hydrothermal solutions. In: Barnes, H. L. (ed.) *Geochemistry of Hydrothermal Ore Deposits*. New York: John Wiley, pp. 568–610.

Helgeson, H. C., Garrels, R. M. & MacKenzie, F. T. (1969). Evaluation of irreversible reactions in geochemical processes involving minerals and aqueous solutions—II. Applications. *Geochimica et Cosmochimica Acta* **33**, 455–481.

Helgeson, H. C., Delany, J. M., Nesbitt, H. W. & Bird, D. K. (1978). Summary and critique of the thermodynamic properties of rock-forming minerals. *American Journal of Science* **287-A**, 1–229.

Hensen, B. J. (1971). Theoretical phase relations involving cordierite and garnet in the system MgO–FeO–Al_2O_3–SiO_2. *Contributions to Mineralogy and Petrology* **33**, 191–214.

Holland, T. J. B. (1980). The reaction albite = jadeite + quartz determined experimentally in the range 600°–1200°C. *American Mineralogist* **65**, 129–134.

Holland, T. J. B. (1989). Dependence of entropy on volume for silicate and oxide minerals; a review and predictive model. *American Mineralogist* **74**, 5–13.

Holland, T. J. B. & Powell, R. (1985). An internally consistent thermodynamic dataset with uncertainties and correlations: 2. Data and results. *Journal of Metamorphic Geology* **3**, 343–370.

Holland, T. J. B. & Powell, R. (1988). An internally consistent thermodynamic data set for phases of petrological interest. *Journal of Metamorphic Geology* **8**, 89–124.

Holland, T. J. B. & Powell, R. (1990). An enlarged and updated internally consistent thermodynamic dataset with uncertains and correlations: the system K_2O–Na_2O–CaO–MgO–MnO–FeO–Fe_2O_3–Al_2O_3–TiO_2–SiO_2–C–H_2–O_2. *Journal of Metamorphic Geology* **8**, 89–124.

Holland, T. J. B. & Powell, R. (1991). A compensated Redlich–Kwong (CORK) equation for volumes and fugacities of CO_2 and H_2O in the range of 1 bar to 50 kbar and 100–1600°C. *Contributions to Mineralogy and Petrology* **109**, 265–273.

Holland, T. J. B. & Powell, R. (1992). Plagioclase feldspars: activity–composition relations based upon Darken's quadratic formalism and Landau theory. *American Mineralogist* **77**, 53–61.

Holland, T. J. B. & Powell, R. (1996a). Thermodynamics of order–disorder in minerals 1: symmetric formalism applied to minerals of fixed composition. *American Mineralogist* **81**, 1413–1424.

Holland, T. J. B. & Powell, R. (1996b). Thermodynamics of order–disorder in minerals 2: symmetric formalism applied to solid solutions. *American Mineralogist* **81**, 1425–1437.

Holland, T. J. B. & Powell, R. (1998). An internally consistent thermodynamic data set for phases of petrological interest. *Journal of Metamorphic Geology* **16**, 309–343.

Holland, T. & Powell, R. (2003). Activity–composition relations for phases in petrological calculations: an asymmetric multicomponent formulation. *Contributions to Mineralogy and Petrology* **145**, 492–501.

Holland, T. J. B. & Powell, R. (2011). An improved and extended internally consistent thermodynamic dataset for phases of petrological interest, involving a new equation of state for solids. *Journal of Metamorphic Geology* **29**, 333–383.

Holland, T. J. B., Baker, J. & Powell, R. (1998). Mixing properties and activity–composition relationships of chlorites in the system MgO–FeO–Al_2O_3–SiO_2–H_2O. *European Journal of Mineralogy* **10**, 395–406.

Holland, T. J. B., Hudson, N. F. C., Powell, R. & Harte, B. (2013). New thermodynamic models and calculated phase equilibria in NCFMAS for basic and ultrabasic compositions through the transition zone into the uppermost lower mantle. *Journal of Petrology* **54**, 1901–1920.

Holloway, J. R. & Wood, B. J. (1988). *Simulating the Earth: Experimental Geochemistry*. Dordrecht: Springer.

Hunziker, P. (2003). The stability of tri-octahedral Fe^{2+}MgAl chlorite. A combined experimental and theoretical study. PhD thesis. University of Basel, 162 pp.

Jennings, E. S. & Holland, T. J. B. (2015). A simple thermodynamic model for melting of peridotite in the system NCFMASOCr. *Journal of Petrology* **56**, 869–892.

Katsura, T., Shatskiy, A., Manthilake, M. A. G. M., Zhai, S., Fukui, H., Yamazaki, D., Matsuzaki, T., Yoneda, A., Ito, E., Kuwata, A., Ueda, A., Nozawa, A. & Funakoshi, K-I. (2009). Thermal expansion of forsterite at high pressures determined by *in situ* X-ray diffraction: the adiabatic geotherm in the upper mantle. *Physics of the Earth and Planetary Interiors* **174**, 86–92.

Kelly, E. D., Carlson, W. D. & Ketcham, R. A. (2013). Magnitudes of departures from equilibrium during regional metamorphism of porphyroblastic rocks. *Journal of Metamorphic Geology* **31**, 981–1002.

Kelly, E. D., Hoisch, T. D., Wells, M. L., Vervoort, J. D. & Beyene, M. A. (2015). An Early Cretaceous garnet pressure–temperature path recording synconvergent burial and exhumation from the hinterland of the Sevier orogenic belt, Albion Mountains, Idaho. *Contributions to Mineralogy and Petrology* **170**, 1–22.

Kelsey, D. E. & Hand, M. (2015). On ultrahigh temperature crustal metamorphism: phase equilibria, trace element thermometry, bulk composition, heat sources, timescales and tectonic settings. *Geoscience Frontiers* **6**, 311–356.

Kelsey, D. E. & Powell, R. (2011). Progress in linking accessory mineral growth and breakdown to major mineral evolution in metamorphic rocks: a thermodynamic approach in the Na_2O–CaO–K_2O–FeO–MgO–Al_2O_3–SiO_2–H_2O–TiO_2–ZrO_2 system. *Journal of Metamorphic Geology* **29**, 151–166.

Kelsey, D. E., White, R. W. & Powell, R. (2003). Orthopyroxene–sillimanite–quartz assemblages: distribution, petrology, quantitative *P–T–X* constraints and *P–T* paths. *Journal of Metamorphic Geology* **21**, 439–453.

Kerrick, D. M. & Jacobs, G. K. (1981). A modified Redlich–Kwong equation for H_2O, CO_2, and H_2O–CO_2 mixtures at elevated pressures and temperatures. *American Journal of Science* **281**, 735–767.

Kohn, M. J. (1993). Uncertainties in differential thermodynamic (Gibbs' method) *P–T* paths. *Contributions to Mineralogy and Petrology* **113**, 24–39.

Kohn, M. J. (2014a). 4.7—geochemical zoning in metamorphic minerals A2. In: Holland, H. D. & Turekian, K. K. (ed.) *Treatise on Geochemistry*, 2nd edn. Oxford: Elsevier, pp. 249–280.

Kohn, M. J. (2014b). 'Thermoba-Raman-try': calibration of spectroscopic barometers and thermometers for mineral inclusions. *Earth and Planetary Science Letters* **388**, 187–196.

Kohn, M. J. & Spear, F. S. (1991). Error propagation for barometers; 2. Application to rocks. *American Mineralogist* **76**, 138–147.

Kohn, M. J. & Spear, F. S. (2000). Retrograde net transfer reaction insurance for pressure–temperature estimates. *Geology* **28**, 1127–1130.

Konrad-Schmolke, M., O'Brien, P. J., de Capitani, C. & Carswell, D. A. (2008). Garnet growth at high- and ultra-high pressure conditions and the effect of element fractionation on mineral modes and composition. *Lithos* **103**, 309–332.

Korzhinskii, D. S. (1936). Mobility and inertness of components in metasomatosis. *Izvestiya Akademiya Nauk SSSR, Seriya Geologicheska* **1**, 58–60.

Korzhinskii, D. S. (1959). *Physicochemical Basis of the Analysis of the Paragenesis of Minerals*. New York: Consultants Bureau.

Koziol, A. M. & Newton, R. C. (1989). Grossular activity–composition relationships in ternary garnets determined by reversed displaced-equilibrium experiments. *Contributions to Mineralogy and Petrology* **103**, 423–433.

Lanari, P. (2012). Micro-cartographie *P–T–e* dans les roches métamorphiques. Applications aux Alpes et à l'Himalaya. PhD thesis. Université de Grenoble, Grenoble, 534 pp.

Lanari, P. & Duesterhoeft, E. (2016). Thermodynamic modeling using BINGO-ANTIDOTE: a new strategy to investigate metamorphic rocks. *Geophysical Research Abstracts* **18**, EGU2016-11363.

Lanari, P. & Engi, M. (2017). Local bulk composition effects on mineral assemblages. In: Kohn, M. J., Engi, M. & Lanari, P. (eds) *Petrochronology: Methods and Applications. Mineralogical Society of America and Geochemical Society, Reviews in Mineralogy and Geochemistry* **83**, 55–102.

Lanari, P., Guillot, S., Schwartz, S., Vidal, O., Tricart, P., Riel, N. & Beyssac, O. (2012). Diachronous evolution of the alpine continental subduction wedge: evidence from *P–T* estimates in the Briançonnais Zone houillère (France–Western Alps). *Journal of Geodynamics* **56–57**, 39–54.

Lanari, P., Riel, N., Guillot, S., Vidal, O., Schwartz, S., Pêcher, A. & Hattori, K. H. (2013). Deciphering high-pressure metamorphism in collisional context using microprobe mapping methods: application to the Stak eclogitic massif (northwest Himalaya). *Geology* **41**, 111–114.

Lanari, P., Rolland, Y., Schwartz, S., Vidal, O., Guillot, S., Tricart, P. & Dumont, T. (2014a). *P–T–t* estimation of deformation in low-grade quartz–feldspar-bearing rocks using thermodynamic modelling and $^{40}Ar/^{39}Ar$ dating techniques: example of the Plan-de-Phasy shear zone unit (Briançonnais Zone, Western Alps). *Terra Nova* **26**, 130–138.

Lanari, P., Vidal, O., De Andrade, V., Dubacq, B., Lewin, E., Grosch, E. G. & Schwartz, S. (2014b). XMapTools: a MATLAB©-based program for electron microprobe X-ray image processing and geothermobarometry. *Computers and Geosciences* **62**, 227–240.

Lanari, P., Wagner, T. & Vidal, O. (2014c). A thermodynamic model for di–trioctahedral chlorite from experimental and natural data in the system $MgO–FeO–Al_2O_3–SiO_2–H_2O$: applications to *P–T* sections and geothermometry. *Contributions to Mineralogy and Petrology* **167**, 968.

Lanari, P., Giuntoli, F., Loury, C., Burn, M. & Engi, M. (2017). An inverse modeling approach to obtain *P–T* conditions of metamorphic stages involving garnet growth and resorption. *European Journal of Mineralogy* **29**, 181–199.

Lanari, P., Vho, A., Bovay, T., Airaghi, L. & Centrella, S. (2018). Quantitative compositional mapping of mineral phases by electron probe micro-analyser. In: Ferrero, S., Lanari, P., Goncalves, P. & Grosch, E. G. (eds) *Metamorphic Geology: Microscale to Mountain Belts. Geological Society, London, Special Publications*, doi: 10.1144/SP478.4.

Laurent, V., Lanari, P., Naïr, I., Augier, R., Lahfid, A. & Jolivet, L. (2018). Exhumation of eclogite and blueschist (Cyclades, Greece): pressure–temperature evolution determined by thermobarometry and garnet equilibrium modelling. *Journal of Metamorphic Geology* **36**, 769–798.

Loomis, T. P. (1975). Reaction of zoning of garnet. *Contributions to Mineralogy and Petrology* **52**, 285–305.

Loury, C., Rolland, Y., Guillot, S., Mikolaichuk, A. V., Lanari, P., Bruguier, O. & Bosch, D. (2015). Crustal-scale structure of South Tien Shan: implications for subduction polarity and Cenozoic reactivation. In: Brunet, M. F., McCann, T., Sobel, E. R. (eds) *Geological Evolution of Central Asian Basins and the Western Tien Shan Range. Geological Society, London, Special Publications* **427**, 197–229.

Loury, C., Rolland, Y., Guillot, S., Lanari, P., Ganino, C., Mélis, R., Jourdon, A., Petit, C., Beyssac, O., Gallet, S. & Monié, P. (2018). Tectonometamorphic evolution of the Atbashi high-pressure units (Kyrgyz CAOB, Tien Shan): implications for the closure of the Turkestan Ocean and continental subduction–exhumation of the South Kazakh continental margin. *Journal of Metamorphic Geology* **36**, 959–985.

Mader, D. & Schenk, B. (2017). Using free/libre and open source software in the geological sciences. *Austrian Journal of Earth Sciences* **110**, 142–161.

Mäder, U. K., Percival, J. A. & Berman, R. G. (1994). Thermobarometry of garnet–clinopyroxene–hornblende granulites from the Kapuskasing structural zone. *Canadian Journal of Earth Sciences* **31**, 1134–1145.

Maier, C. G. & Kelley, K. K. (1932). An equation for the representation of high-temperature heat content data. *Journal of the American Chemical Society* **54**, 3243–3246.

Majumdar, A. J., McKinstry, M. A. & Roy, R. (1964). Thermodynamic parameters for the α–β quartz and α–β cristobalite transitions. *Journal of Physics and Chemistry of Solids* **25**, 1487–1489.

Margules, M. S. (1895). On the composition of saturated vapors of mixtures. *Akademie der Wissenschaften in Wien, Mathematisch-Naturwissenschaftliche Klasse Abteilung 2* **104**, 1234–1239.

Marmo, B. A., Clarke, G. L. & Powell, R. (2002). Fractionation of bulk rock composition due to porphyroblast growth: effects on eclogite facies mineral equilibria, Pam Peninsula, New Caledonia. *Journal of Metamorphic Geology* **20**, 151–165.

Marsala, A. & Wagner, T. (2016). Mass transfer and fluid evolution in late-metamorphic veins, Rhenish Massif (Germany): insight from alteration geochemistry and fluid–mineral equilibria modeling. *Mineralogy and Petrology* **110**, 515–545.

Mayne, M. J., Moyen, J.-F., Stevens, G. & Kaislaniemi, L. (2016). Rcrust: a tool for calculating path-dependent open system processes and application to melt loss. *Journal of Metamorphic Geology* **34**, 663–682.

McCarron, T., Gaidies, F., McFarlane, C. R. M., Easton, R. M. & Jones, P. (2014). Coupling thermodynamic modeling and high-resolution *in situ* LA-ICP-MS monazite geochronology: evidence for Barrovian metamorphism late in the Grenvillian history of southeastern Ontario. *Mineralogy and Petrology* **108**, 741–758.

McMullin, D., Berman, R. G. & Greenwood, H. J. (1991). Calibration of the SGAM thermobarometer for pelitic rocks using data from phase equilibrium experiments and natural assemblages. *Canadian Mineralogist* **29**, 889–908.

Metcalf, R. V., Smith, E. I., Walker, J. D., Reed, R. C. & Gonzales, D. A. (1995). Isotopic disequilibrium among commingled hybrid magmas: evidence for a two-stage magma mixing–commingling process in the Mt. Perkins Pluton, Arizona. *Journal of Geology* **103**, 509–527.

Meth, C. E. & Carlson, W. D. (2005). Diffusion-controlled synkinematic growth of garnet from a heterogeneous precursor at Passo del Sole, Switzerland. *Canadian Mineralogist* **43**, 157–182.

Miron, G. D., Wagner, T., Kulik, D. A. & Heinrich, C. A. (2016). Internally consistent thermodynamic data for aqueous species in the system Na–K–Al–Si–O–H–Cl. *Geochimica et Cosmochimica Acta* **187**, 41–78.

Miron, G. D., Wagner, T., Kulik, D. A. & Lothenbach, B. (2017). An internally consistent thermodynamic dataset for aqueous species in the system Ca–Mg–Na–K–Al–Si–O–H–C–Cl to 800°C and 5 kbar. *American Journal of Science* **317**, 755–806.

Moynihan, D. P. & Pattison, D. R. M. (2013). An automated method for the calculation of *P–T* paths from garnet zoning, with application to metapelitic schist from the Kootenay Arc, British Columbia, Canada. *Journal of Metamorphic Geology* **31**, 525–548.

Nagel, T. J., Duesterhoeft, E. & Schiffer, C. (2018). Garnet-controlled very low velocities in the lower mantle transition zone at sites of mantle upwelling. *Terra Nova* **30**, 333–340.

Navrotsky, A. (1987). Models of crystalline solutions. In: Carmichael, I. S. E. & Eugster, H. P. (eds) *Thermodynamic Modeling of Geological Materials: Minerals, Fluids and Melts. Mineralogical Society of America, Reviews in Mineralogy* **17**, 35–69.

Nestola, F., Pasqual, D., Smyth, J. R., Novella, D., Secco, L., Manghnani, M. H. & Dal Negro, A. (2011). New accurate elastic parameters for the forsterite–fayalite solid solution. *American Mineralogist* **96**, 1742–1747.

Newton, R. C. (1987). Thermodynamic analysis of phase equilibria in simple mineral systems. In: Carmichael, I. S. E. & Eugster, H. P. (eds) *Thermodynamic Modeling of Geological Materials: Minerals, Fluids and Melts. Mineralogical Society of America, Reviews in Mineralogy* **17**, 1–33.

Oliveira, B., Afonso, J. C., Zlotnik, S. & Diez, P. (2018). Numerical modelling of multiphase multicomponent reactive transport in the Earth's interior. *Geophysical Journal International* **212**, 345–388.

Ortolano, G., Visalli, R., Godard, G. & Cirrincione, R. (2018). Quantitative X-ray map analyser (Q-XRMA): a new GIS-based statistical approach to mineral image analysis. *Computers and Geosciences* **115**, 56–65.

Palin, R. M., Weller, O. M., Waters, D. J. & Dyck, B. (2016). Quantifying geological uncertainty in metamorphic phase equilibria modelling; a Monte Carlo assessment and implications for tectonic interpretations. *Geoscience Frontiers* **7**, 591–607.

Parra, T., Vidal, O. & Agard, P. (2002a). A thermodynamic model for Fe–Mg dioctahedral K white micas using data from phase equilibrium experiments and natural pelitic assemblages. *Contributions to Mineralogy and Petrology* **143**, 706–732.

Parra, T., Vidal, O. & Jolivet, L. (2002b). Relation between the intensity of deformation and retrogression in blueschist metapelites of Tinos Island (Greece) evidenced by chlorite–mica local equilibria. *Lithos* **63**, 41–66.

Parra, T., Vidal, O. & Theye, T. (2005). Experimental data on the Tschermak substitution in Fe-chlorite. *American Mineralogist* **90**, 359–370.

Pattison, D. R. M. (1994). Are reversed Fe–Mg exchange and solid solution experiments really reversed? *American Mineralogist* **79**, 938–950.

Pattison, D. R. M. & DeBuhr, C. L. (2015). Petrology of metapelites in the Bugaboo aureole, British Columbia, Canada. *Journal of Metamorphic Geology* **33**, 437–462.

Pattison, D. R. M. & Spear, F. S. (2018). Kinetic control of staurolite–Al_2SiO_5 mineral assemblages: implications for Barrovian and Buchan metamorphism. *Journal of Metamorphic Geology* **36**, 667–690.

Pattison, D. R. M. & Tinkham, D. K. (2009). Interplay between equilibrium and kinetics in prograde metamorphism of pelites: an example from the Nelson aureole, British Columbia. *Journal of Metamorphic Geology* **27**, 249–279.

Pattison, D. R. M. & Vogl, J. J. (2005). Contrasting sequences of metapelitic mineral assemblages in the aureole of the tilted Nelson Batholith, British Columbia: implications for the phase equilibria and pressure determination in andalusite–sillimanite-type settings. *Canadian Mineralogist* **43**, 51–88.

Pattison, D. R. M., Spear, F. S., Debuhr, C. L., Cheney, J. T. & Guidotti, C. V. (2002). Thermodynamic modelling of the reaction muscovite + cordierite → Al_2SiO_5 + biotite + quartz + H_2O: constraints from natural assemblages and implications for the metapelitic petrogenetic grid. *Journal of Metamorphic Geology* **20**, 99–118.

Pattison, D. R. M., Chacko, T., Farquhar, J. & McFarlane, C. R. M. (2003). Temperatures of granulite-facies metamorphism; constraints from experimental phase equilibria and thermobarometry corrected for retrograde exchange. *Journal of Petrology* **44**, 867–900.

Pattison, D. R. M., De Capitani, C. & Gaidies, F. (2011). Petrological consequences of variations in metamorphic reaction affinity. *Journal of Metamorphic Geology* **29**, 953–977.

Pitzer, K. S. & Sterner, M. S. (1994). Equations of state valid from zero to extreme pressures for H_2O and CO_2. *Journal of Chemical Physics* **101**, 3111–3116.

Pitzer, K. S. & Sterner, S. M. (1995). Equations of state valid continuously from zero to extreme pressures with H_2O and CO_2 as examples. *International Journal of Thermophysics* **16**, 511–518.

Pourteau, A., Sudo, M., Candan, O., Lanari, P., Vidal, O. & Oberhänsli, R. (2013). Neotethys closure history of Anatolia: insights from ^{40}Ar–^{39}Ar geochronology and *P–T* estimation in high-pressure metasedimentary rocks. *Journal of Metamorphic Geology* **31**, 585–606.

Pourteau, A., Bousquet, R., Vidal, O., Plunder, A., Duesterhoeft, E., Candan, O. & Oberhänsli, R. (2014). Multistage growth of Fe–Mg–carpholite and Fe–Mg–chloritoid, from field evidence to thermodynamic modelling. *Contributions to Mineralogy and Petrology* **168**, 1–25.

Powell, R. (1978). *Equilibrium Thermodynamics in Petrology*. London: Harper & Row.

Powell, R. (1987). Darken's quadratic formalism and the thermodynamics of minerals. *American Mineralogist* **72**, 1–11.

Powell, R. & Holland, T. J. B. (1988). An internally consistent dataset with uncertainties and correlations: 3. Applications to geobarometry, worked examples and a computer program. *Journal of Metamorphic Geology* **6**, 173–204.

Powell, R. & Holland, T. J. B. (1993a). The applicability of least squares in the extraction of thermodynamic data from experimentally bracketed mineral equilibria. *American Mineralogist* **78**, 107–112.

Powell, R. & Holland, T. J. B. (1993b). On the formulation of simple mixing models for complex phases. *American Mineralogist* **78**, 1174–1180.

Powell, R. & Holland, T. J. B. (1994). Optimal geothermometry and geobarometry. *American Mineralogist* **79**, 120–133.

Powell, R. & Holland, T. J. B. (2008). On thermobarometry. *Journal of Metamorphic Geology* **26**, 155–179.

Powell, R. & Holland, T. (2010). Using equilibrium thermodynamics to understand metamorphism and metamorphic rocks. *Elements* **6**, 309–314.

Powell, R., Holland, T. & Worley, B. (1998). Calculating phase diagrams involving solid solutions via non-linear equations, with examples using THERMOCALC. *Journal of Metamorphic Geology* **16**, 577–588.

Powell, R., White, R. W., Green, E. C. R., Holland, T. J. B. & Diener, J. F. A. (2014). On parameterizing thermodynamic descriptions of minerals for petrological calculations. *Journal of Metamorphic Geology* **32**, 245–260.

Pownceby, M. I., Wall, V. J. & O'Neill, H. S. C. (1987). Fe–Mn partitioning between garnet and ilmenite: experimental calibration and applications. *Contributions to Mineralogy and Petrology* **97**, 116–126.

Ravna, E. J. K. & Paquin, J. (2003). Thermobarometric methodologies applicable to eclogites and garnet ultrabasites. *EMU Notes in Mineralogy* **5**, 229–259.

Reche, J. & Martinez, F. J. (1996). GPT: an Excel spreadsheet for thermobarometric calculations in metapelitic rocks. *Computers and Geosciences* **22**, 775–784.

Reich, M. & Becker, U. (2006). First-principles calculations of the thermodynamic mixing properties of arsenic incorporation into pyrite and marcasite. *Chemical Geology* **225**, 278–290.

Robie, R. A. & Hemingway, B. S. (1995). *Thermodynamic properties of minerals and related substances at 298·15 K and 1 bar (105 pascals) pressure and at higher temperatures. US Geological Survey Bulletin* **2131**, 461 pp.

Robie, R. A., Hemingway, B. S. & Fisher, J. R. (1978). *Thermodynamic properties of minerals and related substances at 298·15 K and 1 bar (105 pascals) pressure and at higher temperatures. US Geological Survey Bulletin* **1452**, 456 pp.

Rubatto, D., Chakraborty, S. & Dasgupta, S. (2013). Timescales of crustal melting in the Higher Himalayan Crystallines (Sikkim, Eastern Himalaya) inferred from trace element-constrained monazite and zircon chronology. *Contributions to Mineralogy and Petrology* **165**, 349–372.

Rubie, D. C. (1998). Disequilibrium during metamorphism: the role of nucleation kinetics. In: Treloar, P. J. & O'Brien, P. J. (eds) *What Drives Metamorphism and Metamorphic Reactions? Geological Society, London, Special Publications* **138**, 199–214.

Sánchez-Roa, C., Vidal, O., Jiménez-Millán, J., Nieto, F. & Faulkner, D. R. (2018). Implications of sepiolite dehydration for earthquake nucleation in the Galera Fault Zone: a thermodynamic approach. *Applied Geochemistry* **89**, 219–228.

Saxena, S. K., Chatterjee, N. & Fei, Y. G. S. (1993). *Thermodynamic Data Set Based on Thermochemistry and High Pressure Phase Equilibrium*. Berlin: Springer.

Schairer, J. F. & Bowen, N. L. (1935). Preliminary report on equilibrium-relations between feldspathoids, alkali-feldspars, and silica. *Transactions, American Geophysical Union* **16**, 325–328.

Scheffer, C., Vanderhaeghe, O., Lanari, P., Tarantola, A., Ponthus, L., Photiades, A. & France, L. (2016). Syn- to post-orogenic exhumation of metamorphic nappes: structure and thermobarometry of the western Attic–Cycladic metamorphic complex (Lavrion, Greece). *Journal of Geodynamics* **96**, 174–193.

Shock, E. L., Helgeson, H. C. & Sverjensky, D. A. (1989). Calculation of the thermodynamic and transport properties of aqueous species at high pressures and temperatures: standard partial molal properties of inorganic neutral species. *Geochimica et Cosmochimica Acta* **53**, 2157–2183.

Siret, D., Poulet, T., Regenauer-Lieb, K. & Connolly, J. A. D. (2009). PreMDB, a thermodynamically consistent material database as a key to geodynamic modelling. *Acta Geotechnica* **4**, 107–115.

Spear, F. S. (1988a). The Gibbs method and Duhem's theorem: the quantitative relationships among *P*, *T*, chemical potential, phase composition and reaction progress in igneous and metamorphic systems. *Contributions to Mineralogy and Petrology* **99**, 249–256.

Spear, F. S. (1988b). Metamorphic fractional crystallization and internal metasomatism by diffusional homogenization of zoned garnets. *Contributions to Mineralogy and Petrology* **99**, 507–517.

Spear, F. S. (1993). *Metamorphic Phase Equilibria and Pressure–Temperature–Time Paths*. Wahington, DC: Mineralogical Society of America.

Spear, F. S. & Pattison, D. R. M. (2017). The implications of overstepping for metamorphic assemblage diagrams (MADs). *Chemical Geology* **457**, 38–46.

Spear, F. S. & Pyle, J. M. (2010). Theoretical modeling of monazite growth in a low-Ca metapelite. *Chemical Geology* **273**, 111–119.

Spear, F. S., Thomas, J. B. & Hallett, B. W. (2014). Overstepping the garnet isograd: a comparison of QuiG barometry and thermodynamic modeling. *Contributions to Mineralogy and Petrology* **168**, 1059.

Spear, F. S., Pattison, D. R. M. & Cheney, J. T. (2016). The Web of Geological Sciences: Advances, Impacts, and Interactions II Geological Society of America. In: *Geological Society of America, Special Papers* **523**, 31–73.

Stixrude, L. & Lithgow-Bertelloni, C. (2005). Thermodynamics of mantle minerals—I. Physical properties. *Geophysical Journal International* **162**, 610–632.

Stixrude, L. & Lithgow-Bertelloni, C. (2011). Thermodynamics of mantle minerals—II. Phase equilibria. *Geophysical Journal International* **184**, 1180–1213.

Symmes, G. H. & Ferry, J. M. (1992). The effect of whole-rock MnO content on the stability of garnet in pelitic schists during metamorphism. *Journal of Metamorphic Geology* **10**, 221–237.

Tajčmanová, L., Connolly, J. A. D. & Cesare, B. (2009). A thermodynamic model for titanium and ferric iron solution in biotite. *Journal of Metamorphic Geology* **27**, 153–165.

Tajčmanová, L., Vrijmoed, J. & Moulas, E. (2015). Grain-scale pressure variations in metamorphic rocks: implications for the interpretation of petrographic observations. *Lithos* **216–217**, 338–351.

Tanger, J. C. & Helgeson, H. C. (1988). Calculation of the thermodynamic and transport properties of aqueous species at high pressures and temperatures: revised equations of state for the standard partial molal properties of ions and electrolytes. *American Journal of Science* **288**, 19–98.

Taylor-Jones, K. & Powell, R. (2010). The stability of sapphirine + quartz: calculated phase equilibria in FeO–MgO–Al_2O_3–SiO_2–TiO_2–O. *Journal of Metamorphic Geology* **28**, 615–633.

Thomas, J. B. & Spear, F. S. (2018). Experimental study of quartz inclusions in garnet at pressures up to 3·0 GPa: evaluating validity of the quartz-in-garnet inclusion elastic thermobarometer. *Contributions to Mineralogy and Petrology* **173**, 1–14.

Thomas, J. B., Watson, E. B., Spear, F. S., Shemella, P. T., Nayak, S. K. & Lanzirotti, A. (2010). TitaniQ under pressure: the effect of pressure and temperature on the solubility of Ti in quartz. *Contributions to Mineralogy and Petrology* **160**, 743–759.

Thompson, J. B. (1955). The thermodynamic basis for the mineral facies concept. *American Journal of Science* **253**, 65–103.

Thompson, J. (1959). Local equilibrium in metasomatic processes. In: Abelson, P. H. (ed.) *Researches in Geochemistry, Volume 1*. New York: John Wiley, pp. 427–457.

Thompson, F. B. (1967). Thermodynamic properties of simple solutions. In: Abelson, P. H. (ed.) *Researches in Geochemistry*. New York, NY: John Wiley, pp. 340–361.

Thompson, J. B. (1970). Geochemical reaction and open systems. *Geochimica et Cosmochimica Acta* **34**, 529–551.

Tinkham, D. K. & Ghent, E. D. (2005). Estimating *P–T* conditions of garnet growth with isochemical phase-diagrams sections and the problem of effective bulk-composition. *Canadian Mineralogist* **43**, 35–50.

Tracy, R. J. (1982). Compositional zoning and inclusions in metamorphic minerals. In: Ferry, J. M. (ed.) *Characterization of Metamorphism Through Mineral Equilibria.*

Mineralogical Society of America, Reviews in Mineralogy **10**, 355–397.

Trincal, V. & Lanari, P. (2016). Al-free di–trioctahedral substitution in chlorite and a ferri-sudoite end-member. *Clay Minerals* **51**, 675–689.

van Laar, J. J. (1906). *Sechs Vorträge über das Thermodynamischer Potential*. Braunschweig: Vieweg.

van Zeggren, F. & Storey, S. H. (1970). *The Computation of Chemical Equilibrium*. Cambridge: Cambridge University Press.

Vernon, R. H. (1977). Relationships between microstructures and metamorphic assemblages. *Tectonophysics* **39**, 439–452.

Vernon, R. H. (1978). Porphyroblast–matrix microstructural relationships in deformed metamorphic rocks. *Geologische Rundschau* **67**, 288–305.

Vernon, R. H., White, R. W. & Clarke, G. L. (2008). False metamorphic events inferred from misinterpretation of microstructural evidence and *P–T* data. *Journal of Metamorphic Geology* **26**, 437–449.

Vidal, O. & Dubacq, B. (2009). Thermodynamic modelling of clay dehydration, stability and compositional evolution with temperature, pressure and H_2O activity. *Geochimica et Cosmochimica Acta* **73**, 6544–6564.

Vidal, O. & Parra, T. (2000). Exhumation paths of high-pressure metapelites obtained from local equilibria for chlorite–phengite assemblages. *Geological Journal* **35**, 139–161.

Vidal, O., Parra, T. & Trotet, F. (2001). A thermodynamic model for Fe–Mg aluminous chlorite using data from phase equilibrium experiments and natural pelitic assemblages in the 100° to 600°C, 1 to 25 kb range. *American Journal of Science* **301**, 557–592.

Vidal, O., Parra, T. & Vieillard, P. (2005). Thermodynamic properties of the Tschermak solid solution in Fe-chlorite: application to natural examples and possible role of oxidation. *American Mineralogist* **90**, 1945–3027.

Vidal, O., De Andrade, V., Lewin, E., Munoz, M., Parra, T. & Pascarelli, S. (2006). *P–T*–deformation–Fe^{3+}/Fe^{2+} mapping at the thin section scale and comparison with XANES mapping: application to a garnet-bearing metapelite from the Sambagawa metamorphic belt (Japan). *Journal of Metamorphic Geology* **24**, 669–683.

Vieillard, P. (2010). A predictive model for the entropies and heat capacities of zeolites. *European Journal of Mineralogy* **22**, 823–836.

Vinograd, V. L., Gale, J. D. & Winkler, B. (2007). Thermodynamics of mixing in diopside–jadeite, $CaMgSi_2O_6$–$NaAlSi_2O_6$, solid solution from static lattice energy calculations. *Physics and Chemistry of Minerals* **34**, 713–725.

Vrijmoed, J. C. & Hacker, B. R. (2014). Determining *P–T* paths from garnet zoning using a brute-force computational method. *Contributions to Mineralogy and Petrology* **167**, 1–13.

Wagner, T., Kulik, D. A., Hingerl, F. F. & Dmytrieva, S. V. (2012). Gem-Selektor geochemical modeling package: TSolMod library and data interface for multicomponent phase models. *Canadian Mineralogist* **50**, 1173–1195.

Warren, C. J. & Waters, D. J. (2006). Oxidized eclogites and garnet-blueschists from Oman: *P–T* path modelling in the NCFMASHO system. *Journal of Metamorphic Geology* **24**, 783–802.

Waters, D. J. & Lovegrove, D. P. (2002). Assessing the extent of disequilibrium and overstepping of prograde metamorphic reactions in metapelites from the Bushveld Complex aureole, South Africa. *Journal of Metamorphic Geology* **20**, 135–149.

Wheller, C. J. & Powell, R. (2014). A new thermodynamic model for sapphirine: calculated phase equilibria in K_2O–FeO–MgO–Al_2O_3–SiO_2–H_2O–TiO_2–Fe_2O_3. *Journal of Metamorphic Geology* **32**, 287–299.

White, R. W., Powell, R. & Holland, T. J. B. (2007). Progress relating to calculation of partial melting equilibria for metapelites. *Journal of Metamorphic Geology* **25**, 511–527.

White, R. W., Powell, R. & Baldwin, J. A. (2008). Calculated phase equilibria involving chemical potentials to investigate the textural evolution of metamorphic rocks. *Journal of Metamorphic Geology* **26**, 181–198.

White, R. W., Powell, R., Holland, T. J. B., Johnson, T. E. & Green, E. C. R. (2014). New mineral activity–composition relations for thermodynamic calculations in metapelitic systems. *Journal of Metamorphic Geology* **32**, 261–286.

White, W. M. (2013). *Geochemistry*. Wiley–Blackwell.

Whitney, D. L. & Evans, B. W. (2010). Abbreviations for names of rock-forming minerals. *American Mineralogist* **95**, 185–187.

Wood, B. J. (1987). Thermodynamics of multicomponent systems containing several solid solutions. In: Carmichael, I. S. E. & Eugster, H. P. (eds) *Thermodynamic Modeling of Geological Materials: Minerals, Fluids and Melts. Mineralogical Society of America, Reviews in Mineralogy* **17**, 71–95.

Wood, B. J. & Nicholls, J. (1978). The thermodynamic properties of reciprocal solid solutions. *Contributions to Mineralogy and Petrology* **66**, 389–400.

Worley, B. & Powell, R. (2000). High-precision relative thermobarometry: theory and a worked example. *Journal of Metamorphic Geology* **18**, 91–101.

Yakymchuk, C. (2017). Applying phase equilibria modelling to metamorphic and geological processes: recent developments and future potential. *Geoscience Canada* **44**, 27–45.

Yakymchuk, C., Clark, C. & White, R. W. (2017). Phase relations and petrochronology. In: Kohn, M. J., Engi, M. & Lanari, P. (eds) *Petrochronology: Methods and Applications. Mineralogical Society of America and Geochemical Society, Reviews in Mineralogy and Geochemistry* **83**, 13–53.

Zunino, A., Connolly, J. A. D. & Khan, A. (2011). Precalculated phase equilibrium models for geophysical properties of the crust and mantle as a function of composition. *Geochemistry, Geophysics, Geosystems* **12**, 1–9.